ABSTRACT

Title of Dissertation:	THERMAL DRILLING AND ANCHORING ON ICY PLANETARY BODIES
	Adam Hugh Halperin **Doctor of Philosophy, 2020**
Dissertation directed by:	Professor Raymond J. Sedwick Department of Aerospace Engineering

Europa is of scientific interest because it is made primarily of water, may have subsurface liquid oceans, and has active cryovolcanoes. Despite the cryogenic surface temperatures, ambient vacuum pressure, and high levels of radiation, potential missions to its surface or its subsurface oceans are topics of current research. Exploring Europa's surface poses an interesting challenge because of these ambient conditions. Furthermore, any regions of crevasses, ridges, penitentes, cryovolcano formations, and other extreme terrains would be inaccessible to existing rover designs.

The "thermal pick" proposed here is a novel system to enable a rover to traverse even the most extreme Europan terrains. It is a dual-function system that first uses a thermal drilling process to burrow into Europa's surface ice and then serves as an anchor, supporting the mobility of the rover to which it is attached. Thermal drilling provides high reliability but can be energetically costly. An intermittent

thermal drilling approach was developed that dramatically reduces the primary drivers of energy cost for thermal drilling in cryogenic ices. Since thermal drilling can cause thermally induced ice fracturing, operational conditions that minimize the likelihood of ice failure modes were established.

Three test rigs, two end effectors, and over ten thermal picks were prototyped and tested. Testing with dry ice at atmospheric pressure and testing with cryogenic water ice in a vacuum chamber provided an understanding of thermal drilling in the sublimation and melting regimes, respectively. This testing demonstrated efficiencies of up to 90% relative to ideal sublimation with dry ice and efficiencies of up to 50% relative to melting with cryogenic water ice under vacuum.

For safe mobility in the toughest icy terrains, a single anchor should be capable of supporting an entire rover's weight. Anchoring strengths in excess of 130N were demonstrated, which is the full weight of 100kg on Europa. This 130N anchoring force was supported by even the weakest anchor tested, suggesting potentially greater anchoring loads can be supported.

THERMAL DRILLING AND ANCHORING ON ICY PLANETARY BODIES

by

Adam Hugh Halperin

Dissertation submitted to the Faculty of the Graduate School of the
University of Maryland, College Park, in partial fulfillment
of the requirements for the degree of
Doctor of Philosophy
2020

Advisory Committee:
Professor Raymond J. Sedwick, Chair
Professor Norman Wereley
Professor David Akin
Professor Kenneth Yu
Professor Yunho Hwang
Professor David Lovell

Acknowledgements

I would first like to thank my advisor, Dr. Raymond Sedwick, for the opportunity to work on this exciting research project while at the Space Power and Propulsion Laboratory. Without his support, guidance, and patience, I could not have done any of this. Dr. Sedwick gave me the academic freedom to learn to solve problems but was always there when I needed help. I cannot overstate the value of our multi-hour meetings in his office. I always left them excited to work through the potential solutions we had discussed. I will always be grateful to have had him as a mentor.

I would like to thank Dr. David Akin for providing a thermal vacuum chamber, lab space, and advice. He has supported me since my time as an undergraduate and my first experience of becoming truly passionate about an engineering project was in his Space Systems Design course, which was a critical step on the path leading me here today. Additionally, I want to thank Dr. Norman Wereley, Dr. Kenneth Yu, and Dr. Yunho Hwang for being on my committee and Dr. David Lovell for being my committee's Dean's Representative.

Particularly helpful to this work were the efforts of Melissa Adams, Arjun Agarwal, and Kahlil Greene. Your contributions were essential to this dissertation and I know you will all be successful in your continued studies and research.

I am grateful for the support of my labmates in the Space Power and Propulsion Laboratory and especially for their friendship. Discussing research projects, going out to the Food Factory, and joking around in the office made each

day fun. Their help in studying for examinations, preparing for presentations, and working through research problems was invaluable.

I would like to extend a special thank you to Howie Grossenbacher. Without Howie's expertise and willingness to brainstorm mechanical solutions, many of my mechanical problems would have been insurmountable roadblocks. I appreciate every lesson I learned from him and his kind heartedness made each meeting a pleasure.

I would also like to thank Dr. William Fourney for his guidance through my undergraduate and graduate studies. I would not be here without his advice and support and I know that there are countless other students that he has helped in a similar manner.

My family has been a constant source of love and encouragement, and to those I have not mentioned, thank you. Thank you to my wife, Meredith, who keeps me on track and is always on my team. Thank you to my son, Clark, whose smiles, hugs, and words always bring me joy. Thank you to my Mom and Dad, Janet and Steve Halperin, who have always been there for me to talk through both personal and technical problems. Thank you to my sister, Nicole, who is my oldest friend, for always lending a helping hand. Thank you to the Osbornes, Weizers, Jerins, Clairs, and Morgans for welcoming me into your family with open arms. Thank you to my friends who have always believed in me. Thank you to Horton for your love, loyalty, and for always being happy to walk with me, even in silence when I am preoccupied with work.

Finally, I would like to thank Dr. Rick Elphic and NASA's Early Stage Innovation program for their financial support of this research.

Table of Contents

List of Figures

Chapter 1: Introduction

1.1 Motivation

Previous and planned missions to Europa and the other icy moons are indicative of the scientific value we see in exploring planetary bodies where water can be found. This is at least in part due to the potential for life and is especially relevant for moons such as Europa where liquid water is suspected to exist. Europa orbiters and fly-bys are an excellent means of gathering information about this Jovian moon, but landers, rovers, and subsurface probes represent further milestones that would enable direct measurements and sampling that are not possible from space. This dissertation proposes an anchoring system for landers and rovers that would interact directly with the surface of Europa.

Landers may require additional stability once they have reached the surface, but rovers are mobile and require a more complex interaction with the surface ice. The success of Mars rovers suggests that rocker-bogie systems with large wheels might be suitable. Tracked systems like those used for terrestrial snowmobiles are similarly appealing. However, both approaches are restricted in the surface topology that can be accommodated, with steep inclines and large obstacles being especially problematic. To explore the cracks, crevasses, cliffs, penitentes, cryovolcanoes, and other features that may be found on Europa, a rover with an ability to handle extreme terrains is required.

To handle these daunting Europan terrains, this work proposes the use of an anchoring end effector that would attach to an actuated rover. By anchoring into the

surface ice of Europa, an actuated rover could leverage a series of holds in sequence to traverse a wide range of icy surfaces at any angle.

An ice anchor on a rover must be inserted into the surface ice by mechanical or thermal means, support applied loads without failure of the ice or the anchor itself, and must be extracted from the ice so that it can be anchored into a new location. A robust design that has potential for real world application must be capable of performing these functions with minimal energy expenditure, mass, complexity, and likelihood of failure. The development and demonstration of the novel thermal pick system in this work achieves those goals and thereby contributes to the state of the art.

1.2 Summary of Contributions

1.2.1 Thermal Pick

The anchoring system that is proposed achieves low complexity and low mass by using a single mechanism to act as both a thermal drill and anchor. This dual function device is referred to as a thermal pick and is the primary focus of this work. A thermal pick achieves its dual function by having an embedded heater that provides heat for the thermal drilling process and a sturdy metal body that can withstand the loads applied during anchoring.

1.2.2 Thermal Drilling

The thermal drilling process that permits insertion of the thermal pick beneath the ice necessitates energy expenditure. The energy cost is the primary concern for the practicality of thermal drilling systems operating in cryogenic environments. This

work proposes a novel intermittent insertion scheme that dramatically reduces conductive heat loss, the primary heat loss mechanism for cryogenic thermal drills. This intermittent insertion scheme targets melting phase transition on the surface of Europa despite its lack of atmosphere. It provides efficient thermal drilling (>30%) and effectively decouples heater power output from efficiency.

1.2.3 Reliable Anchoring

To provide an anchoring system design with high reliability, the anchors proposed in this work avoid the use of moving parts by relying on thermal processes. By contrast, mechanical drilling systems that use moving parts and cutting edges experience wear and tear, leading to concerns for their reliability on autonomous systems. However, thermal drilling systems have different downsides. They create thermal gradients and phase change behaviors that introduce new thermally induced ice failure modes.

Thermal gradients within a block of solid ice cause a relative expansion or contraction that induces mechanical stress. If the mechanical stresses exceed the ice strength and result in ice fracture, it is referred to as thermal shock. This mechanical stress can exceed the strength and fracture the ice and is called thermal shock. Liquid water freezing and expanding within a closed volume can also develop stress that fractures the surrounding ice. These phenomena can be observed in common household freezers, but they are especially problematic in the cryogenic temperature range. These ice failure mechanisms were observed and studied through experimental testing, culminating in establishing a set of operational conditions for thermal drilling that mitigate ice failure.

1.2.4 Experimental Testing at Planetary Conditions

To test and demonstrate the thermal anchoring system, experiments were conducted under simulated Europa surface conditions. This effort required the design and construction of test rigs, the development of test procedures, and the design and manufacturing of prototype thermal picks and end effectors. Three test rigs and corresponding procedures as well as a multitude of prototype components were constructed and tested under both vacuum cryogenic water ice conditions and cryogenic dry ice conditions. A vacuum chamber and a liquid nitrogen cooling process were used to simulate Europa's surface conditions.

Dry ice was used in place of water ice to perform initial testing without requiring a vacuum chamber. However, since dry ice is a partial constituent of the polar ice caps on Mars and can be mechanically or thermally drilled in a similar means to water, the dry ice experimental results are pertinent to that application. Sublimation-based thermal anchoring systems that operate in dry ice are inherently different from water ice systems due primarily to the lack of observed re-freezing.

1.2.5 End Effector

Anchoring was demonstrated using two end effectors that were designed and prototyped. The long thermal pick end effector was designed for deep-anchoring and the short thermal pick end effector was designed for shallow-anchoring. End effectors are made of a thermal pick and a complementary set of components that permit the loading of the anchor in the intended manner, for anchoring loads to be transferred to the rover body, and for the thermal insulation of the thermal pick. The end effectors

were successfully tested in cryogenic water ice at atmospheric pressure in the laboratory, demonstrating the feasibility of the anchoring system in its entirety.

1.2.6 Publications

Thermal Picks for Anchoring on Icy Moons

Adam H. Halperin, Raymond Sedwick, and Arjun Agarwal

Heliyon, Volume 5, Issue 12

DOI: 10.1016/j.heliyon.2019.e02959

Anchoring Thermal Drills for Icy Moon Stability and Mobility

Adam Halperin and Raymond Sedwick

Planetary and Space Science

DOI: 10.1016/j.pss.2020.104967

Chapter 2: Background

2.1 Europa's Surface

Our understanding of the nature of Europa's surface is constantly expanding as new data are acquired and old data are further analyzed. While direct observations are limited, the information that exists can be combined with terrestrial analogues and simulations to provide estimations of what the surface conditions may be. The relevant surface characteristics for an anchoring system that provides stability and mobility are the surface topology, ice strength, ice composition, and surface friction. Thermal drilling systems specifically are also impacted by the temperature, thermal conductivity, specific heat, and latent heat of phase change.

The surface of Europa is young, and the observable characteristics indicate what is referred to as chaos terrains [1] [2] with active tectonics and resurfacing mechanisms [3] [4]. Whether or not the formation of penitentes (fields of ice spikes formed by differential sublimation) is likely on Europa's surface is still a topic of current debate [5] [6], but ridges [7], crevasses [8], and even features created by cryovolcanism [9] are observed and have been modeled. The temperature of the surface has been extensively studied and the mean surface temperature is 90 K (-183 °C) [10]. The pressure on the surface has also been studied and is at vacuum, with sublimation, sputtering, and cryovolcanism sustaining a tenuous atmosphere [11].

While the large-scale features of Europa have been studied because they are discernable with the image resolutions that are available, the meter-scale surface

characteristics are not currently known but are of prime importance to a Europa rover. The surface composition, density, and strength are also unknown, but terrestrial analogues can be used to estimate their potential range. The brittle failure of ice has been studied extensively [12] and its strength as it approaches cryogenic temperatures has also been explored [13] [14]. These works have shown that the strength of ice is inversely correlated with temperature, reaching its highest strength at cryogenic temperatures. It has also been shown that the strength of ice decreases dramatically with increasing porosity [13], but the tensile and compressive strength of ice generally increases with decreasing purity.

These ice strength trends make the measured cryogenic temperature and presence of sulfates [15] potentially positive factors for anchors that rely on load bearing ices. Current porosity estimates show a range as high as 95% porosity at the optical scale [16], between 50% and 75% at the meter scale [17], and as low as 10% [18] at the kilometer scale. The higher porosity range has an especially negative implication for ice strength but requires additional research to confirm. However, an opposing process called sintering may be occurring for porous surface ices, increasing their strength and forming an ice crust [19].

The surface friction on Europa is important for wheeled and tracked Europa rovers. While water ice is associated with low friction on Earth, this is due to a thin meltwater layer that can form and reduce the coefficient of friction of an ice surface. This phenomenon is not observed in cryogenic ices where the cold temperature inhibits the formation of a liquid layer, which in turn causes the surface friction coefficient to be relatively high ($\mu_f > 0.15$) [20].

For thermal drilling systems, the conductivity and specific heat of ice at cryogenic temperatures affect the behavior of the thermal drilling process. These properties have been measured with terrestrial ices that were cooled to cryogenic temperatures [21]. The specific heat reduces to 800 J/kg-K at 90 K from 2100 J/kg-K at 273 K while thermal conductivity increases to 6 W/m-K at 90K from 2.2 W/m-K at 273 K.

2.2 Mechanical Drilling and Anchoring

Mechanical anchoring systems use a cutting process that removes the necessary ices to permit the insertion of the anchor. All mechanical cutting schemes for anchoring require moving parts like motors, gears, and bearings and a cutting edge, all of which will wear over time. This leads to reliability concerns for autonomous use.

Cutting into cryogenic ice was studied and requires a low specific cutting energy cost of 60 MJ/m^3 for cryogenic water ice at 140 K. The axial force required was between 15 N and 25 N for a 25 mm outer diameter coring bit [22]. However, mechanical cutting mechanisms are relatively complex and require motor control and sensors to prevent damage to the ice during the cutting process.

Ice screw based mechanical anchoring systems have been demonstrated in terrestrial ices and their capabilities can be extrapolated to planetary applications. The Ice Screw End Effector (ISEE) is equipped with an alpinist screw for anchoring and is proposed for use on a planetary Rover [23]. The anchoring load capacity demonstrated by the ISEE is in excess of 350 N in terrestrial ices found in fumarolic

caves. This anchoring load corresponds to the full weight of a >250 kg rover on Europa.

A downside of mechanical anchoring systems is the force required to initiate the insertion of the ice screw, which for ISEE is recorded as being between <60 N and 180 N. If these forces are similar to what would be required on Europa, then Europa's low gravity could prove to be problematic. For a rover to perform its first mechanical anchor insertion, it would have to use its own weight to apply the force. To use this approach, a rover would need a minimum mass of 45 kg or 136 kg for a 60 N and 180 N insertion force, respectively. This is potentially restrictive for a Europa mission. Certain terrains may permit the rover to apply this force by bracing against surrounding ices and using actuation to develop the necessary forces, but this is reliant upon finding appropriate surface features prior to anchoring.

NASA's IceWorm is another ice screw based mechanical anchoring system that has been tested in terrestrial ices [24]. The IceWorm is based on the same inchworm morphology found in ISEE and this work. The IceWorm is equipped with sensors and precision motors that are needed to avoid damaging the ice, leading to a relatively complex system.

Mechanical cutting has also been proposed for long-range subsurface drilling [25]. A rotating cutting head is proposed to break up the ice in the path of the subsurface probe, while the cut ice material is melted and passed out of the back of the probe so that forward progress to be made. This approach involves many moving parts and complex mechanisms, leading to concerns regarding its reliability. The process of clearing cut ice from the drill path is inherently solved for the ISEE and

IceWorm systems since alpinist screws passively push cut ice out through the hollow core of the screw.

Regardless of the mechanism used to drill into the ice, anchors require mechanical strength to provide a useful hold in the ice. Despite the limited knowledge of Europa's ice surface characteristics, the holding strength of terrestrial ices can be examined. Terrestrial ices subjected to loading through an ice anchor fail in tension [26] and their strength is correlated with the depth of insertion. The high strength of ice anchors at relatively shallow depths suggests that a Europa rover with low weight will require only a shallow anchor. However, if Europa ice is significantly weaker than terrestrial analogues due to the potentially high porosity or other characteristics, then long anchors with deep insertions may be necessary.

2.3 Water Ice Thermal Drilling

To avoid the complexity and reliability concerns with mechanical drilling systems, thermal drills are an appealing alternative. Thermal drills are used to bore holes or extract ice cores in terrestrial ices and are proposed for similar use in planetary conditions. Thermal drills are based on the core concept of using heat to change the phase of ice into either gas or liquid. Since liquid and gas are mobile forms of water, they will accelerate towards regions of lower pressure. This pressure differential can either be an inherent consequence of a vacuum-pressure atmosphere alongside the increased volume of gaseous water or else be caused by physically pushing the gas and liquid out of the way using the thermal drill. Pushing forces can come from either gravity or actuation. Both means of removing gas and liquid from the path of the thermal drill will allow it to progress farther into the ice, although only

the latter is seen with terrestrial versions of thermal drills given the presence of a substantial atmosphere.

Thermal drills for planetary use are frequently gravity-driven devices that target long duration steady-state operating modes. All that is required for their operation is a steady supply of heat distributed across the edges in contact with the ice, which makes them relatively simple when compared to their mechanical counterparts.

Given the low weight of landers and rovers on Europa due to its low gravity, applying the relatively high insertion forces required by mechanical drilling systems can be difficult. This is one of the benefits of thermal drilling systems, which are usable with small applied insertion forces. However, even with thermal drills, high insertion forces are generally desirable since they are associated with increased thermal drilling velocities and efficiencies [27].

The thermodynamic theory of steady-state thermal drills is dependent upon which phase transition that is dominant. Thermal drills at the surface of Europa are exposed to the surrounding vacuum and generally result in sublimation while thermal drills that operate below the surface are expected to seal off from the surrounding vacuum and result in melting.

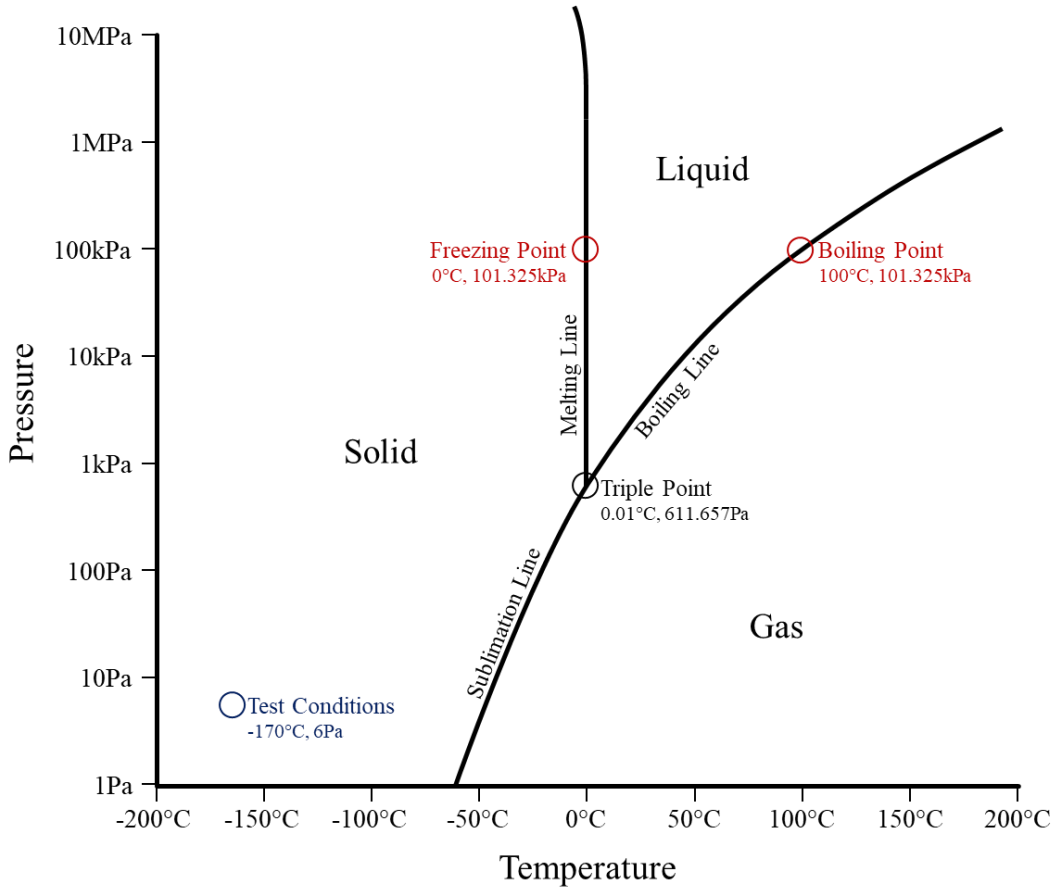

Figure 1: Water ice phase diagram. A description of the test conditions can be found in Section 4.2.

The water ice phase diagram in Figure 1 shows the pressure and temperature at which phase changes will occur. The triple point marks the pressure and temperature at which all three phases of water can exist simultaneously. Only the solid and gaseous states are observed below the triple point pressure (611.657 Pa).

Sublimation is the phase transition where solid water ice bypasses the liquid phase and changes directly into a gas, which is what occurs with water at the vacuum-pressure on the surface of Europa. Sublimation occurs naturally to the highest energy water ice molecules on the surface [11] but the process can be accelerated by warming the ice to its sublimation temperature. Natural and accelerated sublimation

can be thought of as solid-to-gas variants of the more familiar evaporation and boiling processes, respectively. Accelerated sublimation is the basic mechanism by which sublimation-based thermal drilling operates, where a directed transfer of heat converts ice into gas, boring a hole. Sublimation thermal drilling requires supplying the energetic cost of both warming the ice to its sublimation temperature and then changing its phase from solid to gas.

The energy costs of sublimation are dependent upon temperature and pressure at the ice surface and are made of the two distinct processes of warming and phase change. Warming from the ambient temperature requires approximately 180 kJ/kg to 250 kJ/kg and the latent heat of sublimation is approximately 2835 kJ/kg to change the phase of the ice into gas.

Melting is the phase transition of solid into liquid and is the familiar process that occurs when ice is warmed to its melting temperature at pressures above the triple point. While this process is ubiquitous on Earth, it does not naturally occur on the surface of Europa. The tenuous atmosphere means that melting on the surface can only be found when a region of increased local pressure is created. The melting temperature for water is approximately 0 °C (except under extreme pressure) and is hotter than the highest sublimation temperature. Warming from the ambient cryogenic temperature to the melting point takes approximately 250 kJ/kg, while the latent heat of fusion is approximately 334 kJ/kg to change the phase of ice into liquid. The large discrepancy of the required phase change energy between melting (334 kJ/kg) and sublimating (2835 kJ/kg) makes melting-based thermal drilling theoretically more energy efficient.

Both thermal drilling approaches require the surface ice to increase in temperature before it can change phase and be removed from the path of the thermal drill. The pocket of ice that has warmed prior to changing phase will necessarily form a thermal gradient within the ice relative to the cryogenic surroundings. This thermal gradient causes heat to be conductively lost. Models for these conductive losses were developed for thermal drills in terrestrial ices [28] and have been expanded upon to account for subsurface probe geometry [27] [29]. These conductive losses are proportional to the temperature differential of the warmed ices relative to the surroundings.

Conductive loss is the primary driver of the total energy and instantaneous power required for gravity-driven thermal drills, which are the primary issues identified with their use. While the total energy required for thermal drilling in cryogenic water ice is substantial, even a small power generator can produce a large amount of energy if given enough time. However, gravity-driven thermal drills operate in steady-state and require a relatively consistent application of power to their heaters. This is problematic because power generation is limited on and below the surface of Europa. Even if a multi-mission radioisotope thermal generator (MMRTG) by itself were used as a thermal drill, it would not produce enough power to overcome conduction loss and melt through cryogenic water ice [30].

Photovoltaic power generation has limited applicability on Europa due to the low light intensity in the Jovian region of the solar system and is not suitable for subsurface missions unless a tether is used to transfer power. Radioisotope power generators provide consistent power but are costly and often massive devices. This

has led to the conclusion that long-range steady-state subsurface thermal drilling probes are not feasible with current technology [31].

Sediment build-up at the drill-ice interface is another issue that can prevent the use of thermal drills [32] [33]. However, since sediment build-up occurs proportionally with distance travelled, it is a major concern for long-range drilling systems but is not pertinent to the short-range thermal drilling and anchoring described in this work.

2.4 Sublimation-Based Water Ice Thermal Drilling

Sublimation-based systems have been studied using various ices at simulated Europa surface conditions [34]. They have demonstrated that the introduction of heat to the thermal drill head will slowly remove the surface ices. The velocity and efficiency are relatively low for these systems, which is problematic for long-range operation. The low efficiency and velocity of operation is primarily driven by the conductive heat loss into the surrounding cryogenic ice. The efficiency of sublimation-based thermal drills is a topic of continued work and different drill heads are studied to determine which leading edge shapes provide the optimal distribution of heat for efficient operation [35].

An issue with the use of long-range sublimation systems is the concentration of sediment at the melting head, which can halt progress if the sediment layer reaches a thickness that sufficiently impedes heat transfer into the ices below. Given that salts are present on Europa [15], this is potentially problematic. To overcome the deposition of sediment at the leading edge, a combined mechanical-thermal system was proposed and tested [33] [36]. It was determined by Weiss that the introduction

of a mechanical drilling system reduced the reliability of their device due to the moving parts that were necessarily introduced. However, the testing of the IceMole showed that a combined thermal-mechanical approach can work in glacial terrestrial ices with successful dirt layer penetration [36].

Sublimation-based insertion has also been proposed to provide sampling probes with access to subsurface ice [37] where a melting regime would be selectively targeted to retrieve liquid water samples. For these short-range systems, the buildup of sediment will be limited.

Even with sublimation-based thermal drills, it has been observed that melting will occur selectively and intermittently across the heated surface in contact with the ice [34]. This was observed indirectly as periods of increased heat transfer between the thermal drill and the ice, which is due to the thermal contact provided by liquid water. This suggests that the local pressure due to sublimation can briefly rise above the triple point even for steady-state operation of a sublimation device. The intermittent thermal drilling approaches discussed in this work draw on and leverage this type of local pressure buildup.

2.5 Melting-Based Water Ice Thermal Drilling

Despite their many similarities, thermal drills operating in the melting regime are fundamentally different from those which operate in the sublimation regime.

Many advanced melting probes have been designed to operate at terrestrial pressures and temperatures [36] [38]. Under these operating conditions, the melting probe becomes immersed in liquid water shortly after thermal drilling begins. Probes designed for use in water ice on Mars would also naturally trigger the melting regime

[39] due to the ambient pressure being slightly above the triple point of water. These systems can potentially be adapted to use on the icy moons with vacuum-pressure surface conditions, but they will not observe pure melting without alteration.

Melting probes operating in vacuum require some mechanism to ensure that the local pressure rises to and stays above the triple point so that liquids can be sustained. The most frequently proposed means of achieving sustained pressures is through sealing of the borehole using re-freezing water [27] [40] [41]. Any liquid meltwater that is produced as a result of thermal drilling when exposed to a vacuum is unstable and can freeze when in contact with the surrounding cryogenic ice or due to pressure-induced re-freezing. It has also been suggested that melting can be achieved through a tip-sealing mechanism with an internal flowpath, allowing for meltwater sample collection [37] [42].

Melting requires significantly less energy for its phase transition than sublimation, and meltwater is capable of rapidly transferring heat between the drill and ice, both of which increase the maximum achievable velocity for a given drill geometry and power supply. However, the excellent heat transfer properties of a meltwater layer can also be a disadvantage. Probes that operate in steady-state and are completely immersed in meltwater experience conductive cooling caused by the surrounding cryogenic ice. If the meltwater is allowed to freeze then it can bind the thermal drill within the ice and halt thermal drilling [41]. This binding can be solved by distributed heating of the walls of the probe, preventing meltwater layer surrounding the probe from freezing.

The minimum power to maintain the wall temperature of a subsurface thermal drill against the surrounding cryogenic ambient temperature is based on the size and shape of the drill but is substantial and constant. However, progress made from thermal drilling into the ice is variable and a function of heater power output. Progress can only be made with heater powers above what is necessary to keep the walls of the probe warm, but additional power output above this threshold primarily accelerates the thermal drilling process. This inherently couples the efficiency of operation to the power output of the melting probe. The thermodynamics of subsurface melting probes has been modeled [27] and tested. However, even a melting probe with a power output of 600 W designed for use in cryogenic ices is predicted to have efficiencies on the order of 5% based on extrapolation of experimental testing [41].

A tethered thermal drill is one whose power supply is external. A cable connecting the subsurface thermal drill to a power supply on the surface permits the transfer of energy. Smaller thermal drill profiles require less power to drill through the ice and off-boarding the power supply represents a significant size reduction. The cabling also permits communications to pass from the subsurface probe, which would not otherwise be possible when underneath a thick sheet of ice. However, this approach requires a cabling system that either releases cable from the surface or is stored and released from within the probe itself. Cabling that is released from the surface must be heated to prevent binding by re-freezing meltwater, which represents yet another large energy expenditure that scales with length. Cabling that is released from the thermal drill itself increases the size and complexity of the thermal drill, but

the cabling no longer needs to be heated. A cabling system that is released from within the thermal drill itself was designed in a combined thermal-mechanical system called the Search for Life Using Submersible Heated (SLUSH) drill [43].

A tethered thermal drill with a 600 W heater powered by an external source through cabling released from the surface was prototyped and tested [40]. This system demonstrated that binding due to freeze-in could be prevented with distributed heating but that sealing of the borehole was not sustained. Short periods of binding by re-freezing water were observed and the thermal drilling naturally cycles between melting and sublimation.

2.6 Dry Ice Sublimation

Carbon dioxide ice was used in this work because it presented an avenue for atmospheric pressure sublimation testing due to its high triple point pressure (517 kPa). This property of sublimating rather than melting at atmospheric pressure leads to its nickname “dry ice”.

The phenomena demonstrated with dry ice are of vital importance to any thermal drill operating where the ambient pressure is below the triple point of the ice being drilled. The increase in specific volume of carbon dioxide during its phase transition creates a gas barrier that reduces the effective friction between a warmed object and the dry ice and can even lead to levitation. This is known as the Leidenfrost effect [44] or the inverse Leidenfrost effect [45] depending on the orientation of the warmed object and boiling (or sublimating) object. This has led to the development of a sublimation-based engine for use with dry ice [46]. These phenomena have major implications for sublimation-based thermal drills.

Since water ice is the primary focus of this study, the thermal differences between sublimating dry ice and water ice are quantified. The characteristics pertinent to the sublimation process are the density, temperature, and latent heat of sublimation. The dry ice used in testing had a measured average density of approximately 1350 kg/m^3, while the latent heat of sublimation is 571 kJ/kg. On the other hand, the density of water ice is 917 kg/m^3, while the latent heat of sublimation is 2835 kJ/kg. The resulting volumetric sublimation energy required for dry ice is 30% relative to water ice. There are also mechanical differences between dry ice and water ice, but they have not been quantified. However, the cutting of dry ice has been studied and its specific cutting energy is half that of cryogenic water ice [22].

While water ice is below its sublimation temperature on the icy moons, dry ice created on Earth is often at its sublimation temperature and actively sublimating due the ambient temperature being relatively warm. Subcooling of the dry ice below its sublimation temperature was achieved in this study in limited cases using liquid nitrogen.

2.7 Triple Point Thermodynamic Modeling

The physics of a liquid flow reaching the triple point is the focus of current study. Carbon dioxide has a high triple point pressure of 517 kPa but is often stored above this pressure in its liquid state. When liquid carbon dioxide is vented from high to low pressure then it undergoes a transient thermodynamic process that includes passing through the triple point. It is at the triple point that solid carbon dioxide is created and that process has been modeled and experimentally tested [47] [48].

However, these studies are specific to their application and a general model for triple point thermodynamic simulation has not yet been developed.

Chapter 3: Sublimation-Based Thermal Drilling in Dry Ice

3.1 Experimental Setup

Two separate test rigs were developed to assess the sublimation characteristics of a range of prototype thermal picks. The first test rig used linear motion and weights to produce a force-controlled insertion. The second test rig used a "corkscrew" motion (coupled linear and rotational) with a lead screw and a stepper motor that produced a tapping position-controlled insertion.

3.1.1 Linear Test Rig

The linear test rig as seen in Figure 2 used two linear sleeve bearings supported by a frame, a driving rod, and a weighted plate that applied the insertion force. The thermal pick was connected to the driving rod with a G-10 coupling and was inserted linearly into the ice. This linear rig allowed for a weighted force-controlled insertion into the ice but could also be manually controlled. Manual control of the test rig provided useful tactile, visual, and auditory feedback during the sublimation process, which allowed for a more thorough investigation of the sublimation phenomena. The linear test rig was used to test all cylindrical profile thermal picks (a) through (e), but not the screw-type thermal pick (f).

Table 1: Thermal picks used in dry ice experimental testing. All thermal picks were built to a length of 63.5mm to accommodate an insertion distance of 50.8mm.

	Diam.	Tip Shape	Material	Misc.
a	6.35 mm	Flat	Tellurium Copper (Cu 145)	
b	6.35 mm	45° Conical	Cu 145	
c	6.35 mm	45° Inverse Conical	Cu 145	
d	12.7 mm	Flat	Cu 145	
e	12.7 mm	Flat	Cu 145 and Titanium (Ti-6Al-V4)	3.18 mm thick titanium walls
f	12 mm	Flat	Aluminum (EN-AW6060)	Threads have 3 mm pitch and 2 mm depth

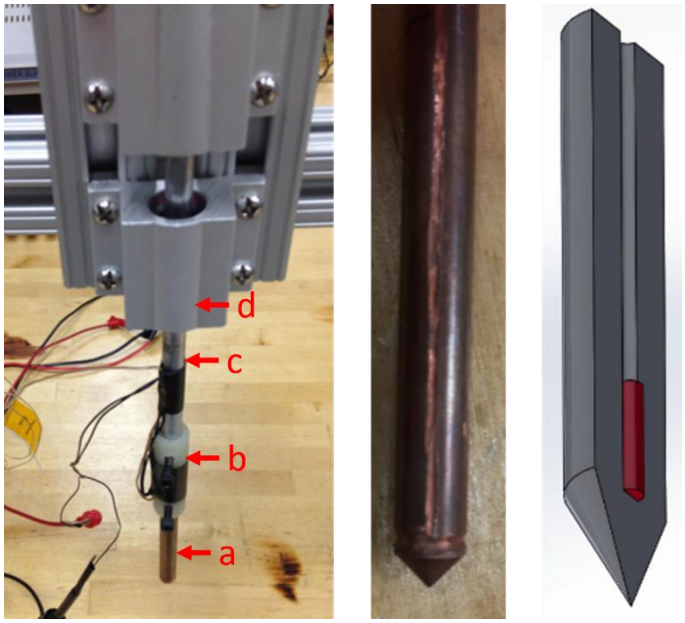

Figure 2: Linear test rig and thermal pick (b). Shown left is the linear test rig with a) thermal pick, b) G-10 thermally insulating coupling, c) driving rod, and d) sleeve bearings. Shown center is the conical pick with pressure relieving grooves. Shown right is the conical pick model cross-cut revealing the embedded heater placement in red.

3.1.1.1 Sleeve Bearings

The two linear sleeve bearings had internal ball bearings that allowed for linear motion and rotation of the driving rod with minimal friction. The two sleeve

bearings were separated by a small gap to reduce driving rod play. With only one sleeve bearing, the driving rod would bind when subjected to off-axial forces on the driving rod. This issue was resolved by the addition of the second sleeve bearing.

3.1.1.2 Driving Rod

The driving rod made of 6.35 mm diameter stock aluminum 6061 was chosen so that the 6.35 mm diameter thermal picks could be attached to the driving rod using a simple coupling tube (the G-10 coupling). The length of this rod sticking out beneath the linear sleeve bearing proved to be problematic. Because of its length, the lateral forces that were incurred during insertion of the thermal pick would cause the driving rod to bend significantly. This caused the thermal pick path to deviate from the desired path. This phenomenon led lateral forces to result in thermal pick path deviation and is described in Section 3.2.2.

To allow insertion depths of over 50 mm and because of the position of the dry ice blocks beneath the test rig, the length of the exposed driving rod could not be substantially reduced. To minimize the bending of the driving rod, test runs were started with the minimum possible exposed driving rod length, but the driving rod was still prone to bending. This drove future test rig design towards the use of components with increased structural rigidity.

3.1.1.3 G-10 Coupling

The G-10 coupling was used to thermally insulate the thermal pick from the driving rod. G-10 has a low thermal conductivity of 0.288 W/m-k and its modulus of elasticity of 7 GPa to 20 GPa makes it relatively stiff, which allowed it to simultaneously serve as a structural member and thermal insulation. Early testing

used an aluminum coupling, but the driving rod would heat up to nearly the same temperature as the thermal pick. After the G-10 coupling was implemented, the temperature of the driving rod was unaffected by testing, indicating that conduction-based losses had been substantially diminished. To make the system adaptable to switching between multiple thermal pick styles, the G-10 coupling was outfitted with two set screws to secure it to the driving rod and thermal pick.

3.1.1.4 Aluminum Frame

The frame of the linear test rig was made of aluminum 80-20, which allowed for rapid construction of the test rig and the use of various dry ice block sizes.

3.1.1.5 Thermal Picks (a), (b), and (c)

The thermal picks (a), (b), and (c) were the first to be designed and tested and are shown in Figure 3. They were made of tellurium copper for its machinability and high thermal conductivity (355 W/m-K). Machinability was a critical feature because of the tight tolerances of the hole for the embedded cartridge heater.

These thermal picks were 63.5 mm long and had three different tip designs. The flat tipped thermal pick (a) was designed as the baseline system against which others could be compared. The 45° conical tip (b) was designed to encourage flow of escaping gas out and around the thermal pick. The 45° inverse conical tip (c) was designed to examine the effect of discouraging the flow of escaping gas during sublimation.

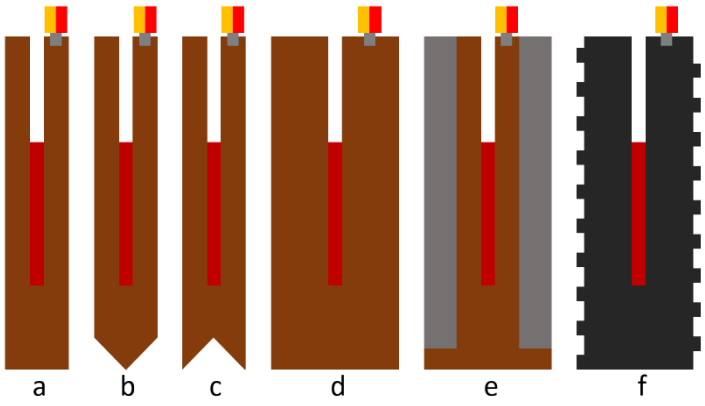

Figure 3: Illustrations of thermal picks (a) through (f). Colors represent copper (light brown), titanium (gray), aluminum (dark gray), cartridge heater (red), and thermocouple (red/yellow/gray).

3.1.1.6 Thermal Pick (d)

Thermal pick (d) was designed to be compared to thermal pick (a). It was the same design but with a larger diameter. The scalability of the thermal picks is a primary concern since a Europa rover has not yet been designed and meter-scale Europan surface ice characteristics are not yet known. While thermal picks with larger profiles require additional energy to insert into the ice, it may be necessary to use large thermal picks when working with weak ices.

The same 30 W cartridge heater was used regardless of thermal pick size. With a larger thermal pick, the rate of warming when exposed to 30 W was relatively reduced, while the rate of cooling during thermal drilling remained relatively unchanged due to the proportional increase of tip surface area.

3.1.1.7 Thermal Pick (e)

Thermal pick (e) was designed to be compared to thermal pick (d). As the sublimated gas escaped between the thermal pick and borehole walls, heat was transferred. This heat transfer was undesirable and so thermal pick (e) was designed with a thermally insulating material on its outer surface, except near the tip. This

insulated the outer surface of the thermal pick from the copper core, limiting the amount of heat lost through the walls without inhibiting the central heat flow path between the heater and tip.

Titanium 6Al-V4 was chosen as the outer wall material due to its combination of high strength of 828 MPa and relatively low thermal conductivity of 6.6 W/m-K. After insertion, thermal picks need to be used as load bearing anchors at potentially cryogenic temperatures, which precluded the use of insulating materials that have low yield strength, or that become brittle when cooled. The titanium did not extend to the leading edge of the thermal pick because the leading edge was an active surface for thermal drilling and required uninhibited heat flow.

3.1.1.8 Embedded Cartridge Heater

Cartridge heaters were selected for their high power density and because they had been used in previous works [32] [39] [49]. Cartridge heaters have a coiled resistive wire surrounded by densely packed magnesium oxide powder. Magnesium oxide powder that has been pressurized is thermally conductive and electrically resistive, which is an uncommon pairing of material characteristics. This allowed the resistive wire of the cartridge heater to be coiled densely for high power density and simultaneously avoided overheating.

The other competitive option for heating the thermal picks was thin film heaters, which had also been used in previous works [34] [37]. Thin film heaters have a relatively low areal power density but were otherwise suitable. Subsurface thermal drills often have a large radius and are not subjected to significant mechanical stresses, permitting relatively thin conductive layers and thin film heaters. However,

thermal picks were mechanically stressed during anchoring and were ideally small in profile to minimize energy cost. This made thin film heaters impractical for thermal picks.

While cartridge heaters are known to have an unequal distribution of heat across their surfaces, our modeling assumed they were isothermal. This assumption is reasonable due to the surrounding copper, which rapidly distributed the heat produced by the cartridge heater.

The cartridge heaters operated at a maximum of 30 W at 24V-DC and had a radius of 3.2 mm and a length of 25.4 mm. They were also used at voltages below their rated maximum to reduce the heater power output. They were procured from Heaters Controls & Sensors.

3.1.1.9 Thermal Paste

Thermal paste was used to create a conduction path between the embedded cartridge heater and the copper thermal pick body. The hole drilled into the thermal pick was made large enough to allow insertion of the cartridge heater, but this created gaps between the two that prevented conductive heat transfer except at the points of contact. Off-the-shelf thermal paste is a conductive filler that was used to improve heater-to-pick conduction. “Arctic Silver” thermal paste was used and has a thermal conductivity of 8.9 W/m-K and a maximum operating temperature of 130 °C. While this thermal conductivity is very low relative to copper, it did not significantly inhibit thermal conduction when only thin layers were used. The maximum operating temperature was the limiting factor that set the upper bound of the thermal pick temperatures used.

3.1.1.10 Thermocouple

Temperature measurements were taken using a K-type thermocouple. The thermocouple wires were attached on the surface opposite from the leading edge as seen in Figure 3. This was because placement of the thermocouple on surfaces closer to the leading edge would have exposed it either to ice or to sublimated gas and would have registered as erroneously cold or caused it to be physically damaged. This placement created a small thermal lag in the system where heating by the cartridge heater and cooling due to thermal drilling took a short time before it was registered by the thermocouple.

3.1.1.11 Arduino and Electronics

The Arduino board was used to control the heater and track the temperature of the thermal pick. The thermocouple temperature was read in as an analog voltage coming from the thermocouple that was amplified with a MAX31850K breakout board.

The Arduino was also manually commanded to turn the heater on and off, which was achieved by opening and closing the circuit between the power supply and cartridge heater with a 10 A DC relay.

3.1.1.12 Power Supply

The DC power supply for the cartridge heater was rated to 10 A and had a variable voltage setting. When the power supply was set to 24 V, approximately 30 W of thermal power was output by the cartridge heater. The power supply was also run at 20.8 V, and 17 V, changing the heater power output to 22.5 W (75% capacity) and 15 W (50% capacity), respectively.

3.1.2 Rotary Test Rig

The rotary test rig in Figure 4 was a partially automated system that controlled the temperature and position of the thermal pick. It had a stepper motor that rotated a lead screw that followed a prescribed path set by the lead screw nut, resulting in a coupled linear-rotational motion. The thermal pick was attached to the lead screw through the G-10 coupling. The discrete steps taken by the stepper motor resulted in a rapid stepwise linear progression of the thermal pick.

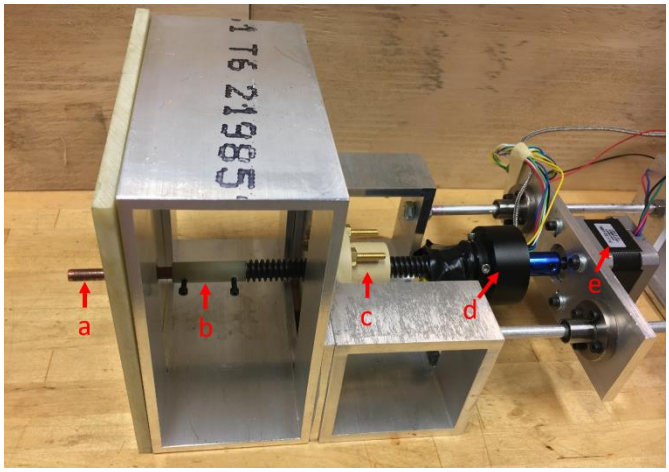

Figure 4: Rotary test rig with a) thermal pick, b) G-10 thermal insulation, c) lead screw nut, d) slip ring, and e) motor.

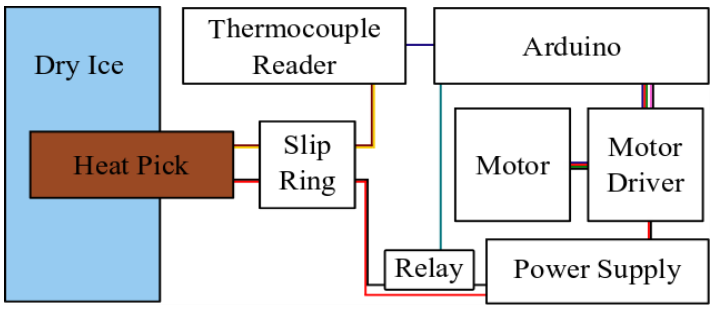

Figure 5: Rotary test rig schematic showing the system's major electronic components.

When the rotary test rig was used with a screw-type thermal pick that had a pitch (distance between each thread) matching that of the test rig's lead screw, the

thermal pick would only contact the dry ice surface at the leading edge of the thermal pick, not along its threading. The lack of contact between the thermal pick's threading and the ice meant that the ice borehole would have an internal threading pattern as seen in Figure 6. The pitch of the lead screw and nut determined the coupling of the linear-rotational "corkscrew" motion.

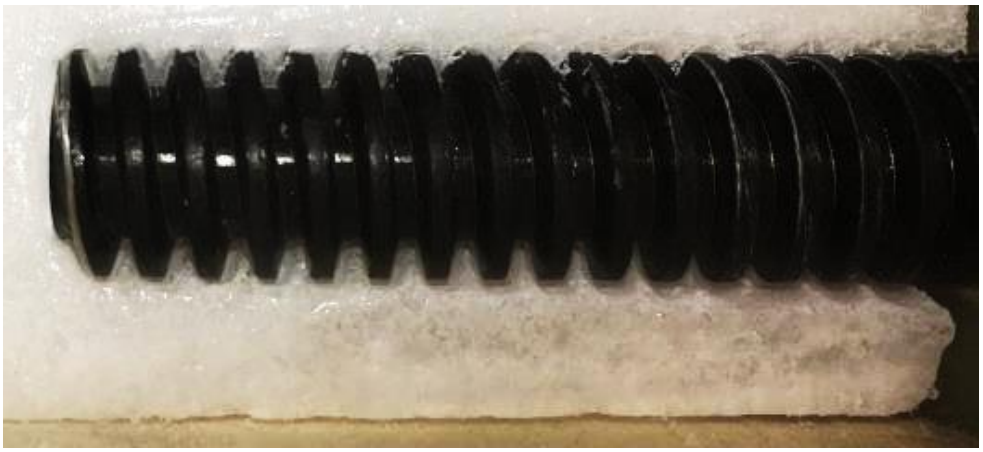

Figure 6: Cross cut of threaded ice borehole and thermal pick (f). Thread quality degrades towards the surface of the ice due to thermal erosion.

Thermal picks (a) through (e) had a cylindrical profile and when used with the rotary test rig would rotate as they progressed linearly into the ice. The rotation of these cylindrically symmetrical picks did not cause any observed differences relative to the linear test rig results. The entire set of thermal picks (a) through (f) were tested on the rotary test rig.

The test rig was controlled by an Arduino MEGA and its associated electronic components. The relay, motor micro-controller, thermocouple amplifier, heater power supply, and motor power supply were all controlled by the Arduino board.

The screw-type thermal pick was distinct from the other thermal picks in that it was an anchor that could not be pulled linearly out of the ice after insertion. Since

the dry ice studies were focused on the thermal behavior of the thermal picks and not their load bearing capabilities, this difference was not pertinent to the reported results.

The embedded cartridge heaters, thermocouples, G-10 coupling, thermocouple amplifier, power supply, relay, and Arduino were unchanged from their descriptions in Section 3.1.1.

3.1.2.1 Stepper Motor

The stepper motor provided the mechanical means of insertion for the rotary test rig, replacing the function of the weights used in the linear test rig. While the linear test rig enabled direct control over the insertion force, the stepper motor could not provide this capability. The stepper motor provided discrete short rotary motions of high torque, which resulted in brief high-force movements of the thermal pick that appeared as a rapid “tapping” type insertion. The pace of insertion could be controlled, but not the force applied between the thermal pick and the ice.

Limited control over the quality of the thermal contact between the thermal pick and ice was achieved by adjusting the pace of insertion. The commanded velocity was controlled by setting the number of steps per unit time and caused the leading edge of the thermal pick to tap against the bottom of the ice borehole with a frequency corresponding to the velocity. Higher commanded velocities improved the thermal contact between the leading edge of the thermal pick and bottom of the ice borehole. This behavior is modeled in Section 3.4.

3.1.2.2 Stepper Motor Driver

The stepper motor driver was the only component of the electrical system that was not used in the linear test rig. The stepper motor driver was a chip that took a set

of command inputs from the Arduino, drew power from the motor power supply, and provided a precise current profile to the stepper motor. This was necessary because the stepper motor required a series of rapidly changing currents to take steps, and the stepper motor driver was designed to produce that tailored current profile.

3.1.2.3 Brace Plate

The brace plate blocked the stepper motor from freely rotating, which caused it to pass the produced torques into the lead screw. It was rigidly attached to the motor and to two linear sleeve bearings running along the two rods of the test rig frame. This setup allowed frictionless linear motion of the brace plate in the direction of insertion, but prevented the motor from spinning.

3.1.2.4 Driving Lead Screw, Nut, and Motor Coupling

The driving lead screw and nut had a pitch of 3mm and were used to couple the linear and rotational motion of the thermal pick. The driving lead screw was rotated by the stepper motor and this rotation caused linear displacement through screw-nut contact. This actuation system permitted the proper use of the screw-type thermal pick, which would otherwise produce an unthreaded ice borehole. The motor coupling was used to rigidly connect the output shaft of the stepper motor to the driving lead screw so that torque could be transferred.

Since the pitch of the lead screw and nut was small, internal friction made the system not backdrivable. This meant that any axial force applied to the system would be blocked and not result in motion, so any position changes made by the stepper motor were held unless an external torque was applied. As a result, pressures developed during sublimation did not reverse progress made by the thermal pick.

3.1.2.5 Slip Ring

Since the pitch of the driving lead screw was 3mm and the insertion distance of the thermal pick was 50.8 mm, the thermal pick rotated approximately 17 times per insertion and extraction. Without a slip ring, this would have resulted in the twisting of wires. The slip ring was a model MT007-S08 (Z2097) and was purchased from Moflon Technology Co., Limited. It provided six 2 A connections and two K-type thermocouple connections. Two of the 2 A connections were used for passing current to the cartridge heaters. Since thermocouples use dissimlar metal junctions to develop voltages, the K-type thermocouple connections were made of nickel-chromium and nickel-alumel and would not otherwise be usable for temperature readings.

3.1.2.6 Thermal Pick (f)

Thermal pick (f) was designed to become locked within the ice after insertion by the threaded borehole that it cut according to its screw shape. It was aluminum with a trapezoidal thread profile and a pitch of 3 mm. It had an outer diameter of 12 mm (outer edge of the threads) and an inner diameter of 8 mm (diameter of the solid unthreaded core). Since copper lead screws were not available off-the-shelf, aluminum was selected for its relatively high thermal conductivity of 200 W/m-K.

3.1.2.7 Stabilizing Sheet

In early testing, a small cyclic lateral deviation of thermal picks was caused by the mating of the driving lead screw and nut. As the lead screw was rotated and driven linearly by the nut, the contact points between the lead screw and nut would shift due to slight misalignments. This was corrected through the use of the G-10 stabilizing sheet.

The G-10 sheet was cut with holes specifically sized for the diameters of the various thermal picks. The thermal picks fit into their appropriately sized holes tightly enough that the G-10 sheet physically restricted lateral motion of the thermal pick. The use of this sheet resulted in some limited additional friction and conductive heat transfer between the sheet and the thermal pick.

3.1.2.8 Aluminum Frame

The frame used a combination of stock and custom machined pieces of aluminum 6061. The square tubes that made up the body of the frame provided structural rigidity and tight machining tolerances, ensuring alignment of the test rig. Two 6.35 mm rods prescribed the motion of the linear sleeve bearings of the brace plate. Using relatively thin rods allowed for some limited bending, which eased the constraints on the alignment between the aluminum rods and the driving lead screw.

3.1.3 Dry Ice Mounts

Given the substantial forces that developed through the sublimation process as gas pressure would build between the thermal pick and ice, mounting was required to hold the dry ice test specimen in place. The custom mounts held the dry ice through a distributed loading schemes that avoided cracking the ice.

For the linear test rig with vertical insertion and therefore primarily vertical forces, taut ropes strung over the ice block adequately secured it to the laboratory testing table and provide stability. In the rotary test rig, the thermal pick with horizontal insertion and primarily horizontal forces meant that a more substantial approach was needed. Two 12.7 mm thick plywood planks were used to sandwich the dry ice block, and a ratchet strap was used to provide the compressive force necessary

to secure the dry ice within. Dry ice blocks would occasionally break under the compressive load of the clamping mechanism, but this was mitigated by shaping the ice surface prior to use so that it conformed to the flat mounting surfaces.

3.1.4 Test Procedure

In designing the test procedure, two distinct approaches were considered. The first was to determine the energy and time required for the insertion of a thermal pick into the ice based on a set of initial conditions and operating conditions. The second was to determine the energy and time required for the insertion of a thermal pick into the ice as well as the energy and time to return to the initial temperature condition.

In practice, a thermal pick would have no reason to return to its initial temperature condition. This made the first approach the best at simulating the intended use of the system, but thermal drills could not readily be compared if this method were used. Thermal drilling by the first approach would cost an amount of energy specific to the mass and material characteristics of the thermal pick since the temperature of the thermal pick changed during use. By using the second approach and ending each test at a temperature matching its initial condition, energy balance could be used to directly solve for the energy cost of the sublimation-based thermal drilling process.

Completing a full thermal cycle involved starting the sublimation process at a target temperature, performing the sublimation action, and then returning to the target temperature. This full cycle (2-3-4-2) negated the impact of the thermal capacity of the thermal pick. The three thermodynamic processes of the test procedure occurred as follows.

Pre-Cycle

State 1: The thermal pick is below the target temperature.

Process (1-2): Heating up to the target temperature.

Thermodynamic Cycle

State 2: The thermal pick is at the target temperature.

Process (2-3): Thermal drilling into the ice with a constant target temperature.

State 3: The thermal pick is below the target temperature within the borehole.

Process (3-4): Removal from ice and settling of the thermal gradient.

State 4: The thermal pick is below the target temperature outside the borehole.

Process: (4-2): Heating back up to the target temperature.

The target temperature was chosen prior to each test run and was used for the entire duration of any one test. While this temperature was the target for the heater to maintain, the actual temperature measured by the thermocouple was often significantly lower. This was due to the rapid cooling that occurs when in contact with cryogenic ice.

3.1.4.1 Linear Test Rig Procedure

While using the linear test rig, the target temperature was representative only of the initial and final temperatures for a test since the heater was kept constantly on until the end of the test. For target temperatures below room temperature, the thermal pick was cooled using spare dry ice to below the target temperature, then the heater would be turned on to raise the thermal pick to the target temperature. The thermal drilling process would then be started by initiating contact between the thermal pick and the ice as soon as the thermocouple registered that the target temperature had

been reached (state 2). Thermal drilling continued until the target depth of 50.8 mm was reached (state 3) after which the thermal pick was removed from the ice (state 4). Once the thermal pick returned to its target temperature (state 2) the heater was turned off and the timing of events were recorded.

The start and end of the total process time (t_p) was marked by the thermal pick reaching its target temperature (state 2) and the timing was recorded by the Arduino microcontroller. The heater time (t_h) was equivalent to the total process time only in the linear test rig because the heater was always on during the test. The insertion time (t_i) of process (2-3) was recorded in the same manner.

3.1.4.2 Rotary Test Rig Procedure

The switch from the linear test rig to the rotary test rig came with automated control over the thermal pick. Heating up to the target temperature (1-2) was followed by an automated initiation of the insertion process and the timing of events was automatically recorded. The stepper motor was commanded to progress at a specified rate of speed until a manual command was issued indicating that the target depth had been reached (state 3). After this command was received, the Arduino microcontroller would automatically quickly extract the thermal pick from the ice (3-4). The heater would then warm the thermal pick back up to the target temperature (4-2) at which point the test was concluded.

Throughout the entirety of each test with the rotary test rig, thermostat control logic was applied, which cycled the heater around the target temperature. If the embedded thermocouple registered a temperature of 1 °C above or below the target temperature, the heater was turned off or on, respectively. The temperature

measurements and thermostat control were performed automatically by the Arduino microcontroller. Given the temperature swings due to thermal lag, a maximum operating temperature of 90 °C was conservatively used to ensure the thermal paste's maximum operating temperature of 130 °C was not violated.

The cycling of the heater meant that the total process time and the heater time (t_h) were no longer equivalent. The Arduino microcontroller would automatically log the duration that the heater was turned on within the test cycle (2-3-4-2).

3.1.5 Theoretical Analysis

The efficiency of the process is calculated as the ratio between the calculated ideal energy required for the sublimation of a perfect borehole (E_i) and the measured energy output by the heater (E_o).

$$\eta = {E_i}/{E_o} \tag{1}$$

Calculation of the ideal energy requires the minimum borehole volume (V), the density of the ice (ρ_{ice}), and the latent heat of sublimation (Δh_{sub}).

$$E_i = V \rho_{ice} \Delta h_{sub} \tag{2}$$

Assuming an average measured dry ice density of 1.35 g/ccm, the ideal energy costs for sublimation are approximately 5.05 kJ for thermal picks (d) and (e), 1.13 kJ to 1.26 kJ for thermal picks (a), (b), and (c), and 3.15 kJ for thermal pick (f).

Due to its variability, the density of each dry ice block was calculated prior to testing. A cylinder of ice was cut and its diameter, length, and weight were measured. The dry ice densities were consistent throughout a given block, but between blocks the densities ranged between 1.2 g/ccm and 1.45 g/ccm.

The heater energy output is calculated from the heater time (t_h) as recorded by the Arduino, the voltage applied to the cartridge heater by the power supply (V_h), and the measured resistance of the cartridge heater (R_h).

$$E_o = {t_h V_h^2}/{R_h} \tag{3}$$

The thermal losses (E_l) are defined as the difference between the output energy and the ideal energy.

$$E_l = E_o - E_i \tag{4}$$

While thermal losses are often a positive value, which indicates that heat is being lost by the thermal pick to the ambient environment by some means, it can also be a negative value. A negative value of thermal loss indicates that the thermal pick is below the ambient temperature and is therefore drawing heat from the ambient environment. Positive values cause the calculated thermal efficiency to be an underestimate of the actual efficiency while negative values cause thermal efficiency overestimates.

The values measured in testing are the thermal pick temperature, total process time (t_p), insertion time (t_i), heater time (t_h), commanded insertion rate of the stepper motor (rotary test rig only), and insertion force (linear test rig only).

The last phase of heating back up to the target temperature represents a large thermal expenditure since the thermal pick cooled to as low as -30 °C during thermal drilling. The energy required to warm the thermal pick is described by Equation (5) where (m_{pick}) is the mass of the thermal pick, ($c_{p,Cu}$) is the specific heat of copper, and (ΔT_{pick}) is the temperature difference involved.

$$E_{warm} = m_{pick}\, c_{p,Cu}\, \Delta T_{pick} \quad (5)$$

The masses of thermal picks (a), (b), and (c) were 14.5 g, the mass of thermal pick (d) was 58 g, and tellurium copper's specific heat is 385 J/kg-K. This corresponded to an energy of 0.67 kJ and 2.7 kJ required to warm the small and large picks, respectively, to their maximum target temperature of 90 °C from their minimum temperature of -30 °C.

The energy required to warm the thermal pick back to the target temperature is equivalent to the latent heat within the thermal pick that was expended during thermal drilling. Without the final warming phase (4-2), an insertion using only latent thermal pick heat without actively returning to the target temperature would appear to have an infinite efficiency by Equation (1).

A thermal pick that approximately maintains its target temperature throughout the duration of a test is undergoing a steady-state thermal process, but a thermal pick that drops in temperature is undergoing a transient thermal process. The transient sublimation processes that were observed were inserted at higher rates as a result of this additional energy expenditure. The use of latent heat is most clearly demonstrated through the insertion of a thermal pick without any active heating. By comparing Equations (2) and (5) it can be calculated that when cooling from 90 °C to -30 °C against the ice, a thermal pick will have expended enough energy to thermally drill approximately 25 mm into the ice without the use of a heater, which was experimentally confirmed.

3.2 Observed Phenomena

The following sections are descriptions of phenomena that were observed during the sublimation process. Since dry ice testing was used primarily as a precursor to water ice testing in a cryogenic vacuum environment, a phenomenological study was the primary focus of this work. The most immediately observable effects of the sublimation process are the normally directed "pushback" force and low surface friction, both of which result from the rapid creation of gaseous carbon dioxide.

3.2.1 Pushback Force

The pushback force observed in these experiments is a variant of the Leidenfrost effect [45]. The thin-film boiling that occurs between a liquid and a hot surface, first noticed by Leidenfrost in 1756 [44], is known to create a local pressure sufficient to levitate droplets of water. A critical temperature was observed by Leidenfrost, below which water droplets would fall into contact with the hot surface and above which water droplets would levitate. This critical temperature is between 150 °C and 210 °C for water droplets. The Leidenfrost effect is caused by heat transferring into the water droplet through a thin gaseous region, which boils the water droplet and sustains the thin gaseous region. If the heat transfer in this manner is insufficient to support the thin gaseous layer, then the water droplet will fall into contact with the heated surface. The counterintuitive aspect of the Leidenfrost effect is that it has an insulating effect, causing a reduction in the rate of boiling of the water droplet. This is because the convective heat transfer that occurs through the thin

gaseous layer is slower than the conductive heat transfer that would occur if the water droplet were in physical contact with the heated surface. There is a critical temperature for the hot surface, above which the Leidenfrost effect will occur, but this temperature is dependent on the materials, ambient conditions, and other factors. The Leidenfrost effect is also observed in sublimating ice (most commonly dry ice) levitating above a relatively hot surface.

The inverted Leidenfrost effect is a variant of the Leidenfrost effect where the boiling or sublimating material is below a hot object that is levitated. The fundamental concept remains the same in that if there is a sufficient temperature differential, a thin gaseous layer can be sustained that supports levitation. The Leidenfrost effect in dry ice has even led to the study of sublimation engines [46].

The size of a water droplet impacts its ability to levitate through the Leidenfrost effect [45]. This is because of the relative scaling of the surface area and weight of the water droplets considered. When the forces pulling the two bodies together can overcome the Leidenfrost levitation force then contact will form and conductive heat transfer becomes dominant.

Within the context of a thermal pick, levitation has the effect of impeding progress and insulating the ice from the thermal pick. Just as heat transfer between a hot surface and water droplets is reduced when a gaseous layer forms between them, heat transfer between a thermal pick and the ice is reduced when a gaseous layer separates them. The width of the gaseous layer depends upon the temperature differential between the thermal pick and the ice as well as the force pressing the thermal pick into the dry ice.

The dependence of the force required to overcome Leidenfrost levitation on pick temperature created a positive feedback loop. If the forces pressing the thermal pick into the ice are sufficient to overcome levitation, then heat efficiently transfers into the ice and cools the thermal pick. Since a cold thermal pick requires relatively smaller forces to overcome levitation, heat transfer efficiency continually increases, further cooling the thermal pick. Conversely, if the forces pressing the thermal pick into the ice are insufficient to overcome levitation, then heat inefficiently transfers into the ice. This inefficient heat transfer into the ice would cause runaway heating without using thermostat control logic.

The critical force has a strong dependence on tip shape and pick-to-ice temperature differential. Since the thermal pick-to-ice temperature differential varies in a transient manner, the critical force is difficult to quantify. When allowed to freely descend into the ice under their own weight, thermal picks universally resulted in runaway heating. An additional force of 2.5 N or 5 N was applied by using either one or two 250 g weights. These forces correspond to between 20 kPa and 160 kPa tip pressure. The 2.5 N additional force was only sufficient to overcome levitation in the coldest cases, while 5 N additional force was sufficient in the vast majority of cases.

3.2.2 Surface Friction

When a gaseous layer formed between the thermal pick and the dry ice, it acted as a barrier, preventing direct contact and removing nearly all surface friction. Unless active measures were taken to prevent it, the low surface friction caused the thermal picks to slip laterally down sloped ice surfaces. The lack of friction combined with the applied forces would bend the driving rod of the linear test rig and deviate

the angle of insertion of the thermal pick. This deviation of the insertion path would result in poor pick-to-ice contact quality and reduce heat transfer into the ice, occasionally causing runaway heating of the thermal pick.

The most impactful effect of a deviated insertion angle was that it would cause an oblong bore volume as seen in Figure 7. An oblong bore volume necessarily involves the sublimation of unintended ices, which implies wasted energy. Unsurprisingly, deviated insertion angles increased energy expenditure during insertion proportional to the volume of additional ice sublimated.

Figure 7: Oblong bore caused by lateral slipping. Visual aid with desired (green) and undesired (red) bore area.

3.2.3 Forced Convection Heat Transfer

Another effect of the rapid production of carbon dioxide gas is the heat transfer that occurs along the walls of the thermal pick. Sublimation occurs primarily at the leading edge of the thermal pick and all sublimated gases must escape to the ambient environment. A thin channel quickly forms around the thermal pick that both

deepens as the thermal pick progresses into the ice and widens as the ice borehole erodes. The escaping gas flows outwards within this thin channel and is exposed to both the hot thermal pick walls and the cold borehole walls. Convective heat transfer from the thermal pick walls increase the temperature of the escaping gas, which can sublimate the borehole ice walls.

Because dry ice thermally equilibrates to its sublimation point, all heat transferred to the ice wall results in unintended sublimation, which is the cause of erosion that widens the channel. Initially, the channel will be no larger than necessary to permit the flow of outgoing gas. However, convective heat transfer rates are a function of channel width and heat transfer into the borehole walls will sublimate and expand the channel. As the channel widens, convective heat transfer slows. This creates a negative feedback loop wherein borehole erosion slows over time.

The width of the borehole gap varied dramatically depending on insertion stability and depth. Stable undeviating insertions with high rates of sublimation produced borehole gaps thin enough that restriction of the outflow of gas caused pressured-based fracturing and expulsion of chips of solid dry ice. However, by the end of any given test, the borehole was always noticeably eroded. For insertion depths of 50.8 mm, the 12.7 mm diameter pick created a borehole width measured between 13.6 mm to 14.2 mm at the lip. This corresponds to a maximum channel width of 0.45 mm to 0.75 mm.

Since the heat required for borehole erosion comes from the thermal pick, erosion represents a distinct heat loss mechanism. To reduce energy lost to convective heat transfer, the thermal pick wall temperature must be reduced, or the flow of the

outgoing sublimated gas must be altered. These considerations are described in Sections 3.3.3 and 3.3.4.

3.2.4 Ambient Losses

Heat transfer to and from the ambient environment occurs through natural convection and conduction. Natural convective losses or gains occur when thermal pick surfaces are exposed to ambient temperatures. Natural convection is gravity-induced heat transfer with the air surrounding any exposed warm or cold surfaces. While this effect would not be present in a vacuum environment, it was present in laboratory testing. Only surfaces above the ice surface were affected by natural convective losses because sublimation flushes the borehole with a consistent supply of carbon dioxide.

Conductive losses (or gains) occur through any material that physically contacts the thermal pick. The primary sources of conductive loss are the G-10 sheet and the G-10 coupling, which are in direct contact with the thermal pick. The material G-10 was selected specifically for its low thermal conductivity, which inhibits this conductive heat transfer.

These convective and conductive losses were experimentally measured by tracking the heater power required to maintain thermal pick temperature when not thermally drilling. The rate of loss is included in the energy accounting in Section 3.5.

3.3 Results

3.3.1 Stability and Insertion Angle

The most impactful characteristic of the insertion of a thermal pick is its path stability. The linear test rig had path stability issues when inserting into sloped ice surfaces stemming from a lack of stiffness in the driving rod while the rotary test rig had a cyclic path deviation of the thermal pick during insertion. The path deviations were difficult to discern by eye but would result in significantly increased bore volumes and wasted energy.

Oblong boreholes as seen in Figure 7 would result from pick path deviation when using the linear test rig. These deviations caused unpredictable efficiency reductions (often over 20%) proportional to the path deviation and resulted in overheating of the thermal pick when the misalignment lowered the thermal pick-to-ice contact area.

The rotary test rig cyclic path deviation was a repeated lateral circular sweeping motion of the thermal pick and caused a significant increase in the bored ice volume. This deviation resulted in efficiency losses of over 50% but was rectified by adding the stabilizing G-10 sheet, which constrained lateral play of the thermal pick. This improved the thermal efficiency up to 90%, matching the maximum that was measured in similar tests with the linear test rig where slipping did not occur.

3.3.2 Temperature and Size

The impact of temperature on thermal efficiency is a consequence of convective and conductive heat losses. Forced convective losses occur along the walls

of the thermal pick beneath the surface of the ice due to sublimated gas, while natural convective losses occur along the rest of the thermal pick surface. Conductive losses occur only at the G-10 attachment points. The convective loss mechanisms all depend on the differential temperature between the thermal pick and the sublimated and ambient gases. The conductive losses depend on the differential temperature between the thermal pick and the adjacent test rig material. For this reason, lowering a pick's operating temperature reduces the rate of convective and conductive heat loss and improves efficiency.

Lower pick temperatures increased thermal efficiency, but also resulted in longer overall process times as seen in Figure 8. The clear increase in efficiency demonstrates that despite the longer overall process times during which losses can occur, the reduction in the rate of heat loss is dramatic enough to decrease the total heat lost.

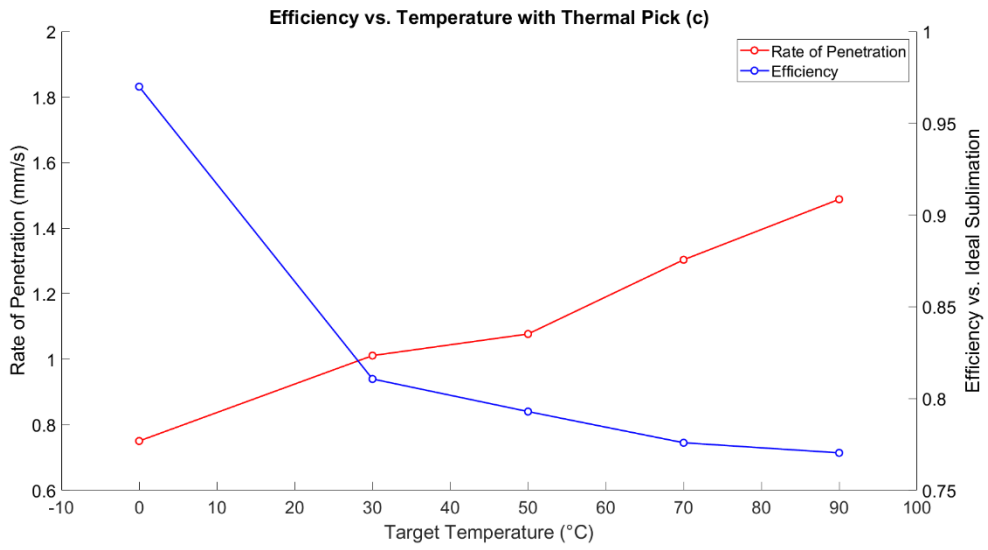

Figure 8: Sublimation efficiency vs. target temperature for thermal pick (c).

The temperature of the thermal pick is a function of both the power output of the heater and the specified target temperature. Adjusting the heater power alone did not directly impact efficiency but could indirectly impact efficiency by changing the temperature of the thermal pick. Tests using heater powers of 15 W, 22.5 W, and 30 W on thermal pick (b) resulted in average thermal efficiencies within 1% of one another when the target temperature was set to 30 °C. This is because each heater power setting was able to maintain the temperature of the thermal pick. In cases where the heater power output was low relative to the size of the thermal pick and its target temperature, the heater was not able to sustain the target temperature despite remaining on throughout the test. This is because the rate of heat transfer into the ice can be in excess of 30 W and cool the thermal pick despite the heater remaining on. If a pick cools below its target temperature, the heat transfer rate decreases and the thermal pick temperature approaches steady-state. However, given the limited timeframe of insertion and changing conditions as the borehole depth increased, steady-state conditions were not reached in this study.

The area of the leading edge impacted the efficiency of the device when it affected the temperature of the thermal pick during the sublimation process. The smaller thermal picks (a), (b), and (c), have the same 30 W heater as the larger thermal picks (d) and (e), but have a smaller surface area to contact the ice. As a result, the smaller picks can maintain higher temperatures throughout the sublimation process. At low target temperatures that could be sustained by both the large and small thermal picks, the efficiencies were similar regardless of pick size. However,

the higher target temperatures could not be sustained by the larger thermal picks due to when their large leading edge surface areas were in contact with the ice.

The minimum target temperature used was 0 °C because as seen in Figure 8, the insertion time would climb dramatically below this temperature. While long insertion times are not inherently problematic, they increase the time during which heat exchange with the ambient environment can occur.

3.3.3 Wall Insulation

Reducing thermal losses from the thermal pick walls was investigated by comparing an insulated and uninsulated thermal pick. As noted in Section 3.2.3, convective heat transfer occurs along the wall of the thermal pick and this leads to heat loss and erosion of the borehole walls. This heat transfer mechanism was the driver of thermal efficiency for the thermal drilling process.

The performance of thermal pick (d) with thermally conducting walls was compared to thermal pick (e) with thermally insulating walls. Both thermal pick (d) and (e) are shown in Figure 9. A standard tellurium copper thermal pick core with a diameter of 6.35 mm was prototyped around which an outer tube making up the walls of the thermal pick was fit. Two outer tubes of 3.175 mm wall thickness were made, one made of tellurium copper and the other made of thermally insulating titanium. The thermal pick core was threaded to a length of 6.35 mm from the leading edge so that a small threaded plug of copper of 12.7 mm diameter could be attached to the bottom of the thermal pick. This allowed heat to flow out across the entire leading edge of the thermal pick where the intended sublimation occurs so that the thermal drilling process would not be inhibited by the thermal insulation.

Figure 9: Thermal picks (d) and (e). Titanium insulated pick (e) shown left and uninsulated copper pick (d) shown right.

Given the end goal of using the thermal pick as an anchor that is subject to loading, titanium was chosen for its combination of high yield strength (828 MPa) and low thermal conductivity (6.6 W/m-K). While other materials may have offered better thermal insulation, they were not adopted due to their lower material strength, machinability, or performance at cryogenic temperatures. However, the titanium used still offers a thermal conductivity that is approximately 50 times lower than that of tellurium copper.

Altering the wall material did not significantly change the thermal efficiency and resulted in a mere 2% efficiency gain, which is within the 2.6% standard deviation of the test data gathered. The lack of improvement is believed to be a result of the low rates of wall heat loss, the relatively large surface areas from which the losses occur, and the timescales involved. If the energy losses from the walls were larger, or if a better thermal insulator were used, then efficiency gains from insulated walls would be expected.

Despite the desire to ensure an efficient thermal drilling process, it is also important to consider the proposed use of a thermal pick as a thermal drill and anchor in a cryogenic water ice environment, not a dry ice environment. Thermal drilling in cryogenic water ice involves re-freezing meltwater, which can cause the walls of a drilling device to become physically obstructed if the walls are not adequately heated [41]. Heating of the walls of a thermal pick is in direct conflict with the goal of insulating them.

3.3.4 Wall Geometry

Three variants on wall geometry were tested for their dry ice thermal drilling performance. The cylindrically symmetrical smooth-walled thermal picks were the standard against which thermal pick (f) with threaded screw-type walls and grooved walls were compared. The development of the rotary test rig made it possible to test a threaded thermal pick because of the coupling of linear and rotational motion. The threaded thermal pick had slightly lower thermal efficiencies than the cylindrical profile thermal picks under similar testing conditions. As seen in Figure 10 the trends in the threaded thermal pick's thermal efficiency and average rate of penetration vary in a manner consistent with that of the cylindrical picks.

To determine the cause of decreased thermal efficiency, the three known modes of heat loss must be considered. Conductive loss occurs through the G-10 thermally isolating coupling based on the thermal pick temperature, but the geometry of this connection, and therefore heat loss, was constant across all thermal picks. However, natural and forced convection have a dependence on the flow of gas along the surface of the thermal pick, which changes with wall geometry.

The threading on the walls of the thermal pick is expected to increase the convective losses from the escaping gas. While any carbon dioxide sublimated at the leading edge of a cylindrical pick has a direct escape path, the threaded thermal pick walls inhibit this flow. The tortuosity of the path between the leading edge of the threaded thermal pick and the surface of the ice is relatively high and this is compounded by the increase in surface area of the walls of the thermal pick. An increase in convective losses is believed to be the cause for the difference in efficiency between the screw-type and cylindrical picks. The repercussions of these convective losses are shown in Figure 6, where significant degradation of the threads in the threaded borehole occurs for the high temperature tests. Borehole erosion is problematic for the use of a screw-type thermal pick as an anchor given that borehole threading is what engages with the thermal pick threads and allows for anchoring. Without the physical engagement of the threading, there is no support against an axial load on the thermal pick.

Due to the required use of the rotary test rig for any experiments involving the screw-type thermal pick, effects on the pushback force were not observed because the rotary test rig cannot measure forces. While it is predicted that a threaded wall geometry may impact the pushback force, that impact was not determined.

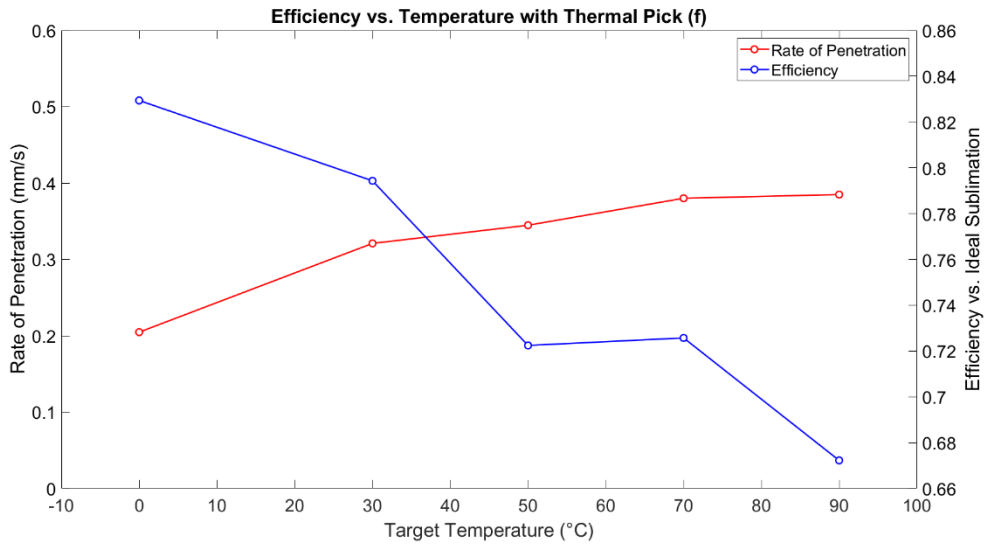

Figure 10: Sublimation efficiency and rate of penetration vs. target temperature for thermal pick (f).

The second wall geometry alteration that was considered was cutting pressure relief grooves into a cylindrically symmetrical thermal pick to further ease the escape of sublimated gases. Grooves of approximately 0.6 mm were cut into the walls of thermal pick (b) to explore the possible impact on the pushback force and thermal efficiency, as can be seen in Figure 2 and Figure 11, but did not have a noticeable impact on either. This result suggests that the primary component of the pushback force is due to pressure across the leading edge surface instead of drag on walls of the thermal pick caused by the escaping gas.

3.3.5 Tip Shape

Figure 11: Thermal picks (a), (b), and (c). Flat, conical, and inverse conical tips shown left to right.

To determine the impact of tip shape, three different thermal picks were compared. The tip shapes used were flat, 45° conical, and 45° inverse conical, shown in Figure 11. Under the conditions tested, the only difference observed was in the pushback force and considerations derived thereof. The inverse conical tip shape resulted in noticeably higher Leidenfrost levitation forces that required increased applied loads to overcome relative to the flat and conical tipped picks. An inability to overcome Leidenfrost lift can reduce thermal pick heat transfer and cause runaway heating in the absence of temperature control.

3.3.6 Duty Cycling

The conduction of heat from the warmed ices being thermally drilled into adjacent cryogenic ices represents a time dependent loss mechanism. This process has been studied analytically [28] [31] and experimentally [41] at steady-state and will be even higher in the initial transient period prior to reaching steady-state. Thermal picks operate in the transient regime where conduction losses are high because of the relatively short depths involved. The use of high heater power outputs is incentivized by these losses to increase thermal efficiency. While the rate of penetration is

correlated with heater power output, conduction losses only increase with temperature, which is not substantially affected by changing heater power. This causes the thermal efficiency to increase with higher heater power [41].

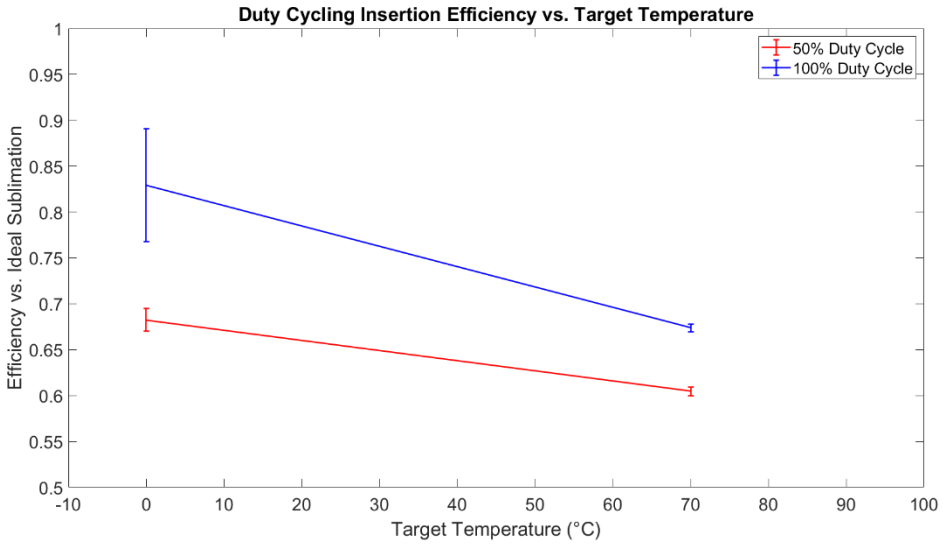

Figure 12: Duty cycling sublimation efficiency vs. target temperature for thermal pick (f).

In the context of a thermal pick, where the position of the thermal pick is actively controlled, an intermittent insertion approach can reduce the conductive losses. Intermittent insertion is characterized by periods of active insertion of the thermal pick into the ice separated by breaks during which it is held in place. This causes the thermal pick to undergo a series of transient thermal drilling processes and is called duty cycling. Duty cycling refers to the percentage of time that a system is actively used.

Intermittent insertion repeatedly interrupts the thermal pick's conduction path because as soon as thermal drilling halts, sublimation generates a thin gaseous layer around the thermal pick that only permits convective heat transfer. With conductive heat loss gone, the thermal pick can warm rapidly. When active insertion resumes, the

thermal pick will be relatively hot and will have increased heat transfer rates. This approach mimics the behavior of a thermal pick operating at a higher rate of power and temperature.

The dry ice used was created days before its use and had undergone an extended period of thermal equilibration and slow sublimation across its external surfaces. Since the external environment is universally warmer than the dry ice, its surface will always sublimate, but at a rate determined by the quality of the thermal insulation of its storage container. Because of this thermal equilibration and sublimation, the internal temperature of the ice will be at its sublimation temperature which prevents conductive losses from occurring. Conductive heat transfer requires a thermal gradient, but any heat added to the surface of the dry ice results in sublimation instead of warming. This means that the intended benefit of an intermittent insertion approach, reducing conductive losses, was not present in dry ice testing. Instead, the intermittent insertion tests in dry ice were used to assess any negative side-effects of the approach that could inform cryogenic water ice testing.

A 50% duty cycle was achieved by repeating a cycle of inserting for 5 seconds then holding steady for 5 seconds. A 100% duty cycle was achieved by constantly applying pressure to insert the thermal pick into the ice. The reduction in efficiency observed in Figure 12 is a consequence of the expected higher operating temperatures during active thermal drilling as well as convective losses in the holding phase that would not be present under vacuum.

While duty cycling represents a net efficiency reduction in this setting, this intermittent approach was essential for cryogenic water ice as described in Chapter 4.

3.3.7 Subcooled Dry Ice

Subcooling of the dry ice was achieved by placing the ice on a liquid nitrogen cooled aluminum block for several hours. Using the aluminum block as a medium through which the dry ice was cooled caused slow changes in temperature and avoided thermal shock-based degradation of the ice that occurs with direct exposure to liquid nitrogen. Testing using thermal pick (d) showed no new phenomenon when penetrating a dry ice block with a measured internal temperature of -146 °C. The limited data set did not show a significant change in heat expenditures when compared to previous tests.

3.4 Thermal Model

A model of thermal pick (d) was created in SolidWorks and used to analyze the transient thermal processes at play. The goal of this model was to estimate the thermal pick leading edge temperature at the thermal pick-to-ice interface given the inability to measure it directly.

The calculated ideal energy expenditure alongside the experimentally measured process time and heater output energy are used to define the settings of the model. The model simulates the four distinct thermal processes: initial heating to the target temperature, sublimation energy expenditure, thermal equilibration, and reheating back to the target temperature.

Figure 13: Simulated exposure of thermal pick (d) to a cold reservoir at the thermal pick tip with thermal losses evenly distributed across the walls of the thermal pick.

This model makes three assumptions:

1. The thermal pick leading edge (tip) temperature (T_t) remains constant throughout insertion. The actual leading edge temperature should start near the target temperature and then approach a constant steady-state temperature. This assumption is valid when good contact between the leading edge of the thermal pick and the ice is quickly established.
2. Heat transfer from the leading edge (tip) of the thermal pick produces the desired sublimation that advances the thermal pick into the ice, while heat transfer from the walls of the thermal pick (E_w) does not.

   This assumption leads to the condition that all undesired losses occur at the walls.

$$E_t = f(T_t) = E_i \tag{6}$$

$$E_w = E_l \tag{7}$$

   This assumption is valid when the leading edge does not significantly heat the sublimated gases, which would be considered a source of loss.
3. All thermal losses (E_l) are distributed either evenly across the entire pick wall or distributed only on the wall surface within 6.35 mm of the leading edge over the full duration of insertion. The power loss (P_l) from the walls does not vary with time and is calculated as follows.

$$P_l = {E_l}/{t_i} \tag{8}$$

The actual wall losses are complex and vary with position, time, channel width, and thermal pick test conditions. This assumption is used in lieu of a model of the fluid dynamics.

The input to the model is the first boundary condition of the leading edge temperature (T_t) and is iteratively set until it meets the condition of Equation (9).

$$E_t = E_i \tag{9}$$

This produces an estimate for the average leading edge temperature. The second boundary condition is at the heater, which is internal to the thermal pick. The heater boundary condition cycles between a constant 0 W or 30 W power input as determined by a modeled thermostat, which follows the same control logic as the rotary test rig's thermostat. The third and final boundary condition is along the thermal pick wall, which is the calculated and evenly distributed constant power loss from Equation (8).

The leading edge temperature estimate determined by the model is affected by many test conditions, but most notably by the commanded insertion rate as seen in Figure 14. As the commanded insertion rate increases, the stepper motor more frequently pushes the thermal pick tip against the dry ice, which drives down the leading edge temperature through improved tip-to-ice contact.

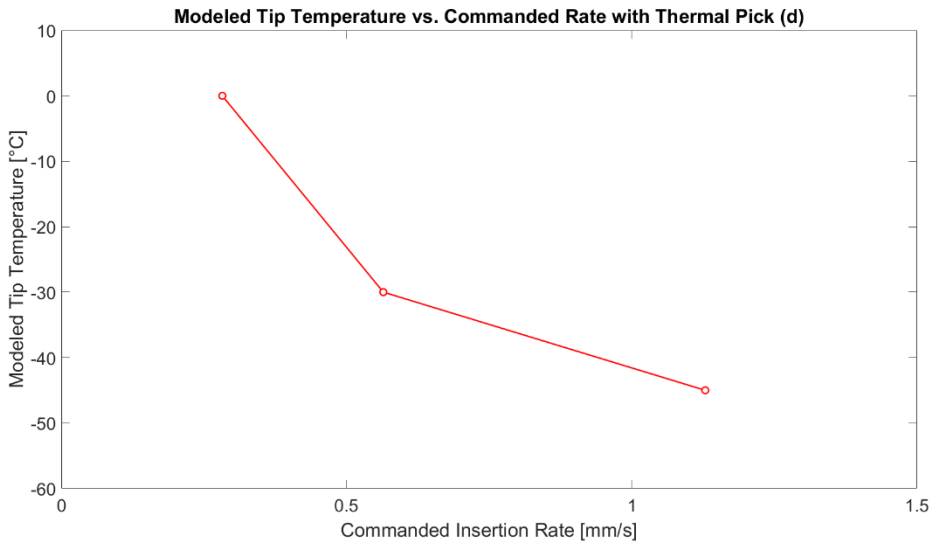

Figure 14: Modeled tip temperature vs. commanded insertion rate with thermal pick (d). Increased commanded motor speed results in better tip contact and reduced leading edge temperatures.

3.5 Energy Accounting

In all cases, the bulk of the energy transfer went towards the desired sublimation. The remaining energy loss is attributed to a combination of forced convection to the escaping sublimated gas, natural convection to the ambient air, and conduction losses internal to the test rig. The forced convective losses due to the escaping gas were not able to be isolated from the other loss mechanisms and experimentally measured directly.

The convective losses to the ambient air and conductive losses to the test rig were quantified by holding the thermal picks at an elevated temperature and measuring the heater power required to maintain a set temperature. By this method, natural convection and conductive losses are measured together and cannot be differentiated. Both loss mechanisms stem from a temperature differential relative to the ambient air temperature in the laboratory since the test rig is assumed to have

initially equilibrated to that temperature. The power loss was a function of this temperature differential and was measured to be 19 mW/K, resulting in estimated losses as high as 1.24 W for the 90 °C tests and gains of as high as 0.47 W for the 0 °C tests.

These heat loss mechanisms affect the calculation of thermal efficiency. Thermal efficiency is intended to describe the efficiency with which energy spent in the thermal drilling process is applied to removing the necessary ice. Any additional energy spent above and beyond this theoretically calculated minimum are loss mechanisms that are undesirable but not entirely avoidable.

The uncertainty in the electrical components and their impact was also evaluated and is shown in Table 2. Errors in the electrical components are generally considered to be small relative to the effects of human error and the inherent variability of test specimens.

Table 2: Uncertainty in electrical components.

Quantity	Variable	Uncertainty	Effect on Efficiency	Description
R_h	Heater resistance	±0.2 Ω	±1%	Cartridge heater (30 W, 24 V-DC)
V_h	Supply voltage	±0.1 V	±0.8%	DC Power Supply
T	Temperature	±0.1 °C	-	Omega HH309 Thermocouple Reader (K-Type)
t	Total insertion and heater timing	±1 ms	-	Arduino MEGA
d	Distances	±0.1 mm	±2%	Digital micrometer

3.6 Conclusions

The study of thermal picks using dry ice in the laboratory environment aimed to provide an understanding of sublimation phenomena that could inform cryogenic vacuum water ice testing and the water ice test rig was designed according to lessons

learned through the dry ice experiments. Lateral pick stability drove the selection of highly rigid test rig components, and high-temperature thermally conductive epoxy was used in place of thermal paste to permit an expanded temperature range.

Lateral pick stability, wall geometry, and temperature were established as the primary factors that affect efficiency. Of these, the stability of the thermal pick had the largest impact on the tests conducted, resulting in significant unnecessary sublimation and reduced thermal efficiencies. The G-10 stabilizing sheet laterally constrained the thermal pick at the surface of the ice and the resolved stability issues. Increasing the complexity of the thermal pick wall geometry increased heat loss due to the larger surface area and by impeding the flow of sublimated gas. Higher operating temperatures decreased thermal efficiency by increasing convective and conductive losses.

The axial force required to overcome the Leidenfrost effect and permit efficient heat transfer into the ice surface depends on tip geometry and temperature. The tip geometry of thermal pick (c) that impedes the escape of sublimated gas created higher pushback forces due to increased tip pressure. Relieving tip pressure by introducing channels in the thermal pick wall was not an effective approach to reducing the pushback force, although only one channel geometry was tested. Reducing the temperature reduced the force necessary to overcome Leidenfrost levitation.

Thermal efficiencies as high as 90% were consistently achieved for low temperature tests when stability was ensured. The convective and conductive

mechanisms are functions of temperature and had a direct impact on thermal efficiency.

Some of the studied characteristics yielded clear results that can be implemented in sublimation-based thermal picks. For example:

- Tips should provide an easy gas escape path.
- Wall insulation provides minimal benefit within the bounds of the materials tested.
- The required applied axial force is correlated with temperature and tip shape.
- Complex wall geometries impede gas flow and increase convective losses.
- Size directly increases energy costs but does not impact thermal efficiency.
- Stability of the thermal pick is essential for energy efficiency.

Other results yielded benefits that trade off against deficits that must be considered, such as:

- High thermal pick temperatures speed up the sublimation process but incur larger energy losses. Energy and time dependencies must inform the temperature choice.
- Duty cycling amplifies heat loss mechanisms present in atmospheric testing but may increase efficiency in vacuum environments.

The lessons learned through this study were applied to the creation of a water ice test rig and prototype water ice thermal picks that are discussed in Chapter 4.

Chapter 4: Intermittent Thermal Drilling in Water Ice

4.1 Experimental Setup

The water ice test rig was designed to test thermal picks in an environment that simulated Europa's surface. To approximate Europa's mean surface temperature of -183 °C, liquid nitrogen was used to cool the water ice used for testing. The surface pressure was simulated by a vacuum chamber, which required that each test rig component be vacuum-compatible. The tasks performed by the test rig were monitoring and controlling the position and temperature of the thermal pick, setting the force between the thermal pick and the ice, and providing either rigid or translating connections between components as necessary.

The water ice experimental setup was made of five separate systems: the thermal pick that is the focus of the study, the test rig that positioned and applied loads on the thermal pick, the ice mount that cooled and held the cryogenic ice block, the vacuum chamber that simulated Europa's surface pressure, and the external electronic components that monitored and controlled the test rig and thermal pick.

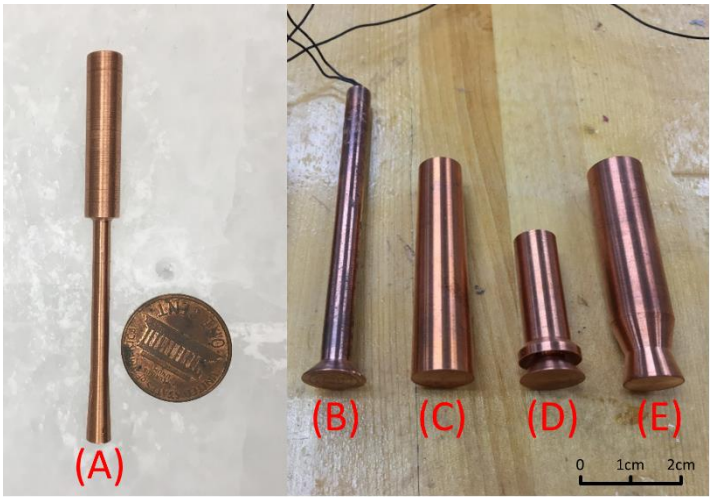

Figure 15: Thermal picks (A) through (E). The leading edge of the thermal picks are the bottom surfaces in the orientation shown.

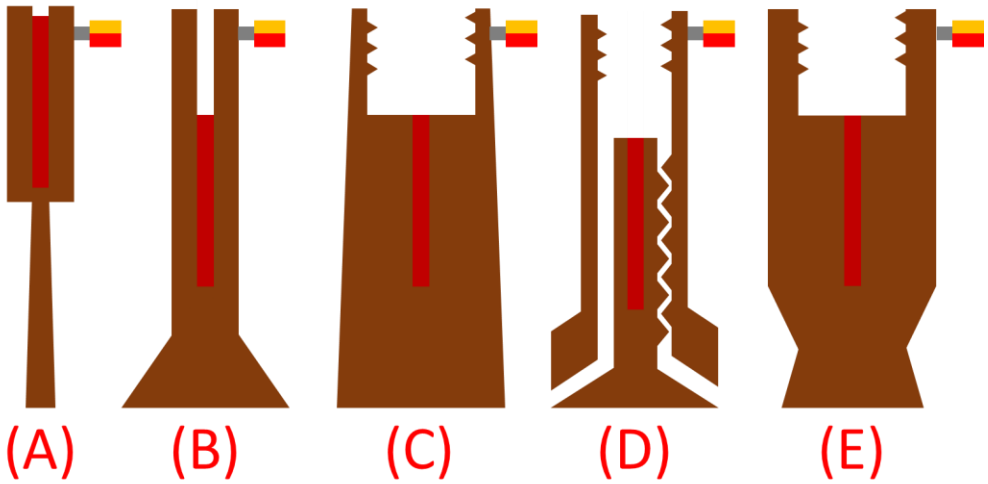

Figure 16: Illustrations of thermal picks (A) through (E). Shown are copper bodies (brown), embedded heaters (red), and thermocouple tip locations (grey). The leading edge of the thermal picks are the bottom surfaces in the orientation shown. Not to scale.

4.1.1 Thermal Pick

The five tested thermal picks (A) through (E) had a copper body and an embedded cartridge heater and are shown in Figure 15 alongside their cross-cut schematics in Figure 16. The thermal picks were flat-tipped, made of Tellurium copper because of its high thermal conductivity (355 W/m-K) and machinability, and

except for thermal pick (D), were cylindrically symmetrical. The tested thermal picks were all designed to be used with a linear insertion due to the difficulty of implementing multiple insertion styles with the test rig. The embedded heaters were the same 30 W, 24 V-DC, 25.4 mm x 3.18 mm cylindrical custom cartridge heaters discussed in Section 3.1.1.8. Thermal picks (C), (D), and (E) required a partially threaded 6.35 mm diameter copper coupling to attach to the G-10 insulating tube.

The temperature of the thermal pick was measured by placing a thermocouple in physical contact with the top of the thermal pick as seen in Figure 16. This placement avoided contact with the ice and the outgoing flow of water during thermal drilling.

The five thermal picks were designed to achieve five different goals: thermal pick (A) was as small as could be machined to minimize energy expenditure, thermal pick (B) had a large tip-to-core taper to encourage re-freezing of meltwater, thermal pick (C) had high bending strength while maintaining a taper, thermal pick (D) had an internal flowpath to mitigate thermally induced ice failure, and thermal pick (E) had an hourglass shape to increase pressure around the tip. Thermal picks (C), (D), and (E) were used for insertion and extraction only, while thermal picks (A) and (B) were used for insertion, extraction, and anchoring testing. Thermal picks (D) and (E) were not used for anchoring since their design features were deemed unnecessary, while thermal pick (C) was not used due to electrical failure of its cartridge heater.

4.1.1.1 Thermally Conductive Epoxy

The cartridge heaters were glued within a cavity of the thermal pick body using EP21TCHT-1 vacuum-compatible thermally conductive epoxy procured from

Master Bond. This epoxy had an operational temperature range between -270 °C and 204 °C. This range comfortably covered the minimum temperature that could be reached with liquid nitrogen cooling, but the upper temperature bound was a limiting condition. This glue was specifically formulated to have high dimensional stability and low outgassing, which made it well suited to this application.

While epoxy resins often have thermal conductivities in the range 0.15 W/m-K to 0.25 W/m-K, this epoxy had a thermal conductivity of 1.44 W/m-K. This thermal conductivity was almost 250 times lower than the copper that surrounded it, but when applied in a very thin layer it did not significantly inhibit the flow of heat from the cartridge heater.

4.1.1.2 Thermal Pick (A)

Thermal pick (A) was the smallest prototyped pick and was the final iteration of the thermal pick design. It demonstrated scaling down the system size as well as the functionality of a very shallow taper angle (3.58°). This thermal pick had a tip diameter of 4.8 mm, which tapered down to a minimum diameter of 3.2 mm over the course of 12.7 mm in length. The minimum diameter was then maintained for an additional 25.4 mm. The top portion of the thermal pick was markedly larger at a diameter of 6.4 mm over a length of 31.8 mm. This section of increased diameter was necessary to accommodate the cartridge heater within a 3.2 mm diameter cavity.

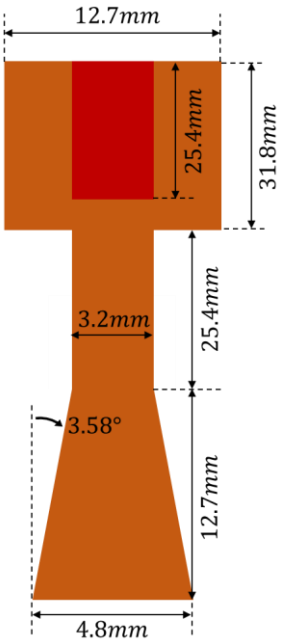

Figure 17: Illustration of thermal pick (A) showing relevant dimensions. Not to scale.

This thermal pick was intended for use as a tensile anchor, lacking the structural integrity to support bending loads. Its diameter was the minimum that could be prototyped with the available machining capabilities, thereby achieving the minimum feasible energy expenditure. Because the strength of the ice in response to a tensile load is a function of both the depth and the width of the anchor, this thin pick inserted to a minimum depth was used to examine the weakest feasible anchoring hold as described in Section 4.5.6.

4.1.1.3 Thermal Pick (B)

Thermal pick (B) was designed with a sharp taper (45°) to ensure that a large volume of ice would re-freeze behind the tip during insertion. It had a tip diameter of 12.7 mm, which tapered down to a minimum diameter of 6.4 mm over the course of 6.35 mm in length. Within the 6.4 mm diameter section was a cavity of 3.2 mm diameter in which the cartridge heater is placed.

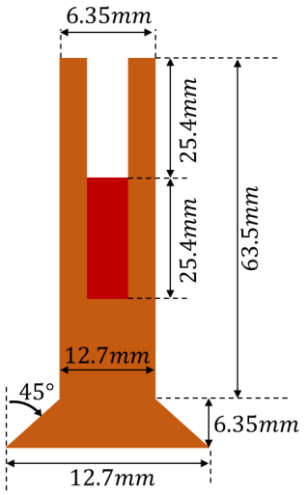

Figure 18: Illustration of thermal pick (B) showing relevant dimensions. Not to scale.

With respect to the failure of the ice, this thermal pick was expected to be the strongest. Since this pick had a large projected volume (tip area multiplied by insertion depth) in comparison to its root diameter, it had a low bending strength relative to its energy cost. This thermal pick style is optimal for the case in which ice failure is the limiting factor and is best suited to applications where only tensile loads are applied.

A secondary consequence of having a small material volume in comparison to projected volume was the low ratio of the thermal pick warming energy cost (proportional to mass) to the thermal drilling energy cost (proportional to projected volume). The warming energy cost is discussed in Section 4.4.8 and simulated in Section 4.6.

4.1.1.4 Thermal Pick (C)

Thermal pick (C) was designed to maximize the bending strength of the thermal pick while maintaining a taper. It had a tip diameter of 12.7 mm, which matched that of thermal pick (B), but tapered gradually over its entire length rather

than quickly. The gradual taper left minimal room for meltwater to re-freeze behind the tip during insertion. This minimized the extraction energy cost.

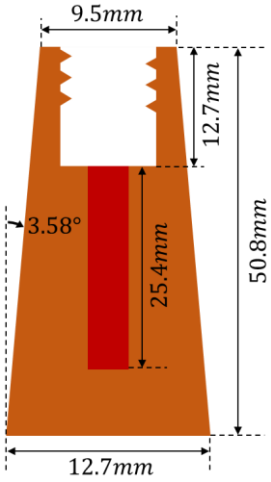

Figure 19: Illustration of thermal pick (C) showing relevant dimensions. Not to scale.

This thermal pick had a small projected volume to pick volume ratio, meaning it had high mass and warming energy required relative to its thermal drilling energy cost. Because of its large root diameter relative to its length, it was best suited for applications where bending loads were applied to the thermal pick.

4.1.1.5 Thermal Pick (D)

Thermal pick (D) was designed with a slotted screw internal attachment point and a two-tiered lip structure. This design was entirely focused on providing an internal flowpath through which meltwater could escape. Internal flowpath systems have been proposed [37] and successfully tested [42] in previous works.

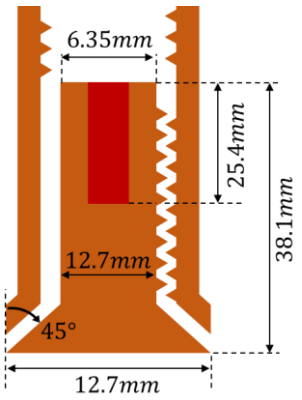

Figure 20: Illustration of thermal pick (D) showing relevant dimensions. Not to scale.

The outer and inner portions of thermal pick (D) were mated through internal and external threading. This thread mating would ordinarily obstruct flow (shown on the right side of the thermal pick in Figure 20), so the inner portion had two cut-out "flats" that created a gap for water to pass through (shown on the left side of the thermal pick in Figure 20). The internal portion of thermal pick (D) had a tip diameter of 12.7 mm with a taper of 45° down to the externally threaded 6.4 mm diameter core. The external portion of thermal pick (D) had a 12.7 mm outer diameter and tapered at 45° to an internally threaded section that mated with internal portion of the thermal pick.

The ice failure mechanisms that are discussed in Section 4.5.3 were caused by the exposure of the cryogenic borehole walls to meltwater and warm gaseous water. This pick was expected to permit the meltwater to freely escape to vacuum without contacting the borehole walls and therefore mitigate ice failure. The downsides of this thermal pick design style were the large internal surface area across which heat was transferred to the outgoing flow of water and the lack of structural integrity and mass inherent to its cavernous structure. This pick was unsuccessful because it had low

thermal energy storage, limiting its ability to support intermittent thermal drilling and would quickly undergo thermal stall, a phenomenon described in Section 4.5.2.1.

4.1.1.6 Thermal Pick (E)

Thermal pick (E) was designed with an hourglass taper that was intended to encourage melting and re-freezing at the tip. The hourglass taper started with a tip diameter of 11.1 mm, which tapered down to a diameter of 7.9 mm over a length of 6.35 mm, then tapered back out to a diameter of 12.7 mm over a length of 6.35 mm. The diameter of 12.7 mm was maintained for the remainder of its length. The hourglass taper, with a final diameter that was larger than the tip diameter created a secondary pinch where active thermal drilling would occur. The objective of a secondary pinch was to increase the pressure that would build upstream (closer to the tip).

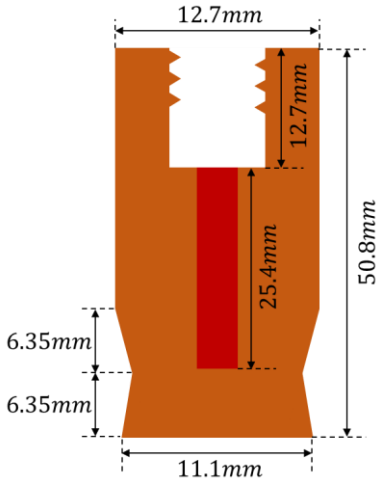

Figure 21: Illustration of thermal pick (E) showing relevant dimensions. Not to scale.

Given the high rate of re-freezing that occurred when meltwater was exposed to the cryogenic borehole walls, re-freezing meltwater in the hourglass cavity was expected to lock the thermal pick within the ice. However, it was determined through

testing of other thermal picks that melting and re-freezing could be achieved without a secondary pinch, negating the need for this thermal pick.

4.1.2 Test Rig Hardware

The purpose of the water ice test rig shown in Figure 22 and Figure 23 was to securely hold, position, and apply loads to a thermal pick. It was made of positioning slides, thermal insulation, frame components, a crossed roller bearing, constant force springs, and an extension spring.

The schematic in Figure 24 shows the approximate position of test rig components and where relative motion of the components occurred.

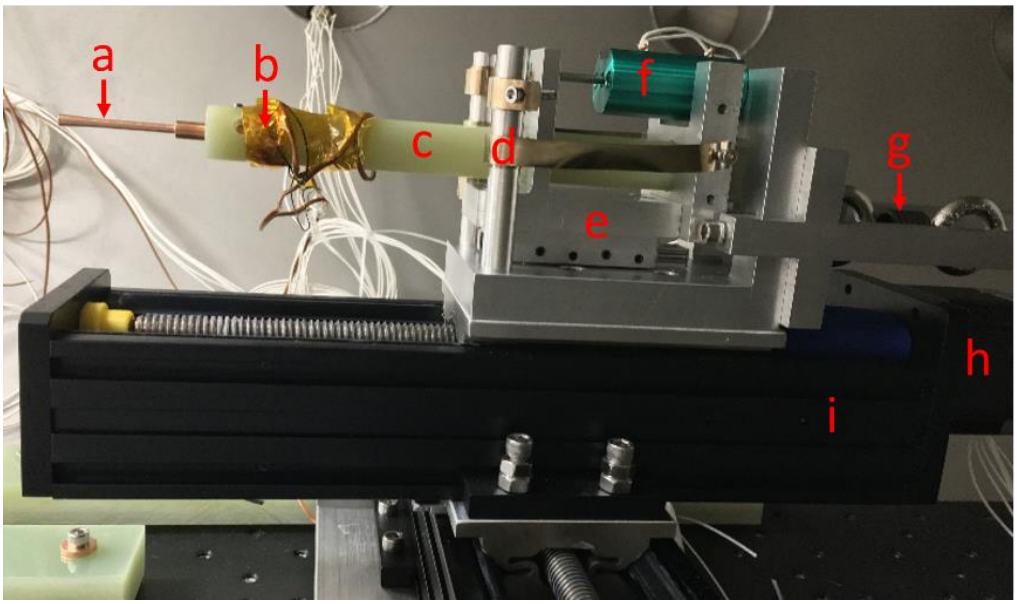

Figure 22: Water ice test rig side view. Shown are the thermal pick (a), thermocouple location (b), G-10 thermal insulation (c), constant force springs (d), crossed roller bearing (e), linear potentiometer (f), extension spring (g), stepper motors (h), and positioning slides (i).

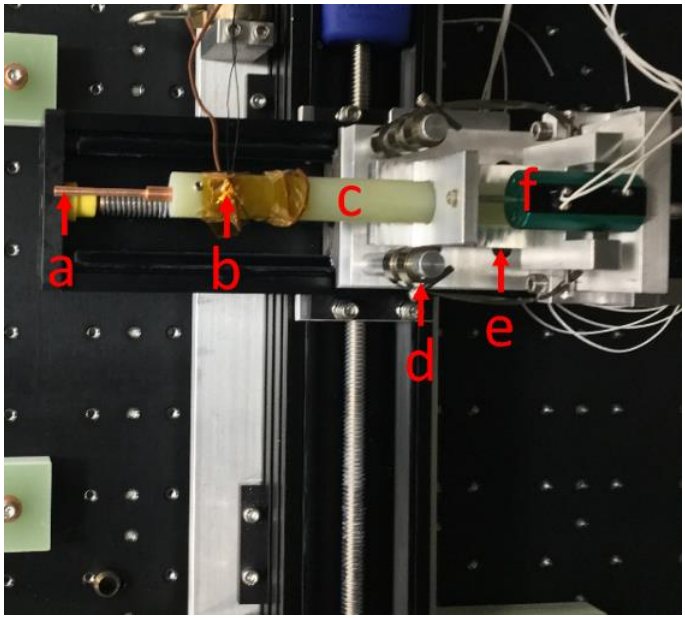

Figure 23: Water ice test rig top-down view. Shown are the thermal pick (a), thermocouple location (b), G-10 thermal insulation (c), constant force springs (d), crossed roller bearing (e), and linear potentiometer (f).

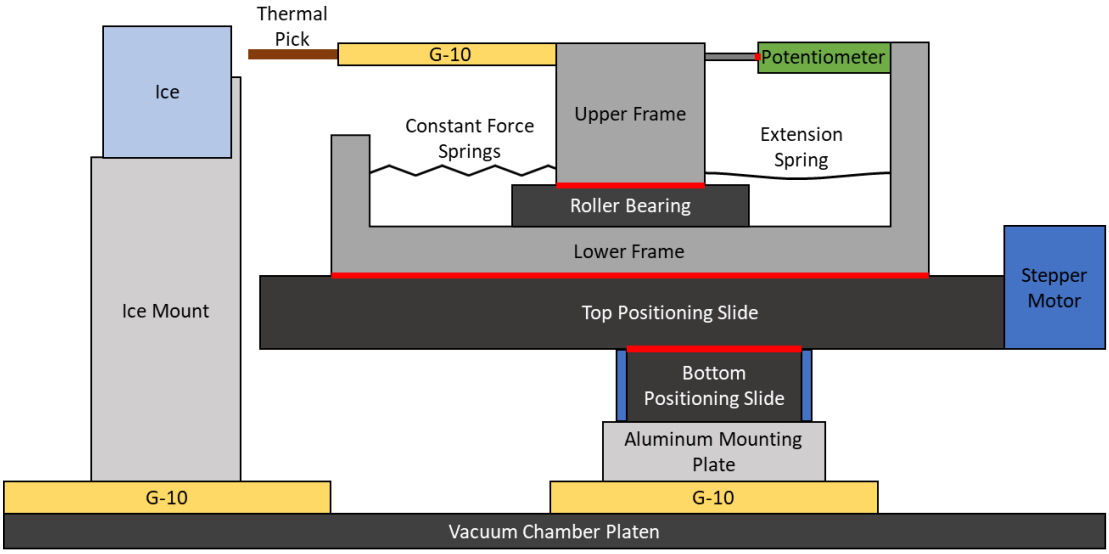

Figure 24: Schematic of the water ice test rig showing the relative position of major components. Red borders denote boundaries across which the relative motion of components can occur. Not to scale.

4.1.2.1 Vacuum Chamber

The vacuum chamber used for testing was a DVI 3600B made by Diversified Vacuum Inc. This vacuum chamber had an Adixen/Alcatel roughing pump that

provided a minimum pressure of 0.013 Pa (10^{-4} Torr). The vacuum chamber was equipped with a cryo-pump that could have enabled reaching pressures that are more representative of Europa's surface, but cryo-pumps are incapable of maintaining vacuum pressures when active sublimation is occurring. To avoid potentially damaging or contaminating the cryo-pump, it was always kept sealed.

The large vacuum chamber volume of 0.9 m^3 allowed the maximum drilling step to have a small impact on the overall chamber pressure. The pressure change resulting from thermal drilling was calculated according to Equation (12).

$$m_{water} = d_{step} A_{tip} \rho_{ice} \tag{10}$$

$$v_{water} = \frac{V_{chamber}}{m_{water}} \tag{11}$$

$$\Delta P = f(v_{water}, T_{water}) \tag{12}$$

A conservative estimate of the chamber pressure change (ΔP) assumed a solid ice density (ρ_{ice}) of 0.92 kg/m^3, the maximum insertion step length of 6 mm (d_{step}), that all of the water thermally drilled in an insertion step (m_{water}) was converted into vapor, and its temperature (T_{water}) was increased to the maximum operating condition of 160 °C. The mass of water filling the chamber yielded a specific volume (v_{water}) of 1284 m^3/kg and this corresponded to a pressure change of 150 Pa for the largest thermal picks (B) through (E) and 22 Pa for the smallest thermal pick (A). Even in this conservative assumption, and without considering any pressure-reducing mechanisms, the overall chamber pressure could reach at most 25% of the way towards the triple point.

4.1.2.2 Thermal Platen

The vacuum chamber contained a thermal platen on which the test rig was rigidly mounted. It was outfitted with a repeating two-dimensional arrangement of threaded holes spaced every 5.08 cm (2”). The vacuum chamber platen had a liquid nitrogen cooling line and resistive heaters that were controlled by an automated thermostat temperature control system but was limited to a minimum temperature of -100 °C. To achieve Europa-realistic ice temperatures of below -143 °C (the maximum equatorial temperature), the ice block had to be thermally insulated from the thermal platen and cooled externally in a liquid nitrogen bath. For initial non-cryogenic ice tests, the thermal platen was used and ice temperatures of -40 °C were achieved.

4.1.2.3 Insulating Mounting Bars

To rigidly affix the test rig components to the thermal platen while simultaneously providing thermal insulation, G-10 bars were used. The material G-10 was used for its low thermal conductivity of 0.288 W/m-k and its relatively high modulus of elasticity of 7 GPa to 20 GPa. These mounting bars were bolted into the thermal platen with spacers, creating significant thermal resistance that ensured the cryogenic components maintained their temperature throughout each test. Steady-state heat transfer through the G-10 mounting bars was modeled in SolidWorks, providing estimates that losses on the order 5 W would be observed when assuming the temperature differential between either side was 190 °C.

The conductive warming of the ice block is the limiting factor in the total duration of a test run. Given that no active means of cooling was used after the

cryogenic components were inserted into the vacuum chamber, test runs were limited to two hours so that the ice temperature stayed beneath -170 °C.

4.1.2.4 Base Mount

The base mount was used to rigidly attach the lower positioning slide to the insulating mounting bars. It was made of a sheet of 6.35 mm thick aluminum 6061 with bolt cutouts.

4.1.2.5 Positioning Slides

The positioning slides were Velmex MN10 lead screw slides driven by Vexta PK266 stepper motors. These slides provided the motion necessary for the insertion and extraction of the thermal pick as well as lateral translation that enabled multiple test locations on a single ice block. The stepper motors were rigidly mounted to the slide and their rotary motion turned a lead screw to linearly translate the carriage with high precision and accuracy.

The lower of the two slides had a stroke length of 50.8 cm and the carriage of the lower slide mounted to the frame of the upper slide. Positioning of the lower slide was used to move the thermal pick in a motion parallel to the surface of the ice. The upper slide had a stroke length of 25.4 cm and the carriage of the upper slide mounted to the custom frame and accompanying components. Positioning of the upper slide moved the thermal pick in a motion perpendicular to the surface of the ice.

4.1.2.6 Custom Frame

This custom frame was made of two distinct components machined from aluminum 6061. The purpose of the frame was to provide two structures that could move relative to one another in a single degree of freedom with minimal play and hold the necessary components. The degree of freedom defined the direction of

insertion and was perpendicular to the ice surface. The base of the custom frame was rigidly attached to the carriage of the upper slide. The top of the custom frame was attached to the base of the frame through the crossed roller bearing. The crossed roller bearing, constant force springs, and extension spring were all attached to the both the base and the top of the custom frame, although only the crossed roller bearing was a structural connection.

4.1.2.7 Crossed Roller Bearing

The crossed roller bearing was a Tusk Direct Inc. RX3-1 and it allowed the top of the custom frame and thermal pick to translate in the direction of insertion relative to the base of the custom frame with minimal friction. The crossed roller bearing had a range of motion of 12.7 mm between its two ground-out positions. The position of the crossed roller bearing was determined by a balance of spring forces and pick-to-ice forces. Forces developed through pick-to-ice interaction could result in a deviation of the crossed roller bearing position and deform the springs.

Prior to the implementation of the extension spring, the unopposed force of the constant force springs caused the neutral position of the crossed roller bearing to be in its forward ground-out position. This position was held until the thermal pick-to-ice force exceeded the constant spring force, after which displacement occurred. This introduced compliance to the insertion of the thermal pick and ensured that the thermal pick-to-ice force was less than or equal to the constant spring force. Without this compliance, it would have been possible to damage the test rig with the full blocking force of the positioning slides. Figure 25 shows the position of the frame and crossed roller bearing with the constant spring force (F_{cf}) and pick-to-ice forces

(F_{ice}). The stiffness and quantity of constant force springs used allowed for control over the insertion force.

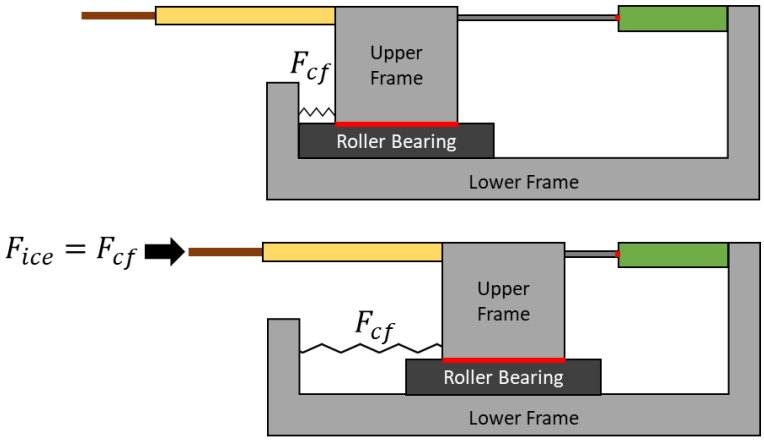

Figure 25: Illustration of constant force spring positions prior to the implementation of the extension spring. Component illustration style based on Figure 24. Not to scale.

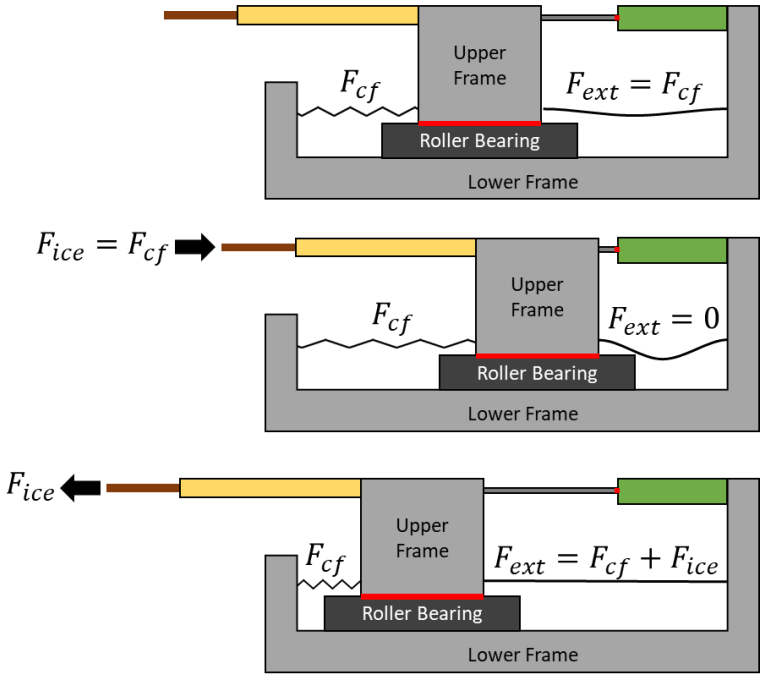

Figure 26: Illustration of spring positions after the implementation of the extension spring. Component illustration style based on Figure 24. Not to scale.

After the inclusion of the extension spring, the neutral position of the crossed roller bearing was determined by the force balance between the constant force and

extension springs. The initial force required for deformation of the extension spring was 53 N. Since this was greater than the constant spring force, the neutral position settled to where the extension spring was taut but undeformed. Figure 26 shows the position of the frame and crossed roller bearing with the addition of the extension spring force (F_{ext}).

The force generated from pick-to-ice pressure was supported by the constant force springs and their deformation caused the extension spring to hang loose and apply no force. This arrangement still ensured that the maximum force resisting pick-to-ice insertion was less than or equal to the constant spring force. However, pressure developed by an attempted but resisted extraction of the thermal pick (during anchoring) caused the extension spring to stretch and produce a high resistive force. The force of the extension spring varied linearly with its deformation while the constant spring force remained unaffected, which allowed control over the anchoring force by adjusting the slide position.

4.1.2.8 Constant Force Springs

The constant force springs were made of metal strips formed into a spiral shape. When the exposed end of the spring was pulled relative to the core of the spiral, the metal strip fed out like a tape measure. The restoring force that resulted from this deformation was a constant pulling force that was maintained until the neutral position was restored. The core of the spiral was attached to the base of the frame, while the exposed end was attached to the top of the frame. This placement led the constant force springs to produce a tension force throughout the entire range of motion of the crossed roller bearing, constantly pulling the top of the frame forward.

An external force applied to the thermal pick that was less than the constant spring forces was balanced by spring tension, but any force in excess thereof caused deformation of the springs and displacement of the crossed roller bearing.

The constant force springs had a tension force of 6.5 N and up to six springs could be used in a parallel arrangement, leading to a maximum net tension force of 39 N. The number of springs that were used on a given test set the maximum force that was applied between the thermal pick and the ice during insertion.

4.1.2.9 Extension Spring

The extension spring was added to introduce a controllable anchoring force. The extension spring was mounted on the rear of both the base and top of the frame. The extension spring could sustain a tension force of 53 N before deformation began, which was higher than what the constant force springs could provide. This meant that the extension spring could not be deformed prior to the anchoring phase.

During the anchoring phase, the tension force of the constant force springs and the pick-to-ice force would act to deform the extension spring. After the initial required total force of 53 N was reached, continued increase in the pick-to-ice force resulted in deformation of the spring according to its stiffness of 28N/mm. Adjustment of the test rig allowed the target maximum spring force of 130N to be reached at the forward ground-out position.

4.1.2.10 Thermally Insulating G-10 Tube

The thermal pick was connected to the frame by a G-10 thermally insulating tube. As with the insulating mount bars, G-10 was chosen for its thermally insulative properties and its structural rigidity.

Experimentation with thermal drilling in dry ice showed that stability of the thermal pick was the characteristic that had the greatest impact on thermal efficiency. To ensure a high degree of stability during insertion in the water ice test rig, a G-10 tube with an outer diameter of 19.1 mm and inner diameter of 6.35 mm was selected. This provided the desired level of rigidity, but also meant there was a large cross-section through which heat could conduct. The resulting conductive losses are discussed in Section 4.5.8.

4.1.2.11 Ice Mounting System

The ice mounting system was composed of a 30.48 cm x 10.16 cm x 15.24 cm block of aluminum, two aluminum and copper clamps, and an aluminum brace plate. The assembled mount can be seen in Figure 27.

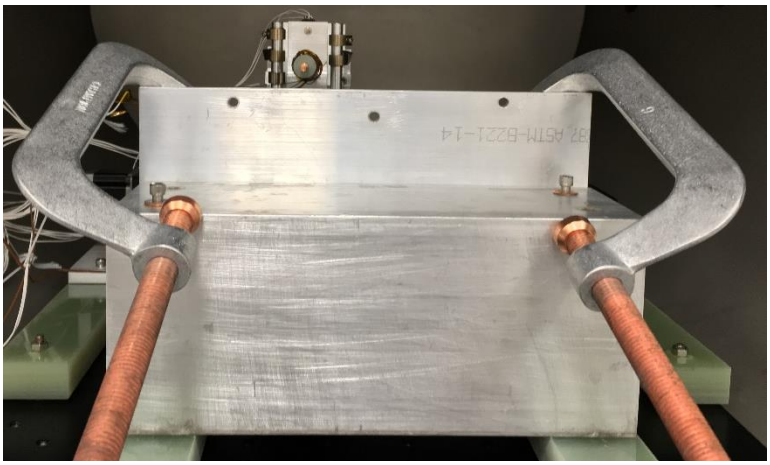

Figure 27: Ice mounting system with clamps.

The block of aluminum was used as a thermal medium through which the ice block was cooled. After the liquid nitrogen bath cooled the ice mounting system components down to temperatures below -170 °C, the aluminum block was bolted onto its G-10 insulating mounting bars. The clamps were used to secure the ice block

to the front plate of the aluminum block. The brace plate served to distribute the load of the clamps across the back surface of the ice block, mitigating cracking.

Previous iterations of the ice mounting system did not involve cryogenic cooling of all components. However, placing non-cryogenic components in contact with the cryogenic ice block resulted in severe degradation of the ice through thermal shock.

4.1.3 Test Rig Electronics

The electronic components associated with the test rig were the power supply, thermocouple reader, linear potentiometer, stepper motors and motor controller, heater relay, Arduino microcontroller, and computer with NI LabVIEW.

4.1.3.1 Vacuum Chamber Feedthroughs

The wiring of the thermocouple, linear potentiometer, stepper motors, and cartridge heater were all connected via feedthroughs installed into the vacuum chamber's ports. The linear potentiometer required a 5 V supply, ground, and an analog sensor wire. Each stepper motor required six wires connected to the motor controller. The cartridge heater required an input and output through which up to 1.5 A flowed. Finally, the K-type thermocouple feedthrough required one nickel-chromium and one nickel-alumel wire.

4.1.3.2 Linear Potentiometer

Displacement of the crossed roller bearing was measured as an analog voltage with a Midori America LP-20F-2K linear potentiometer. The body of the linear potentiometer was rigidly attached to the base of the frame while the piston was attached to the top of the frame as seen in Figure 24. As the crossed roller bearing

position changed, the piston stroke caused a varying voltage to be output on the analog signal line of the potentiometer. This analog voltage was linearly proportional to the displacement of the piston. The analog voltage passed through the feedthrough to the Arduino microcontroller and was converted into a digital value that was then sent to the computer. The digital signal was converted to a measured displacement using a linear scaling scheme that was calibrated using the linear positioning slides.

4.1.3.3 Power Supply

The power supply provided 0 V to 24 V to the cartridge heater and could sustain currents of up to 10 A. Since the heaters had a measured resistance varying between 18 Ω and 21 Ω, this corresponded to maximum heater powers of 27.4 W and 32 W when operating at 24 V. For any test, control over the power provided by the heater was achieved by cycling between the on and off states. However, between tests, the voltage supplied to the heater could be changed by adjusting the output voltage of the power supply.

4.1.3.4 Heater Relay

The heater relay was the component that opened and closed the circuit between the power supply and heater. The state of the relay was controlled by a 5 V signal sent from the Arduino.

4.1.3.5 Stepper Motor Driver

The stepper motor driver was a device that took in digital commands from the computer dictating the desired slide motion and enacted those commands through precisely timed current pulses to the stepper motors. The stepper motor driver was a model VXM-1 that was procured from Velmex, Inc. and controlled both stepper motors.

The stepper motors had velocity and acceleration settings and could accept commands of distance and direction. The velocity and acceleration settings were constant throughout any single commanded motion. The commanded velocity was maintained at 12.7 mm/s while the acceleration was tuned to the maximum possible setting without triggering motor stall.

Exceeding this velocity or over-tuning the acceleration resulted in missed steps and motor stall. This led to uncertainty as to the true pick position since the commanded position would have deviated from the actual position. Uncertainty in the position of the thermal pick was potentially problematic because the positioning slides could ground out and incur damage.

A limited number of pre-cryogenic tests were performed with velocities greater than 12.7 mm/s, though they often failed due to motor stall. During the anchoring phase when pick-to-ice forces developed torques on the carriages, the velocities were reduced to 1.27 mm/s to ensure motor stall was avoided.

4.1.3.6 Arduino

The Arduino MEGA was used for two purposes. Automated commands issued at the computer were passed through the Arduino to the relay to implement thermostat control logic of the heater. Also, the analog voltage from the linear potentiometer was read in, processed, and passed on to the computer in a digital form.

4.1.3.7 Thermocouple Reader

The thermocouple reader was used to read the analog voltage produced by the K-type thermocouple affixed to the tip of the thermal pick, as seen in Figure 15. The

thermocouple reader took the analog voltage and sent digital signals to the computer at a rate of 0.33 Hz. The thermocouple reader was an OmegaTherm HH309.

4.1.3.8 LabVIEW Computer

The computer with NI LabVIEW controlled the thermal pick position and the heater state, automated all necessary processes, and calculated the values derived from the measurements and commands.

The position of the thermal pick was altered by either manual or automated commands. Automation of the insertion phase occurred using a pre-programmed series of commanded steps and delays or through using manual inputs. While automation of the insertion of a thermal pick was used liberally in early testing, automated control lacked the adaptability necessary to handle ice failure. There was limited feedback from within the vacuum chamber, but the potentiometer reading, temperature, and auditory feedback were used to discern the processes that were occurring. Reacting to changes in the behavior of the thermal pick allowed for ice failure to be avoided and for new phenomena to be explored. All testing reported here was performed using manual commands, allowing for ad hoc changes to the step size, temperature, inter-step delay, and for test aborts to be rapidly enacted.

Control over the temperature of the thermal pick was achieved indirectly through the adjustment of the target temperature. The target temperature of the thermal pick was the setpoint around which thermostat logic was implemented in the LabVIEW script. Any temperature registered by the thermocouple reader that was greater than 1 °C above the target temperature would turn the heater off, while any temperature less than 1 °C below the target temperature would turn the heater on.

Finally, the LabVIEW computer calculated the net spring force and the actual tip position based on the position of the crossed roller bearing as measured by the linear potentiometer. It then recorded all values in a data file at a rate of 1.67 Hz.

4.2 Test Preparation

Test preparation required acquiring and preparing the ice block, cooling and mounting the cryogenic components, pumping down the vacuum chamber, mapping the ice surface, and warming the thermal pick to its operational temperature.

4.2.1 Ice Block Preparation

Testing was performed on either compressed ice blocks or optically clear ice that was frozen in-house. The compressed ice blocks were sourced from a local vendor, Apollo Ice Inc., and measured to have an average density of 0.85 g/cm^3. The density of the compressed ice blocks was below that of pure ice due to the presence of air. The effects of this air on the testing process are quantified in Section 4.5.10. The ice blocks were cut using a hand saw to conform to the test mount size. After the cutting process, the compressed ice block surfaces were thermally levelled. Thermal levelling was the process of pressing a flat metal sheet against the ice, causing selective melting until the ice surface conformed to the shape of the metal sheet.

Due to variability in the manufacturing process, density gradients were visible as differing air bubble densities. To ensure conservatism of the calculated ideal energy costs, thermal picks were always inserted into the densest section of the ice while the average measured density was used for any calculations.

The optically clear ice blocks were custom-frozen uniaxially in a freezer over the course of several days. When the water was frozen, air was pushed across an advancing freezing boundary. Uniaxial freezing pushed the air to one side, preventing it from becoming trapped. This led to a solid ice block density of 0.92 g/cm^3 and this clear ice was cut and thermally levelled in the same manner as the compressed ice blocks.

4.2.2 Cooling Phase

The cooling phase started by placing all the components of the ice mounting system in a liquid nitrogen bath in an insulated box. The test ice was placed on top of the aluminum block after it reached a temperature of 0 °C. The bottom of the aluminum block was kept submerged in the liquid nitrogen, making the aluminum block a thermal medium through which the ice was cooled to -170 °C. Using a thermal medium slowed the cooling of the ice which minimized thermal gradients and therefore thermal shock. When exposed directly to liquid nitrogen, the ice would crumble because of thermal shock. A thermal equilibration period of two hours was observed after the ice temperature measurement read below -170 °C. The two-hour timeframe was conservatively set based on transient thermal simulations of ice in SolidWorks.

After all the components of the ice mounting system and the ice block itself had cooled to below -170 °C, the ice was rigidly clamped to the ice mounting system. The entire ice mounting system was then lifted into the vacuum chamber and bolted down to the insulating mounting bars.

4.2.3 Pump-Down

The vacuum chamber was sealed and pumped down to vacuum once the cryogenically cooled components had been inserted and secured. While the surface of Europa is exposed to hard vacuum, such low pressures were not achievable with the hardware available. However, it was assumed that accurately simulating Europa's ices could be achieved at soft vacuum if the relevant thermodynamic region was reached. The behavior of water changes most dramatically at and around its triple point, but these changes slow as the pressure continually drops towards hard vacuum. The phase diagram of water can be seen in Figure 1. To ensure the thermodynamic behavior of water mimics operations on Europa, it was assumed that a pressure two orders of magnitude below water's triple point would suffice.

There were two mechanisms acting to reduce the pressure in the vacuum chamber. The first mechanism was the use of the vacuum chamber's roughing pump, which was run continuously throughout the entire testing process. This was the only mechanism causing the nitrogen and oxygen in air to be evacuated from the chamber. The second mechanism was the de-sublimation of gaseous water on the liquid-nitrogen cooled surfaces of the ice mounting system, given their temperature of -170 °C. This mechanism was invaluable to ensuring that the pressure did not significantly rise during testing by actively de-sublimating the gaseous water byproducts of thermal drilling. Oxygen and nitrogen have freezing points below -170 °C and so they would not de-sublimate on the ice mounting system surfaces.

Mapping of the ice surface using the thermal pick started at 600 Pa, since at that point melting of the ice would not easily occur. Testing was started at 6 Pa, which is two orders of magnitude below water's triple point and considered sufficiently close to hard vacuum.

4.2.4 Ice Surface Mapping

When the pressure in the vacuum chamber dropped below 600 Pa, the room-temperature thermal pick was first advanced by the positioning slides to initiate and sustain contact with an otherwise unused edge of the ice block. This contact would form a conduction path that cooled the thermal pick, but also avoided the warming of ice surfaces that were used for testing.

Once the thermal pick dropped to a temperature of approximately -10 °C, it was assumed that any further contact with the ice would result in sufficiently slow rates of heat exchange. The thermal pick was commanded to undergo a sweep to each future test location on the ice block. At each test location, the cold thermal pick was advanced until contact with the ice was observed as a measured displacement in the linear potentiometer. The calculated position of the thermal pick tip could then be used as the reference point for the surface of the ice at that test location.

Test locations were spaced 25.4 mm apart and always more than 25.4 mm from either edge of the ice block. This meant that a maximum of between 4 to 8 tests could be performed on a single ice block.

Once the ice surface position had been mapped for each test location, then the thermal pick would be warmed by the heater to its target temperature and positioned in front of the ice block prior to the first test run. The thermal pick was held at the

target temperature prior to the first test until the rate of heat loss settled. This heat loss was due to internal conduction into the G-10 insulating tube, which is discussed in Section 4.5.8.

4.3 Test Procedure

4.3.1 Test Philosophy

The goal of the thermal analysis was to gain an understanding of the energy expenditure required to insert a thermal pick beneath the ice where it could be used as an anchor. The actual operation of a thermal pick as would be performed on an icy moon involves warming from an initial temperature to the operational temperature, internal heat losses, the thermal drilling process during insertion, and cooling during anchoring. Since warming, internal heat losses, and cooling of the thermal pick are well defined behaviors, they can be estimated and modeled for any given thermal pick design.

The test procedure was designed to isolate and assess the thermal drilling process specifically. While steady-state thermal drilling processes have been modeled and validated experimentally, the transient thermal drilling process of an intermittent insertion of a thermal pick has not. This is because they involve multiple phase changes, changing boundary conditions, and rapid transient behaviors that are challenging to model. To isolate and experimentally measure the intermittent insertion and extraction processes, tests were based on a thermodynamic cycle containing only the thermal drilling process. These cycles allowed energy balance equations to be applied.

4.3.2 Test Procedure Variations

Controlled insertion and extraction tests made up the majority of testing, allowing the isolated assessment of thermal drilling and for the comparison of the effects of thermal pick design. Since the goal was to model a complete thermodynamic cycle, the insertion began when the thermal pick reached the specified target temperature and ended when the thermal pick returned to that same temperature. The insertion of the thermal pick was then followed either by thermal extraction of the thermal pick from the ice or anchoring. The test procedure used the following discrete processes.

1. Warming of the thermal pick to its target temperature.
2. Stepped thermal insertion into the ice with maintained temperature.
3. (a) Stepped thermal extraction from the ice with maintained temperature.

   OR

3. (b) Cooling of the thermal pick against the ice to halt melting/sublimation followed by attempted extraction of the cold thermal pick, inducing an anchoring load.

After extracting the thermal pick, it was possible to move to a new test location and perform another insertion. Tests were always concluded once one of the following conditions had been met.

1. All test locations mapped in the test preparation phase were used.
2. A sustained heat conduction path had formed between the thermal pick and the ice.
3. Ice failure or positioning slide stall were observed.

4.3.3 Testing Processes

The distinct thermal processes that occurred during the testing phase were warming, insertion, extraction, anchoring, and cooling.

4.3.3.1 Warming

The warming process was automated according to thermostat control logic. This required an amount of energy proportional to both the temperature differential of the process and the thermal pick's mass.

During a warming process, thermal gradients developed within the thermal pick and the G-10 insulating tube. Because of copper's high thermal conductivity, thermal gradients within the thermal pick were relatively shallow and short-lived. However, the low thermal conductivity of G-10 and the temperature differential between the test rig and thermal pick allowed the G-10 insulating tube to support steep thermal gradients. These conductive losses are explored in Section 4.5.8. The warming process was considered complete once conductive losses had slowed to a steady rate.

4.3.3.2 Insertion

The intermittent insertion process used a series of rapid insertion steps of the thermal pick into the ice separated by delay periods. A single insertion step was defined as a contiguous motion of the thermal pick that moves it deeper below the surface of the ice. During each insertion step, heat was rapidly transferred into the ice.

Between insertion steps, the thermal pick was held steadily in place for a period referred to as the delay period. If the thermal pick had maintained a sufficient temperature throughout an insertion step, then all ice that was physically in contact

with the thermal pick at the start of the delay period would melt or sublimate and escape to the surrounding vacuum environment. This formed a vacuum gap around the thermal pick that would effectively halt heat transfer into the ice and allow thermal re-equilibration of both the thermal pick and the cryogenic ice borehole. If the temperature of the thermal pick dropped below a critical threshold value during the insertion step, then the thermal drilling process would not be completed and contact with the ice would remain.

An incomplete thermal drilling process that left ice in contact with the thermal pick during the delay period would permit conductive heat transfer between the thermal pick and the ice. Incomplete thermal drilling processes were marked either by a partial insertion of the thermal pick and/or sustained heat transfer into the ice.

All heat transfers between the thermal pick and the ice were transient processes that reduced the temperature of the thermal pick. These heat transfers caused the internal temperature of the thermal pick to vary, despite maintaining thermostat temperature control.

The start of an insertion process followed the warming process and was timed to coincide with the heater cycling off. This meant that the thermal pick had reached its target temperature as measured by the thermocouple. There was some degree of thermal inertia within the thermal pick body that caused a lag between thermal events and changes in temperature registered at the thermocouple. The end of an insertion test was also timed to coincide with the heater cycling off to make the start and end condition of a test as similar in both temperature and internal thermal gradient as possible.

4.3.3.3 Extraction

For the tapered thermal picks (A) through (E), extraction was an intermittent stepwise rapid removal of the thermal pick from within the ice. Because re-frozen ice would lock the thermal pick within the ice, the thermal removal of ices was required during the extraction process. As was the case during the insertion process, heat was rapidly transferred into the ice during each step and if the thermal pick maintained a sufficient temperature then a vacuum gap would form around the thermal pick at each delay period.

4.3.3.4 Cooling

There were two distinct cooling processes. The first was the active cooling of the thermal pick used to halt thermal drilling and allow anchoring to begin. The second was the continuous passive cooling of the thermal pick during the anchoring phase when contact with the ice was maintained.

If an anchoring phase was attempted with a thermal pick at a high temperature, then the thermal pick would thermally drill the ice rather than be anchored against it. To cool the thermal pick prior to an anchoring phase, a modified intermittent insertion process was used. The heater was forced into and kept in its off state and a series of insertion steps of incrementally decreasing length were performed. The heat that was expended during these insertion steps progressively cooled the thermal pick until no further progress into the ice could be made. Once the temperature of the thermal pick had dropped such that thermal drilling would halt, the thermal pick was left in contact with the ice and allowed to undergo further

conductive cooling to a temperature below 0°C to ensure no localized melting could occur.

After an anchoring load had developed between the thermal pick and the ice, a transient conductive heat transfer between the thermal pick and ice occurred until steady-state was reached. While steady-state was not reached within the testing timeframe, it would be determined by the balance of heat transfer from the G-10 insulating tube and heat transfer to the cryogenic ice.

4.3.3.5 Anchoring

The measurement of the anchoring strength of a thermal pick occurred when a cooled thermal pick was commanded to extract from the ice after it had been inserted. An anchoring hold could only be achieved by a tapered thermal pick because re-freezing meltwater locks the tapered thermal picks within the ice. After undergoing a period of active cooling, a commanded extraction of the thermal pick would be resisted by the ice, developing forces that stretched the extension spring. The magnitude of the force was calculated based on the extension spring displacement and stiffness.

Using a series of short extraction steps, the anchoring load was applied by the extension spring until failure of the ice was observed or the maximum load of 130 N was reached. In all test cases the maximum load was reached, and failure of the ice was never observed.

4.3.4 Test Variables

The thermal pick design and operational characteristics that could be varied and have an impact on the behavior of the thermal drilling processes were the thermal

pick area, temperature, heater power, insertion pressure, total depth, step size, inter-step interval, and total time.

4.3.4.1 Thermal Pick Area

The thermal pick design characteristic that had the most straightforward impact on the thermal drilling behavior was the cross-sectional area of the thermal pick tip. The tip area was proportional to both the bored ice volume and the energy required during the thermal drilling process. The root diameter of a thermal pick determined its ability to withstand bending and tensile loads. Since tapered thermal picks were wider at the tip than the root, the tip area was a limiting factor for its strength.

Thermal picks (B), (C), and (D) had tip areas of 127 mm^2 that were the largest that tested. Thermal pick (A) was the smallest and had a tip area of 17.6 mm^2, representing the smallest pick that could be reliably machined. This thermal pick cannot support bending loads and so it could only be used with purely tensile loading. Thermal pick (E) had a two-tiered tip with a total area of 127 mm^2.

4.3.4.2 Temperature

The target temperature of the thermal pick varied between 0 °C and 160 °C. At temperatures below 70 °C, the melting regime was not noticeably sustained. The upper bound of 160 °C was based on a material limitation of the thermally conductive epoxy used.

The target temperature range that yielded melting represented only a small change in the total temperature differential relative to the ice temperature of -170 °C.

Despite that, varying temperature had dramatic impacts on the thermal drilling process.

4.3.4.3 Power

The instantaneous power supplied to the cartridge heater was varied by changing the voltage of the power supply within a range of 18 V to 24 V. The corresponding effect on power varied from approximately 16 W to 32 W, depending on the resistance of the specific cartridge heater.

While the instantaneous power supplied by the heater is of paramount importance to steady-state thermal drilling systems, its impact on the behavior of intermittent thermal drilling was limited. An insertion step lasted approximately one second, and at such short timescales, thermal inertia effectively prevented the heater from contributing substantially to the rate of heat transfer at the tip. This is discussed in Section 4.5.4

The instantaneous power supplied by the heater was only needed to return the thermal pick to its target temperature by the time of the next step. Between insertion steps, the duty cycle of the heater was as low as 5% for thermal pick (A) and as high as 50% for thermal pick (B). The duty cycle would rise dramatically if a sustained conduction path into the ice formed.

4.3.4.4 Insertion Pressure

The insertion pressure was varied by altering the number of constant force springs or the tip area. Each constant force spring provided 6.5 N and by using between 1 and 6 springs, the total insertion force could be varied between 6.5 N and 39 N. For the range in tip areas tested, this corresponded to pressures between

105 kPa and 1500 kPa. The total insertion force is relevant to the use of a thermal drilling device on an icy moon due to the low gravity that can make it difficult to apply loads. However, the insertion force and pressure did not impact the thermal behavior within the range of forces tested.

4.3.4.5 Total Depth

The depth of insertion was correlated to the bored ice volume and therefore the energy required for the insertion of the thermal pick. Insertion depths as shallow as 6.4 mm and as deep as 37.7 mm were successfully tested. While the length of the thermal pick determined the achievable total depth, ice failure mechanisms and the formation lip were also limitations on the total depth. The ice failure mechanisms described in Section 4.5.3 were functions of depth within the ice, while the formation lips described in Section 4.5.2.3 could physically obstruct motion, preventing further insertion of the thermal pick.

4.3.4.6 Step Size

The step size referred to the distance travelled in a single continuous motion during thermal drilling. The step size had a distinct effect on the efficiency of the thermal drilling process and was limited by the thermal capacity of the thermal pick. Small step sizes resulted in a large amount of vaporization, which approached the expected behavior of a sublimation thermal drill. Large step sizes drained the thermal pick's thermal reserves and resulted in the slowing or halting of the thermal drilling process.

Step sizes varying between 1 mm to 6 mm were successfully tested and ice failure mechanisms were shown to depend on step size and is explored in Section 4.5.3.

4.3.4.7 Inter-Step Interval (Delay Period)

The inter-step interval was the length of time the thermal pick was held steady between insertion steps. The lower bound for the delay between steps was determined by the tolerance of the ice block to thermal shock. Heat was introduced into the ice during each insertion process and caused thermal gradients develop in the ice. These thermal gradients in the ice dissipated over time during the delay period. If insertion steps were taken with only a short delay between steps, then the thermal gradients in the ice would build. Since ice is a brittle material, excessive thermal gradients caused thermal shock. Delays between 10 to 110 seconds were tested and did not have an impact on the thermal drilling process past causing thermal shock.

4.3.4.8 Total Time

The total time taken for an insertion process was measured as the time between the first insertion step and the thermal pick returning to its target temperature after the final step. The total time was a function of step size, inter-step interval, and total depth. The total time did not have an impact on the thermal drilling process.

4.4 Theoretical Thermodynamic Analysis

4.4.1 Fundamental Thermodynamic Properties

For water to melt, the pressure and temperature must both be above its triple point. The pressure of water's triple point is 611 Pa, above which water can exist in a

liquid state. While this pressure is only 0.6% of Earth's atmospheric pressure, it is significantly above Europa's atmospheric pressure. The temperature of water's triple point is 0.01 °C, which is also well above Europa's mean surface temperature of -183 ˚C.

In this project, Europa's surface conditions were simulated in testing by reaching a chamber pressure of below 6 Pa and an ice temperature below -170 °C. However, the local temperature and pressure around the thermal pick were affected by thermal drilling. Thermal drills often operate in a steady-state mode where heat is transferred into the ice at a relatively constant rate throughout the device's operation. By contrast, the thermal picks used in this study store large amounts of thermal energy within a high temperature copper body and conductively release that thermal energy into the ice within a short period of time. This rapid introduction of heat to a cryogenic water ice surface under vacuum causes a transient set of processes as the local temperature and pressure change with time.

4.4.2 Conductive Warming

Before the onset of pick-to-ice contact, the ice will be at the ambient cryogenic temperature. Once contact has been initiated, conduction between the thermal pick and the ice will cause the local ice to warm. This requires a specific energy of 0.8 J/g-K (-170 °C) to 2.1 J/g-K (0 °C) and has a thermal conductivity of 5 W/m-K (-170 °C) to 2 W/m-K (0 °C). The variation of specific energy and thermal conductivity are approximately linear within the relevant temperature range. Ice warming causes the thermal conductivity to decrease while the specific heat increases and both trends serve to slow the rate of further warming of the ice.

4.4.3 Sublimation and Further Warming

The surface of Europa is constantly undergoing a slow background rate of sublimation and any additional warming of the surface ice increases the rate at which sublimation occurs. This sublimation occurs to the most energetic surface molecules in a manner akin to evaporation and requires the latent heat of vaporization, which has the high energy cost of 2835 kJ/kg. Since only the highest energy molecules will sublimate, the remaining ice will be relatively less energetic overall than before each sublimation event, which has a cooling effect. The molecules that sublimate will also have a significantly higher specific volume as a result of their phase change.

Since sublimation is inhibited by external pressure, a negative feedback loop forms where sublimation increases the local pressure and cools the remaining ice, both of which inhibit further sublimation. If the surface temperature is warmed to the sublimation temperature, then the rate of sublimation rapidly increases in a manner akin to boiling. If heat is rapidly transferred to the surface ice, then a cycle of increasing temperature, sublimation, and increasing local pressure will occur, which couples the pressure and temperature of the ice.

4.4.4 Melting and Further Warming

Once the process of sublimation has warmed the surface ice and produced enough gaseous water for the local pressure to reach the triple point, melting can occur. As soon as the triple point is reached, liquid water can be sustained. Melting immediately becomes the dominant phase transition because it is energetically preferable, requiring only 334 kJ/kg.

Melting is not a self-sustaining process in a vacuum given that the specific volume of liquid water is slightly less than that of ice. This specific volume decrease means that transition into liquid causes the local pressure to drop, so the local pressure can only be sustained by a separate process. The processes that can sustain the local pressure are heat-induced boiling of liquid water or pressure-induced boiling of liquid water.

Given that a vacuum atmosphere will always surround these localized regions of increased pressure, the liquid and gas produced will accelerate towards the surrounding vacuum. As meltwater moves towards the surrounding vacuum, then unless it makes contact with an external boundary (hot thermal pick wall or cryogenic ice surface), it will undergo the following processes that serve to sustain the localized pressure environment.

4.4.4.1 Adiabatic Pressure Drop and Boiling

Once the process of sublimation has increased the local pressure to above the triple point, heat transfer between the thermal pick tip and the ice will cause the surface ice to melt. This meltwater is mobile and accelerates in the direction of decreased pressure. Since pressure is what inhibits the boiling of meltwater, as the meltwater advances into a lower pressure region, boiling will be induced. The pressure at which this occurs is dependent upon the temperature of the meltwater. Due to conservation of energy, boiling of high energy meltwater molecules leaves the remaining meltwater at a relatively lower average energy state. This can be viewed as a cooling effect on the remaining meltwater following Equation (13).

$$h_{vap}\Delta m_{vap} + c_p m_{liq}\left(\Delta T_{liq}\right) = 0 \tag{13}$$

$$\Delta m_{vap} > 0 \quad (14)$$

$$\Delta T_{liq} < 0 \quad (15)$$

The mass of water that turns to steam is (Δm_{vap}), the latent heat of vaporization (h_{vap}) is 2500 kJ/kg for boiling, the specific heat of liquid water is (c_p) is 4.2 kJ/kg-K, the mass of liquid remaining after boiling has occurred is (m_{liq}), and the change in temperature of the remaining liquid relative to its initial temperature is (ΔT_{liq}).

The boiling of meltwater results in a large increase in specific volume and therefore helps sustain the local pressure environment. The outgoing flow at this point will be two-phase with both liquid water and gaseous water being present simultaneously. This process continues as the escaping mixture of liquid water and gaseous water advance to regions of further reduced pressure. Boiling continues until the pressure and temperature of the remaining meltwater drop down to the triple point.

4.4.4.2 Adiabatic Triple Point Phase Transition

Once the outgoing flow reaches a region of pressure that is at the triple point, the remaining liquid cannot reduce in pressure any further without triggering a phase change. Further vaporization will only be possible for the highest energy liquid water molecules, while the remaining molecules are forced to freeze. Conservation of energy dictates the relative rates of vaporization and freezing according to Equation (17). The latent heat of vaporization (boiling) and fusion (freezing) are $\left(h_{vap}\right)$ and (h_{fus}), respectively. While all of the water described in this process begins in the liquid state with mass (m_{liq}), the final products of gas and ice have a

mass described by (Δm_{vap}) and (Δm_{ice}), respectively. The latent heat of vaporization here is the transition of liquid to gas at the triple point and 0 °C, which requires approximately 2500 kJ/kg.

$$\Delta m_{ice} + \Delta m_{vap} = m_{liq} \tag{16}$$

$$h_{vap}\Delta m_{vap} = h_{fus}\Delta m_{ice} \tag{17}$$

$$\Delta m_{vap} = \frac{h_{fus}}{h_{fus} + h_{vap}} m_{liq} \tag{18}$$

$$\Delta m_{ice} = \frac{h_{vap}}{h_{fus} + h_{vap}} m_{liq} \tag{19}$$

Both vaporization and freezing involve an increase in specific volume and will contribute to sustaining the local pressure. Once this process begins there will be all three phases of water present in the outgoing flow. This process will continue with the local pressure balancing around the triple point pressure while the specific volume of the water increases as it expands into the surrounding vacuum. This process ends when there is no liquid water left to undergo further phase transition. This is a material-specific ratio and for water the solid-to-gas mass ratio is approximately 7.5 to 1.

4.4.4.3 Adiabatic Sublimation

Once the pressure has dropped below the triple point, the remaining gas and ice are relatively less volatile. While the gas has no pressure-induced phase transitions left to undergo, the temperature of any ice formed through phase transition at the triple point will be at approximately 0 °C. While the ice does not itself undergo expansion, its inertia and the adjacent gas flow can carry the ice to regions of reduced pressure. A reduction in local pressure will cause the ice to undergo sublimation. This

sublimation helps sustain the local pressure while the temperature of the ice decreases. The ice progressively reduces in temperature and pressure until it equilibrates to the ambient conditions.

The temperature drop experienced by ice undergoing sublimation is calculated by applying the conservation of energy principle and depends on the specific heat of ice and the sublimation energy according to Equation (20). The energy required for the sublimation phase change (h_{sub}) is 2835 kJ/kg, the specific heat of ice (c_p) is 2.1 kJ/kg-K at 0 °C, the temperature change of the ice during this process is (ΔT_{ice}), and the mass of gas that is produced in this process and the mass of ice that remains afterwards are (Δm_{vap}) and (m_{ice}), respectively.

$$h_{sub}\Delta m_{sub} + c_p m_{ice}(\Delta T_{ice}) = 0 \tag{20}$$

Once the ice equilibrates to the ambient conditions, sublimation will continue at the natural background rate.

4.4.4.4 External Boundaries

At any point in the processes described above, liquid, gas, or ice may contact the boundaries of the thermal pick or cryogenic ice surface. At the boundary of the thermal pick, gas may warm, liquid may warm and/or boil, and ice may warm and/or melt. Which process results from contact with a boundary depends on the boundary temperature, the local pressure, and the temperature and phase of the water. The energy required for warming or phase transition against the thermal pick walls is an energy loss for the thermal pick.

At the boundary of the ice, gas may cool and/or condense, liquid may cool and/or freeze, and ice may cool. The reciprocal heating of the cryogenic ice boundary

when in contact with the outgoing flow can result in ablation of the ice surface. However, changing the phase of the outgoing flow can result in buildup of the ice surface. While only ablation of the borehole occurred in dry ice as described in Section 3.3.4, cryogenic water ice tests resulted in substantial build-up of ice formations in and around the borehole as described in Section 4.5.2.3.

This boundary condition is particularly active when it aligns with adiabatic triple point phase transition where the escaping flow is three-phase. During this phase, liquid is readily separating into solid ice and gas, which allows for the rapid buildup of new ice along the existing ice boundary.

When a thermal pick is inserted below the surface of the ice, the balance of ablation and buildup of the ice surface is of vital importance. If the outgoing flow is sufficiently cool and warming at the thermal pick boundary is insufficient, then buildup of ice can encroach on the thermal pick. The encroachment of ice onto a thermal drill has been observed in previous works [40] [41], although this phenomenon can be mitigated by maintaining a sufficient thermal pick wall temperature. A high temperature thermal pick wall will warm the adjacent outgoing flow and prevent encroachment of the ice.

4.4.5 The Ideal Thermal Drilling Process

The energy expended by a thermal pick for the purposes of the thermal drilling process can be separated into the essential energy required to complete the process and the energy that is expended but not inherently required to complete the process. The former is considered the ideal energy and when taken by itself is a description of a perfect thermal drilling process. The latter is considered the energy

loss of the system and this is sought to be reduced through the design and operational characteristics of the thermal pick.

The ideal energy required is a function of the volume of ice that must be removed to make room for the thermal pick and the optimal thermal processes that would cause the removal of the ice. A relevant consequence of entering a melting regime rather than a sublimation regime is in the ideal energy required for progress of the thermal pick into the ice. The theoretical energy expended during the operation of a sublimation-based thermal drill (E_{sub}) is shown in Equation (24) and is compared to the heater output energy (E_o) in Equation (25). Equation (21) describes the volume of ice that must be thermally removed and is dependent on the depth of insertion (D) and the tip area for tapered thermal picks. This volume is used in Equation (22) to define the mass of ice that must be thermally drilled using the density of the ice (ρ_{ice}).

$$V = D\pi {r_{tip}}^2 \tag{21}$$

$$\Delta m_{sub} = V\rho_{ice} \tag{22}$$

$$E_{i,sub} = (h_{sub} + c_p \Delta T_{ice})\Delta m_{sub} \tag{23}$$

$$E_{sub} = E_{i,sub} + E_{con}\left(t_{contact}, T_{ice}, T_{pick}\right) + E_l \tag{24}$$

$$\eta_{sub} = \frac{E_{i,sub}}{E_o} \tag{25}$$

The first term of Equation (24) is the ideal sublimation energy cost ($E_{i,sub}$) to warm the ice to its sublimation temperature and induce the phase transition and is proportional to the mass of ice that is thermally drilled, all of which is assumed to be sublimated in the idealization. The second term is the conductive loss into the bulk

cryogenic ice (E_{con}) and is a function of time and temperature. The third term is the loss from the thermal pick to the outgoing flow (E_l) and is a function of time, gap width, and flow properties. This can be compared to the ideal energy required for the operation of a melting-based thermal drill ($E_{i,melt}$) that is shown in Equation (26).

$$E_{i,melt} = (h_{fus} + c_p \Delta T_{ice}) \Delta m_{melt} \tag{26}$$

$$E_{melt} = E_{i,melt} + E_{con}\left(t_{contact}, T_{ice}, T_{pick}\right) + E_l \tag{27}$$

$$\eta_{melt} = \frac{E_{i,melt}}{E_o} \tag{28}$$

Equations (25) and (28) show the efficiency of the sublimation and melting processes, respectively. In the definition of the efficiency of a process, the idealized theoretical minimum energy expenditure of the thermal drilling process (numerator) is compared to the energy spent in an experiment or simulation (denominator).

The ideal energy cost for warming and phase transition is reduced for melting relative to sublimation due to the phase transition energy costs occurring, whereas the total energy expended is impacted by other factors. Operating in the melting regime rather than the sublimation regime impacts both the conductive and wall losses.

4.4.6 Ice-Based Conductive Losses

The energy that is conductively transferred into the bulk ice (E_{con}) represents a transient heat transfer process that can consume a large amount of heat from the thermal pick. To melt or sublimate ice that has an initially cryogenic temperature, it must first be warmed. This warming inherently creates a thermal gradient in the ice relative to the surrounding cryogenic ices, which in turn causes conductive heat

transfer into the surrounding ice. The rate of conductive heat transfer is proportional to how steep the thermal gradient is.

For a thermal drilling system, at the moment when contact is initiated, the thermal gradient will be steep as the immediately adjacent ices are heated, but the surroundings will still be cryogenic. The high initial rate of heat transfer quickly warms the nearby ice, smooths out the thermal gradient, and leads to reduced rates of conductive heat transfer. Over time, the high initial rates of heat transfer will slow. Any energy that is transferred in this method is provided indirectly by the thermal pick heater and is an energy loss mechanism.

The steady-state rate of conductive heat transfer has been analytically modeled [29] and represents the largest single energy expenditure for currently developed steady-state thermal drills. To mitigate these losses, it is necessary to reduce either the total time or temperature of contact between the thermal pick and the ice. However, these are inversely related, since decreasing temperature increases the insertion time.

The intermittent insertion approach proposed in this study transfers heat into the ice for only short periods of time. This means that conductive heat transfer rates will be high, but the total energy transferred will be low.

4.4.7 Wall Losses

Heat transferred into the outgoing water flow represent another loss mechanism of the thermal drilling process. Wall losses occur when the outgoing flow contacts the thermal pick boundary which can be seen illustrated in Figure 28. Wall losses are functions of the ice borehole geometry and temperature, thermal pick wall

geometry and temperature, and outgoing flow temperature, phase, and pressure. Each of these characteristics, including the shape of the ice borehole, changes rapidly with time, making it difficult to model this process.

Recent computational fluid dynamics models have made steps towards modeling flows that cross the triple point [47] [48] in a similar fashion to the water flow at play here. However, even these state-of-the-art thermodynamic models do not account for the time-varying boundary conditions that are present. Variation in the temperature of the boundary is caused by the transient behavior of both the thermal pick and the ice borehole and will impact flow parameters. Ablation or buildup of the boundary affects the geometry of the gap and will also affect flow parameters. However, despite the lack of a model, the impacts of wall losses can still be explored.

If wall losses are to be reduced, it is through the reduction of heat transferred through the walls of the thermal pick and into the outgoing flow. However, even in the case where boundary losses were entirely negated, this would only represent a reduction in energy of 13.2% for the current system as demonstrated in Section 4.6.

Wall losses are to some degree bounded by the case where wall losses cause the vaporization of the entire outgoing flow. If all the outgoing flow is vaporized by wall heating ($E_{l,max}$), then the energy expended by the thermal pick to change the water phase approaches the energy cost of the ideal sublimation process.

$$h_{fus}\Delta m + E_{l,max} \approx h_{sub}\Delta m \tag{29}$$

While vaporization of the entire outgoing flow can be considered a bounding case matching $\eta_{sub} = 1$ in Equation (28), the energy that is expended during

experimental testing is below this bounding case, suggesting that the outgoing flow is not entirely vaporized.

4.4.8 Thermal Pick Warming

In addition to the sum of energy that is transferred into the water through thermal drilling ($E_{i,melt}$), conduction (E_{con}), and wall losses (E_l), it is also required that the thermal pick be warmed to and held at its operational temperature from its initial temperature. This warming energy cost is proportional to the temperature differential required. For an autonomous Europa rover moving slowly across the surface and taking infrequent steps, the initial temperature can be as low as the cryogenic ambient temperature, leading to non-negligible energy costs. For a copper-bodied thermal pick with a specific heat ($c_{p,Cu}$) of 0.385 kJ/kg-K, the warming energy cost (E_w) for a temperature change of -170 ℃ to 160 ℃ (ΔT_{pick}) is 1.13 kJ by Equation (30) for the thermal pick (A) given its mass of 8.93 g. The operational temperature must also be maintained against the effects of conductive losses internal to the mechanism itself ($E_{con,int}$), which represents a time dependent loss by Equation (31). Including these additional energy expenditures, the total energy cost (E_{total}) of the insertion of a thermal pick into the ice is given by Equation (32).

$$E_w = (c_{p,Cu}\Delta T_{pick})m_{pick} \tag{30}$$

$$E_{con,int} = f(t_{total}, \Delta T_{pick}) \tag{31}$$

$$E_{total} = E_{i,melt} + E_{con} + E_l + E_w + E_{con,int} \tag{32}$$

4.4.9 Intermittent Thermal Drilling

The thermodynamic response to the thermal pick insertion step can be viewed as a set of transient processes. Initial sublimation leads the way to melting and back to sublimation again in a process that takes place in approximately one second. The details of the insertion process are inferred from test results and observations and this process is divided into nine phases as shown in Figure 28. Each phase of the insertion process is described below in more detail.

A. Prior to contact with the ice, the thermal pick is at a raised temperature and the ice is cryogenic. The local pressure is at vacuum, matching the ambient conditions.
B. Upon contact with the ice, the thermal pick rapidly transfers heat into the adjacent ice. A thermal gradient forms within ice and causes internal conduction in the ice.
C. Once the surface ice reaches the sublimation temperature corresponding to the ambient pressure, sublimation will accelerate. Sublimation develops a local pressure gradient that accelerates the gaseous water towards the vacuum.
D. Sublimation creates a gas barrier between the thermal pick and the ice due to the Leidenfrost effect. The thermal pick continues to transfer heat into the ice through convection and the resulting sublimation increases the local temperature and pressure.
E. Once sublimation has caused the local pressure to reach the triple point, melting can begin. Meltwater forms a barrier between the thermal pick and the ice, through which heat is transferred by convection. The pressure gradient

causes the meltwater to accelerate to regions of lower pressure and pressure-induced phase change processes will occur, yielding gas and ice at low pressure.

F. As meltwater reaches the ice surface where rapid expansion can occur, it will undergo flash separation into gas and ice. The existing ice surface will act as a catalyst against which the meltwater will freeze, building up the formation lip.

G. As the thermal pick extends deeper below the surface of the ice, meltwater will no longer be able to reach the top of the formation lip, halting its growth. Due to the increasing thermal pick depth, the exposure of the outgoing flow to the borehole and thermal pick walls is also increased. It is this region in which the wall losses occur.

H. Once motion of the thermal pick stops, the pressure gradient rapidly collapses until no liquid water is present, after which gas will still be drawn out towards vacuum or de-sublimate against any cryogenic ice surface.

I. After the gas has been evacuated, heat transfer between the thermal pick and ice will effectively halt and both bodies will thermally equilibrate.

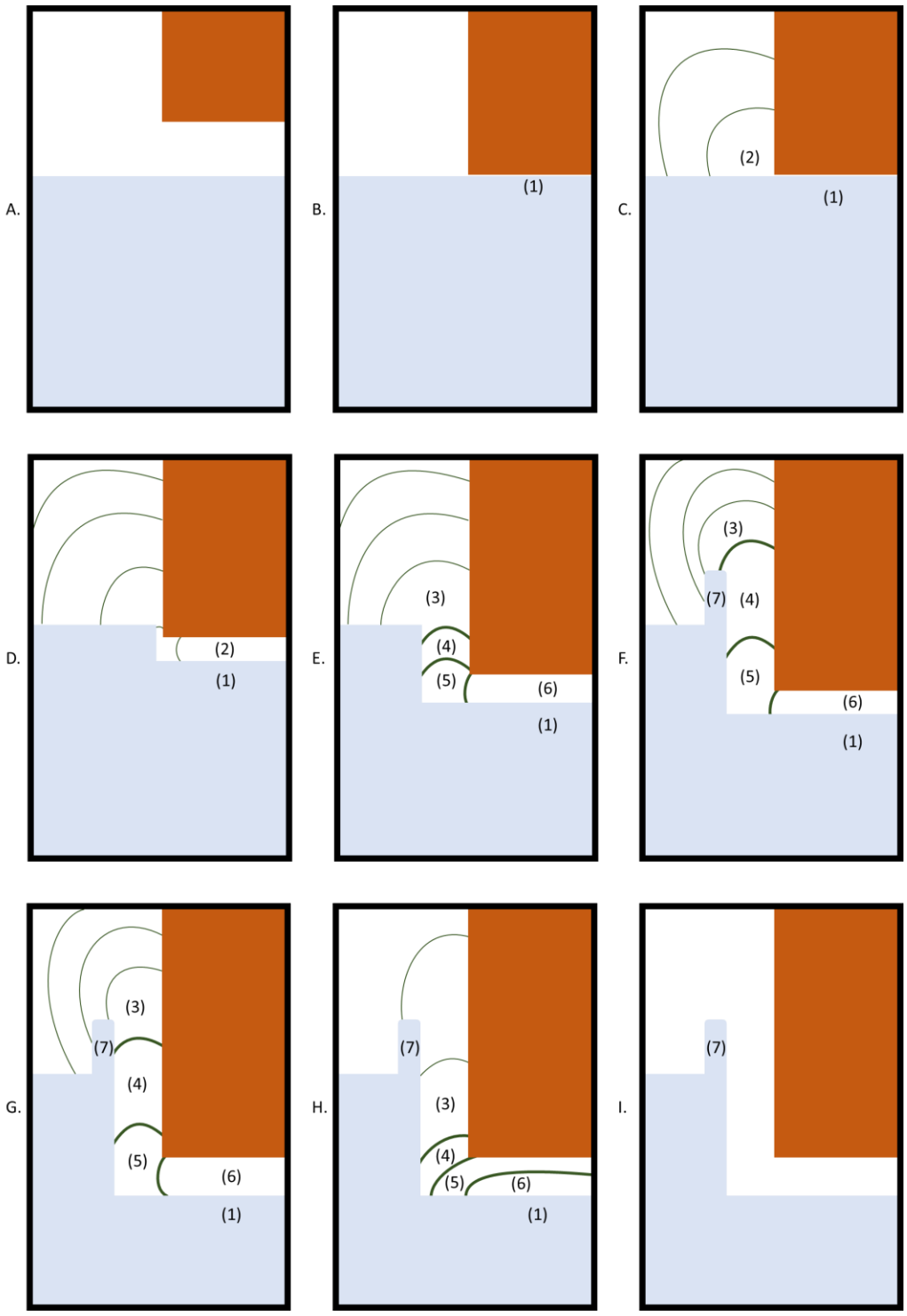

Figure 28: Illustration of the insertion process showing (1) conduction into the ice, (2) gaseous water, (3) ice and gaseous water, (4) triple phase water, (5) liquid water and gaseous water, (6) liquid water, and (7) the formation lip. Lines of constant pressure shown with thickened lines indicating phase change boundaries, ice is shown in light blue, and thermal pick shown in brown.

4.5 Results and Analysis

4.5.1 Overview

Cryogenic vacuum water ice test results come from analyzing three sensor data streams, the recorded timing of events, and a post-test visual inspection of the ice block. The three real-time data streams are the thermocouple temperature (the location of which is shown in Figure 15), the commanded position of the thermal pick tip, and the spring displacement (indicating pick-to-ice contact) as measured by the linear potentiometer. The energy expenditure was calculated as the product of the heater power and the duration over which the heater was on. All efficiencies listed are with respect to the ideal melting process defined in Equation (26) unless otherwise specified. Figure 29 and Figure 45 are example data streams showing tests of thermal pick insertion, extraction, and loading while in cryogenic water ice under vacuum.

Distances are measured relative to the position of the ice surface that is measured during the ice mapping phase described in Section 4.2.4, with positive values indicating insertion beneath the ice surface. The position was calculated by taking the commanded linear slide position and adjusting by the linear potentiometer reading, which is a measure of spring displacement. The commanded linear slide position was accepted at the end of a step, meaning that until a step is completed, displacements of the linear potentiometer are interpreted as pick motion in the opposite direction.

The neutral position of the linear potentiometer is a force-balanced position determined by the extension and constant springs used. Positive spring displacements about the neutral position indicate that insertion into the ice is being resisted and the

constant force springs are applying an insertion force. Negative spring displacements about the neutral position indicate that extraction from the ice is being resisted and the extension spring is applying a loading force.

The measured temperature determines the cycling of the heater. Any temperature above/below the target temperature value means that the heater was turned off/on, respectively, unless otherwise specified. Decreasing temperature was due to the intended energy cost of insertion during an insertion step, internal conduction into the test rig by way of the G-10 thermally insulating tube, convective heat loss to the outgoing flow, or conduction into the ice. Conduction into the ice occurred during anchoring, when an insertion step was not fully completed, or when failure of the ice changed its shape and created sustained physical contact between the thermal pick and the ice. Increasing temperature was exclusively the result of heater power being conducted into the thermal pick body or thermal inertia within the thermal pick resulting from a previous heater power input.

4.5.2 Insertion Step

The efficiencies and variables associated with each insertion test are shown in Table 3.

Table 3: Insertion test data with efficiency measured relative to an ideal melting process. The term β is a metric of resilience to failure of the ice and is defined in Equation (33). Explanation of Notes can be found in Appendix A.2.

Test [#]	Temp [°C]	η	Step [mm]	Depth [mm]	Time [sec]	Pressure [kPa]	Period [sec]	Pick Type	Fail Y/N	Notes
1	90±10	.35	6.35	12.3	182	375	90	A	Y	Low β
2	100	.1	5.715	18.6	284	375	45	A	Y	Low β
3	120	.15	1.27	24.8	550	1499	27.51	A	Y	Low β
4	120	.27	2.54	24.8	369	1499	41	A	N	
5	120	.35	3.81	27.5	216	1499	30.8	A	N	
6	120	.18	5.08	28	324	1499	40	A	Y	Low β
7	120	-	-	16.5	-	1499	20	A	N	Latent heat insertion
8	100	.16	1.27	18.5	353	1499	23.2	A	Y	Low Temp vs. Depth
9	140	.26	2.54	28.7	287	1499	24	A	N	
10	140	.32	3.81	29.3	255	1499	27	A	N	
11	140	.52	5.08	19.05	193	1499	30	A	Y	Low β
12	100	-	-	6.37	-	1499	7	A	N	Latent heat insertion
13	140	.25	2.54	26.45	305	1499	27.2	A	N	
14	140	.39	3.81	26.88	217	1499	24.4	A	N	
15	140	.52	5.08	33.49	164	1499	20.6	A	N	
16	140	.07	2.54	11.5	202	749	10	A	Y	Clear Ice: Low period
17	140	.05	3.81	15	370	749	27	A	Y	Clear Ice: Conduction path formed
18	160	.23	3.81	14.7	192	749	30	A	N	Clear Ice
19	160	.32	3.81	11.8	100	749	15	A	Y	Clear Ice: Low period
20	160	.29	3.81	32.2	254	749	26	A	N	
21	160	.36	2.54	28.55	180	749	28	A	N	
22	160	.34	6.096	28.5	143	749	30	A	N	
23	160	.26	3.81	21.6	119	749	10	A	Y	Low period
24	160	.26	5.08	29.4	350	749	29	A	N	
25	120	.46	3.81	28.1	358	211	41.25	B	N	
26	120	.29	3.81	37.7	704	105	66	B	N	
27	120	.33	2.54	26.2	684	105	55	B	N	
28	120	.29	3.175	19.9	768	105	110	B	N	
29	120	.34	3.175	26.29	8876	105	90	B	Y	Low Temp vs. Depth
30	80	-	3.175	3.11	46	105	-	C	Y	First step failure
31	80	.21	1.588	10.67	482	105	60	D	Y	Low β
32	85	-	6.35	7.26	38	105	-	E	Y	First step failure
33	85	-	6.35	6.94	34	105	-	E	Y	First step failure
34	85	.32	3.81	13.3	239	105	60	E	Y	Low β

Energy efficient insertion was achieved when the melting regime was triggered and the creation of sustained conduction paths into the ice was avoided. These conduction paths were observed as a sustained displacement of the spring and/or a temperature drop of unexpectedly large size or duration. A successful insertion step avoiding sustained conduction was only possible when the thermal pick had sufficient thermal capacity to complete its entire step and also melt or sublimate any adjacent ices until a vacuum gap had formed as shown in Stage I of Figure 28. Once a vacuum gap had formed around the thermal pick, only inefficient radiative heat transfer remained, allowing time for the thermal pick to warm up and for thermal gradients to settle.

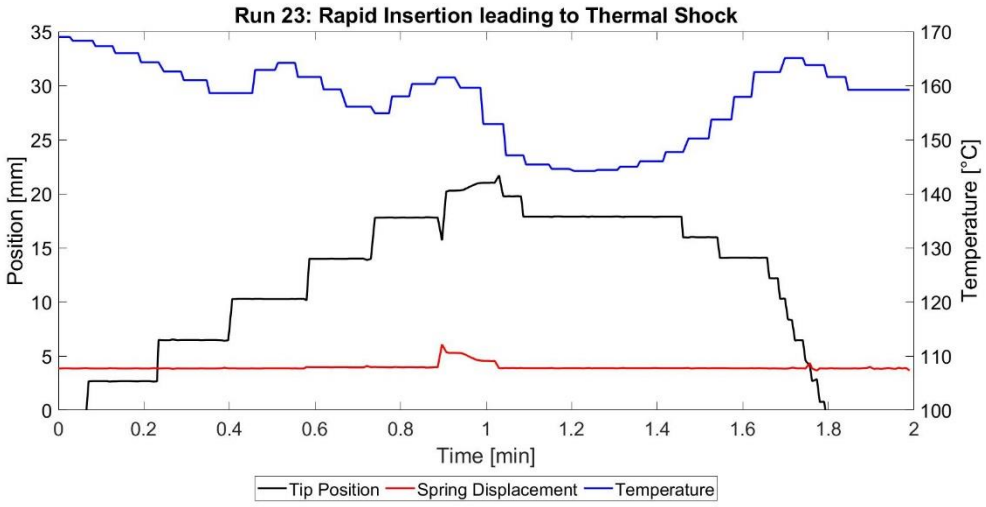

Figure 29: Test run 23 using thermal pick (A). The thermal pick was inserted with short inter-step delay leading to thermal shock failure, heat loss, and extraction.

To achieve the commanded velocity of 12.7 mm/s during insertion, the necessary power transfer rates are higher than the 30 W heater alone can support for longer than brief intervals. However, the high thermal conductivity and thermal

capacity of the copper pick allows these high rates of heat transfer for short periods but are not sustainable. The intermittent insertion approach allowed these high heat transfer rates to be achieved and enabled the triggering of the melting regime.

The insertion step was performed with applied forces between 6.5 N and 35 N depending on the number of constant force springs used. This insertion force compares favorably to mechanical anchoring systems like the ISEE [23] which requires between 60 N and 180 N of applied force. For rovers on planetary bodies with low gravity, this is an important benefit of thermal drilling systems.

4.5.2.1 Thermal Stall

The high rates of heat transfer during an insertion step cause the thermal pick to cool rapidly during active use. This cooling limits the speed of thermal drilling and can halt the thermal drilling process entirely. A thermal pick that is cooling off due to insertion will have progressively reduced melting rates, so conduction loss into the surrounding cryogenic ice can become dominant. This phenomenon is referred to as thermal stall. Once thermal stall occurs, thermal drilling progress into the ice halts, conduction into the ice will persists, and the thermal pick continues to cool.

If insertion steps are sufficiently short, then thermal stall can be avoided. A short insertion step intentionally halts thermal drilling by stopping the motion of the thermal pick so that conduction paths can be broken during the inter-step delay. Experimental testing showed that thermal stall could lead to ice failure but could be avoided with increased temperature and/or decreased step length (see Appendix A.3).

4.5.2.2 Insertion Efficiency

The measured efficiency of thermal pick insertion was calculated by taking the ratio of the measured heat output by the heater and the heat required for the ideal melting process, as shown in Equation (26). The efficiency of the insertion tests performed are shown in Table 3 and Figure 30. The measured efficiency range is between 0.05 and 0.52, while the efficiency of tests without ice failure range between 0.23 and 0.52. Given that the ideal energy cost of sublimation is 4.6 times higher than that of melting, any test with an efficiency greater than 0.21 implies melting rather than pure sublimation.

Figure 30: Efficiency relative to ideal melting vs. insertion step size for all water ice insertion tests.

The efficiency of insertion was influenced by losses directly into the bulk ice when a permanent conduction path was formed. Ice failure occurred in nearly half of all tests, resulting in the formation of a permanent conduction path. These tests were subsequently aborted since conductive losses would persist, prevent further progress, significantly reduce efficiency, and often negatively affect the structure of the ice.

The efficiency of the insertion process is shown in Figure 31 through Figure 36 against all additional test variables. Heater power was notably excluded given its limited negligible effect on an intermittent mode of operation. As shown, the efficiency does not clearly correlate with any of the considered variables, which is believed to be due to the large natural variability in the insertion process, variation in ice structure, and internal conduction-based losses.

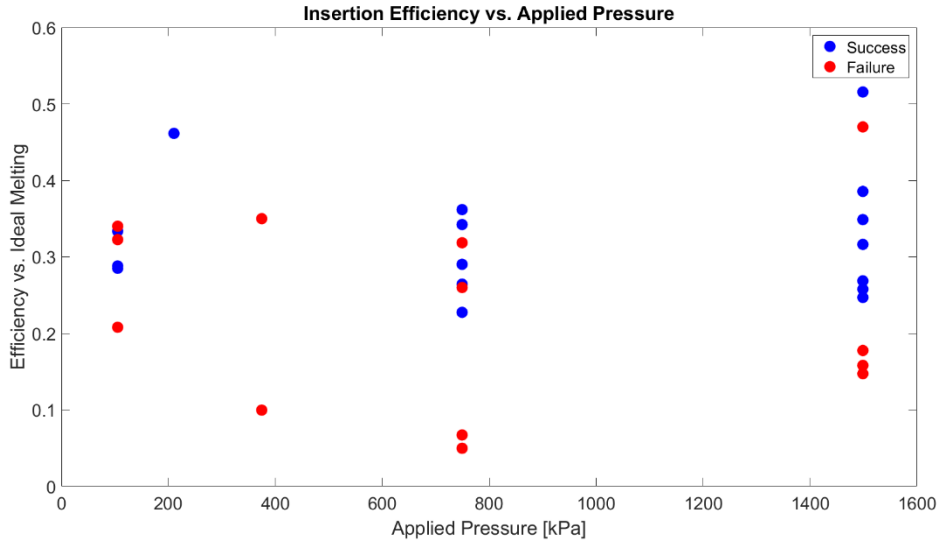

Figure 31: Efficiency relative to ideal melting vs. applied pressure for all water ice insertion tests.

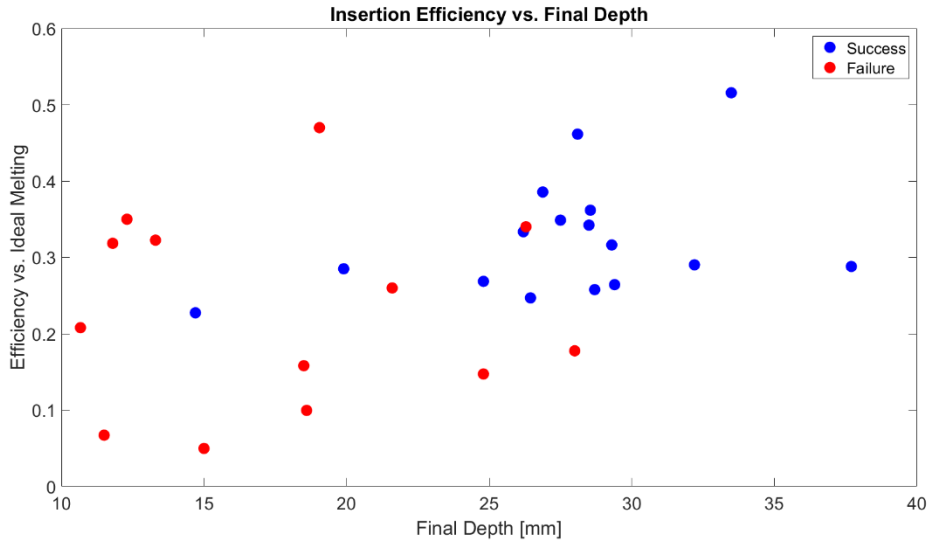

Figure 32: Efficiency relative to ideal melting vs. final insertion depth for all water ice insertion tests.

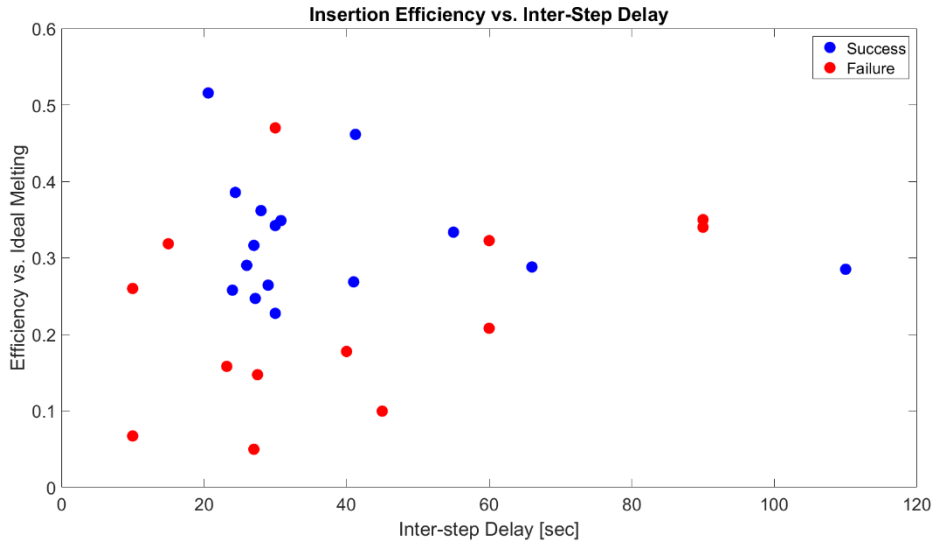

Figure 33: Efficiency relative to ideal melting vs. inter-step delay for all water ice insertion tests.

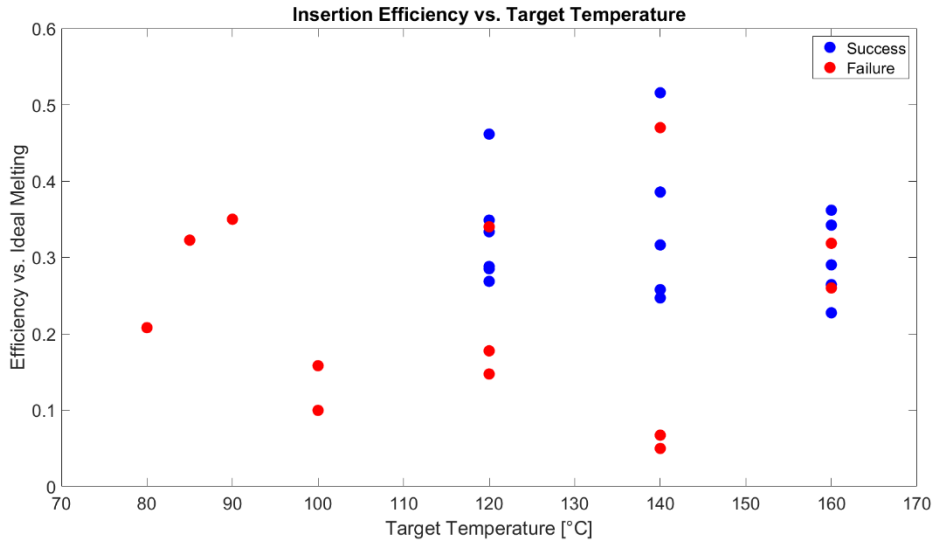

Figure 34: Efficiency relative to ideal melting vs. target temperature for all water ice insertion tests.

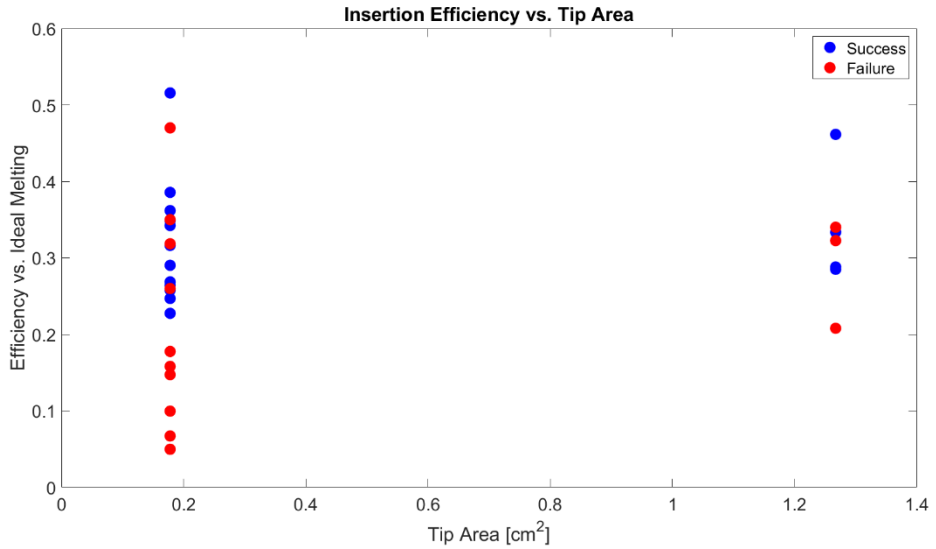

Figure 35: Efficiency relative to ideal melting vs. tip area for all water ice insertion tests.

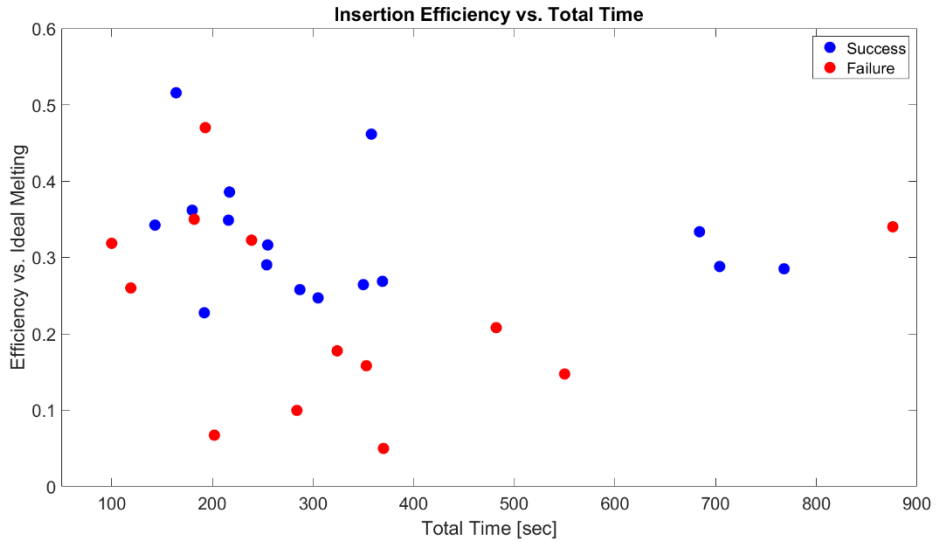

Figure 36: Efficiency relative to ideal melting vs. total insertion time for all water ice insertion tests.

While the efficiency of successful tests varied by approximately a factor of 2, even the lower end of the efficiency range is appealing for use on Europa. The energy required for the insertion of a thermal pick is the sum of the energies for warming, insertion, extraction, and internal conduction. Steady-state melting thermal drilling systems operate in cryogenic water ice at estimated efficiencies of 5% [41] and their transient operation would necessarily be even lower. A thermal pick operating at 5% efficiency means the energy cost of insertion would be a primary energy cost. However, a thermal pick operating at an efficiency on the order of 30% makes the energy cost of insertion a secondary energy expenditure. These energy expenditures are explained in more detail in Section 4.6.

After demonstrating an insertion efficiency on the order of 30%, the primary objectives become ensuring the reliability of the anchoring strength within the ice and reducing warming and internal conduction energies.

4.5.2.3 Re-Freezing Ice Formations

A consequence of a thermal pick entering the melting regime is the production of thermodynamically active meltwater. The meltwater produced by the heated thermal pick is not stable due to the surrounding vacuum, rapidly accelerates according to the pressure differential, and changes phase as the pressure drops. The existing ices surrounding the thermal pick are the base on which meltwater would securely freeze. This process led to the build-up of what is referred to as the formation lip and can be seen in Figure 37. The formation lip was not observed in atmospheric pressure tests at cryogenic temperatures but was observed in non-cryogenic vacuum tests. This suggests that the vacuum environment was the mechanism for triggering the build-up of the formation lip. This phenomenon also extended beneath the surface of the ice, causing the tapered thermal picks to become trapped within the ice after insertion. It is unclear whether this phenomenon was entirely a result of pressure-induced phase transition or was in any way enhanced by conduction at the cryogenic ice surface.

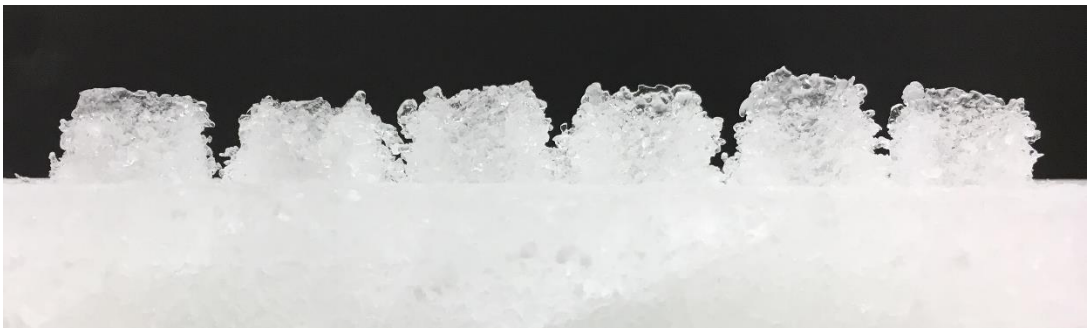

Figure 37: Formation lip shown for multiple tests on the same ice block.

Variants on this phenomenon have been previously observed [40] in experimental testing where the melting regime was triggered by sealing off the borehole with re-freezing meltwater. Sealing off the borehole in this case restricted

the outgoing flow and allowed pressure to build up such that melting could occur, which was a design goal of the study. This implies that the formation lip is a function of the geometry and insertion scheme of the thermal drill used. In sublimation-based experimental testing [34], there was no evidence of ice formations in either solid or porous ices when the thermal drill was not sealed off within the ice, suggesting that ice formations are specific to the melting regime. The ice formation results of this work differ from previous studies in that the active melting surface was not sealed off from the surrounding vacuum. For the purposes of a thermal pick ice anchor, ice formations are critical because they can be leveraged to provide active control over the final borehole shape.

Ice formations were observed whenever active thermal drilling was exposed to vacuum. A secondary exposure to vacuum was created in a single test by cutting and separating an ice block. A thermal pick was then inserted at the gap location and an ice formation conforming to the thermal pick insertion developed as seen in Figure 38. This re-freezing meltwater created a sealed structure surrounding the thermal pick, re-connecting the two sides of the ice block. This formation ice was not structurally significant, and the two sides of the ice block were easily pulled apart.

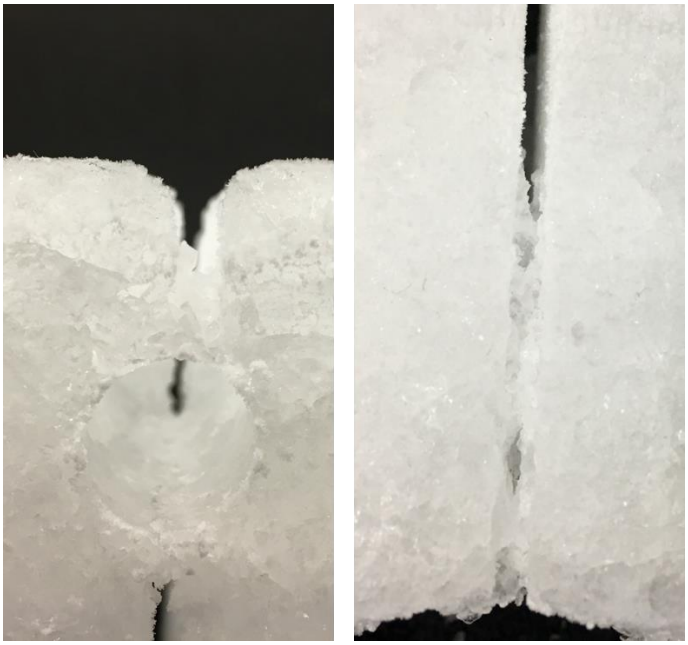

Figure 38: Ice formation fusing two ice blocks together. Views shown are straight into the borehole (left) and perpendicular to the borehole (right).

4.5.3 Ice Failure

Fracturing of the ice block could occur during insertion of the thermal pick. This is believed to be the result of thermal shock or re-freeze-based expansion. These fractures were always centered around the test site and can be seen in Figure 39 to have resulted in a weakened ice structure. Shifting ices during failure could also initiate unintended pick-to-ice contact, leading to a path for conductive heat loss.

Figure 39: Ice fracture resulting from improper operating conditions. Ice blocks were physically separated so that the extent of the fracture could be seen.

Inserting the thermal pick with a short inter-step delay always caused failure and suggests thermal shock at the borehole occurred. Figure 29 shows an example test data stream in which insertion steps were taken every 10 seconds. During the last of six successive insertion steps, thermal stall and temperature drop were observed. Post-test inspection of the ice block confirmed fracture at the test site. This type of fracture is believed to be the result of thermal shock and the damaging effects were easily discerned. While thermal simulations of the copper thermal picks showed that a delay of 10 seconds allowed for the approximate smoothing of its internal thermal gradients, the thermal gradients in the ice are sustained for longer timespans due to its relatively low thermal conductivity.

Allowing the thermal pick to undergo thermal stall could also result in fracture of the ice block. It is suspected that meltwater surrounding the thermal pick re-freezes during thermal stall due to a lack of heat supplied by the thermal pick. Freezing water

expanding within a closed volume causes significant stresses to develop and fractures the surrounding ice.

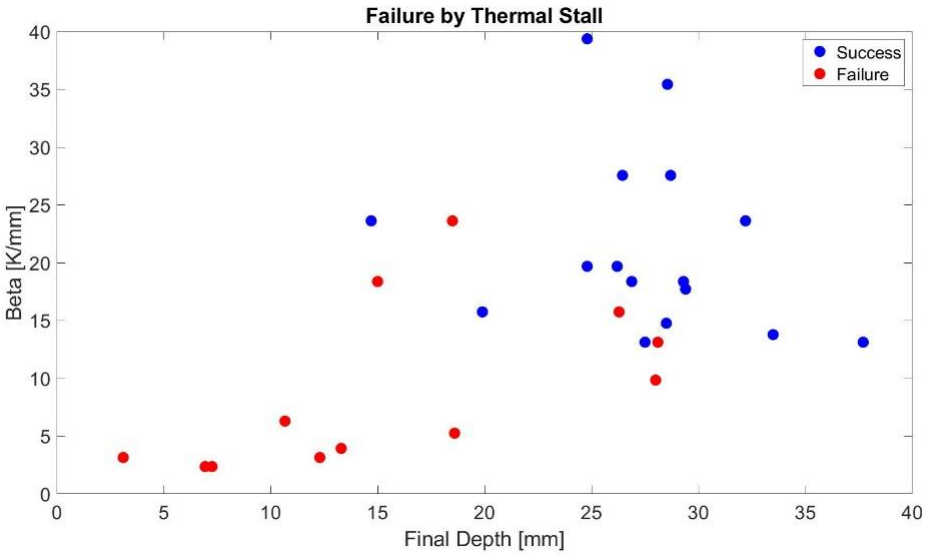

Figure 40: The Beta function vs. final insertion depth, demonstrating the impact of operating conditions on ice failure. Ice failures caused by insufficient inter-step delay (test runs 16, 19, and 23) have been removed from this data set.

The data in Table 3 shows that failure occurred regularly throughout the testing process. While thermal shock is correlated with the inter-step delay, thermal stall is correlated with temperature and step size. Given that thermal stall is believed to be caused by a thermal pick running out of useful thermal energy storage, a metric was developed to compare the stored thermal energy and required thermal energy for an insertion step and is described in Equation (33).

The minimum temperature to achieve melting was experimentally observed to be 70 °C as seen in Figure 45 (see Appendix A.3) when an insertion step is resisted entirely by the ice. Temperatures above this critical value are considered as adding to the useful energy storage of the thermal pick. The thermal energy required to take an insertion step is proportional to the step depth. These values combine to form the term

β in Equation (33) and Figure 40 shows that tests with low β values have a higher likelihood of thermal stall based failure than those with high β values.

$$\beta = (T - 70°C)/d_{step} \quad (33)$$

4.5.4 1-D Thermal Insertion Model

A SolidWorks model of thermal pick (A) was created to simulate the heat transfer that occurs when the thermal pick is brought into contact with the bottom of the ice borehole. Heat transfer across this boundary is assumed to provide all the energy used in active thermal drilling that converts ice at the bottom of the borehole into meltwater. Any heat transfer that occurs along the side walls of the thermal pick are assumed to have negligible contribution towards thermal drilling at the leading edge.

A simulation was created according to the illustration in Figure 41 where the thermal pick was set to a heated initial temperature and then exposed to a cold reservoir. The energy transferred into the cold reservoir models heat transferred across the leading edge during thermal drilling. This simulation used an equilibrated initial temperature condition of 160 °C, corresponding to the maximum target temperature used. The cold reservoir temperature was set to 70 °C, corresponding to the minimum temperature at which a melting layer could be supported. The thermal gradients that form within the thermal pick, meltwater, and ice during this simulated insertion are illustrated in Figure 42.

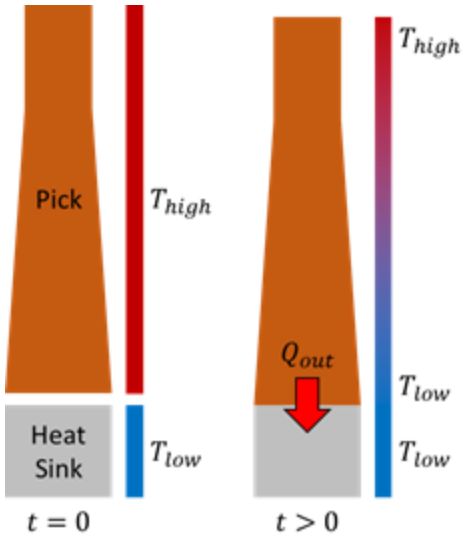

Figure 41: Illustration of the simulation of thermal pick (A). An infinite heat sink of low temperature (representing an isothermal melting boundary) is brought in contact with a hot isothermal copper rod. The energy exchanged between the two bodies is simulated.

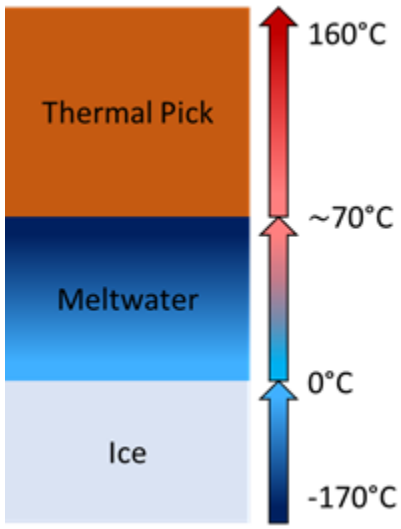

Figure 42: One-dimensional illustration of thermal gradients during insertion showing the thermal pick, meltwater layer, and ice.

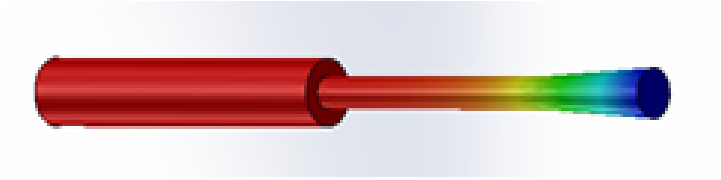

Figure 43: Simulated exposure of thermal pick (A) to a cold reservoir at the tip showing the thermal gradient that forms as a result of heat transfer.

The thermal simulation estimates the energy transfer (E_{sim}) across the leading edge over time for thermal pick (A) when in contact with the ice. This energy transfer is then compared to the theoretical energy expenditure according to Equation (36) to determine the step size (d_{step}) that can be achieved. The efficiency assumed for this mode of heat transfer is 1 since significant losses are not expected across the thermal pick tip.

$$E_{sim} = \eta_{melt} E_{i,melt} = E_{i,melt} \tag{34}$$

$$E_{sim} = \eta_{melt}\left(h_{fus} + c_p \Delta T_{ice}\right) A_{pick} d_{step} \rho_{ice} \tag{35}$$

$$d_{step} = \frac{E_{sim}}{\eta_{melt}\left(h_{fus} + c_{p,ice} \Delta T_{ice}\right) A_{pick} \rho_{ice}} \tag{36}$$

The simulated maximum step size that can be taken by thermal pick (A) when starting at an initial temperature of 160 °C can be seen in Figure 44. The simulation was run in four cases to show the minimal impact of heater output on leading edge heat transfer. The heater was either left off for the entire simulation, turned on 5 seconds prior to contact with the cold reservoir, turned on 3 seconds prior to contact, or turned on at the exact moment of contact.

This shows that theoretically achievable step sizes of approximately 5.5 mm to 6 mm are expected. As seen in Table 1, the maximum experimental step size without failure was 6.1 mm. The alignment between the simulation and observation

implies that heat transferred through the thermal pick tip is efficient in producing melting. This is possible if conductive loss into the cryogenic ice through the bottom of the borehole is minimal, the overall meltwater flow does not undergo much warming across the leading edge, and pick wall loss mechanisms do not significantly affect the temperature at the tip of the thermal pick.

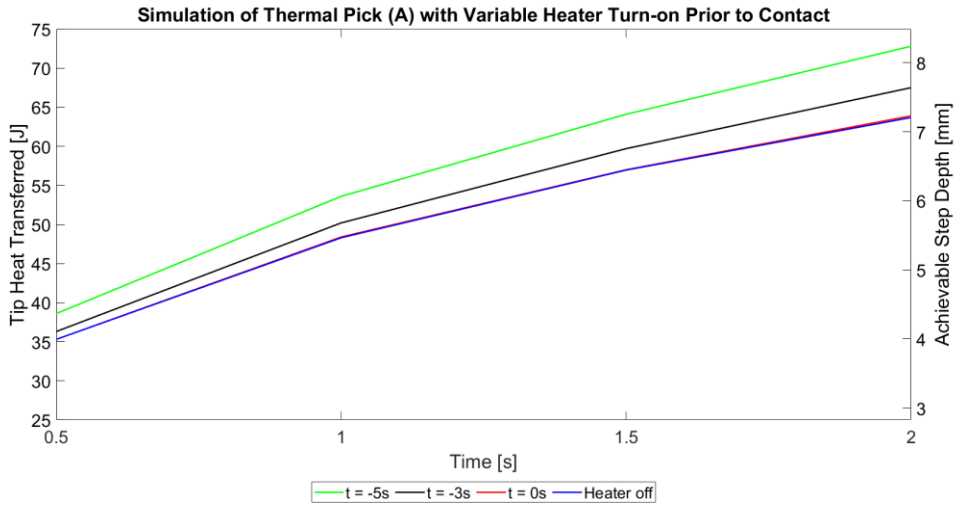

Figure 44: Simulated heat transferred and achievable step depth vs. time through the tip of thermal pick (A). The heater was turned on at time (t) relative to initiation of contact with the cold reservoir.

The two assumed values that affect this simulation are the cold reservoir temperature and contact time. Experimental observations indicating that melting does not occur below 70 °C set the lower bound for tip temperature. While higher tip temperatures are possible, they would decrease the achievable step depth below what is experimentally observed and are therefore not likely. The contact time cannot be accurately discerned from measurements given the data refresh rate of approximately 1.67 Hz. The commanded velocity sent to the positioning slide motor controller is 12.7 mm/s and so the minimum time a 6mm step could take is 0.5 seconds. However,

acceleration and deceleration of the positioning slide cause the actual contact time to be somewhat longer.

4.5.5 Operational Characteristics

4.5.5.1 Thermal Pick Temperature and Insertion Step Size

Avoiding failure of the ice is essential to the reliable use of thermal picks for anchoring and temperature and step size have been shown to impact ice failure. Higher target temperatures of the thermal pick enabled progressively larger step sizes without thermal stall and ice failure. Temperatures only up to 160 °C were tested due to concerns with exceeding the rated temperature of the thermally conductive epoxy. It can be seen in Table 3 that none of the 160 °C tests failed due to thermal stall, although they were still susceptible to thermal shock. It is possible that temperatures above 160 °C may enable further increased resistance to thermal stall related ice failure.

The step size is critical in preventing ice failure and ensuring efficient operation. Step sizes below 2 mm are correlated with low efficiencies as shown in Figure 30, which is suspected to be a result of trending towards a sublimative process due to the limited meltwater produced during a short insertion step. Smaller step sizes have a relatively shorter melting phase (Stages E, F, and G in Figure 28) but will not change the initial sublimation phases (Stages B, C, and D in Figure 28). Conversely, larger step sizes could cause thermal stall, ice fracture, and form conduction paths.

Within the operational condition ranges used in this study, step sizes between 2 mm to 5 mm were capable of yielding efficient operation while also reliably avoiding failure when operated at high temperatures.

4.5.5.2 Total Insertion Depth

The total insertion depth of this testing was practically limited by the length of the thermal picks and the test apparatus. Depths of up to 37 mm were achieved, which can feasibly be expected to yield anchoring strengths in the kN range if terrestrial data is an adequate analog [26]. The limitation on the theoretical maximum achievable depth for a thermal pick is failure of the ice, which depends on the β value shown in Figure 40 and increasing the total insertion depth past the 37 mm achieved here may require even higher β values.

4.5.6 Anchoring

If the thermal pick temperature is cooled below 70 °C through the process of active cooling described in Section 4.3.3.4, then thermal drilling will be halted and it is possible to develop anchoring forces. The application of an anchoring force using the extension spring simulates a tension load that an autonomous Europan vehicle might apply to a thermal pick. Anchoring was tested using the thermal pick styles (A) and (B) at depths between 6.5 mm and 28.1 mm. The maximum rated load for the test rig is 130 N, corresponding to the weight of 100 kg on Europa, and was reached without failure for every anchoring test performed. While this is the result predicted by the extrapolation of terrestrial ice anchor strength, it confirms anchoring into cryogenic ice can feasibly support large anchoring loads after thermal drilling.

The anchoring test case shown in Figure 45 was developed to test the limits of anchoring strength. It was performed using the smallest thermal pick (A) and with only the active cooling process for insertion. The thermal pick was initially warmed to 100 °C and inserted using only the latent heat within the thermal pick, reaching a

shallow depth of 6.5 mm. Despite these conditions, the maximum applied tension load of 130 N was reached without ice failure.

The ice used for this testing ranged from moderately fractured (a result of thermal shock prior to testing) compressed ice to a solid block of monocrystalline ice, though it is unknown if either are representative of the surface ice on Europa.

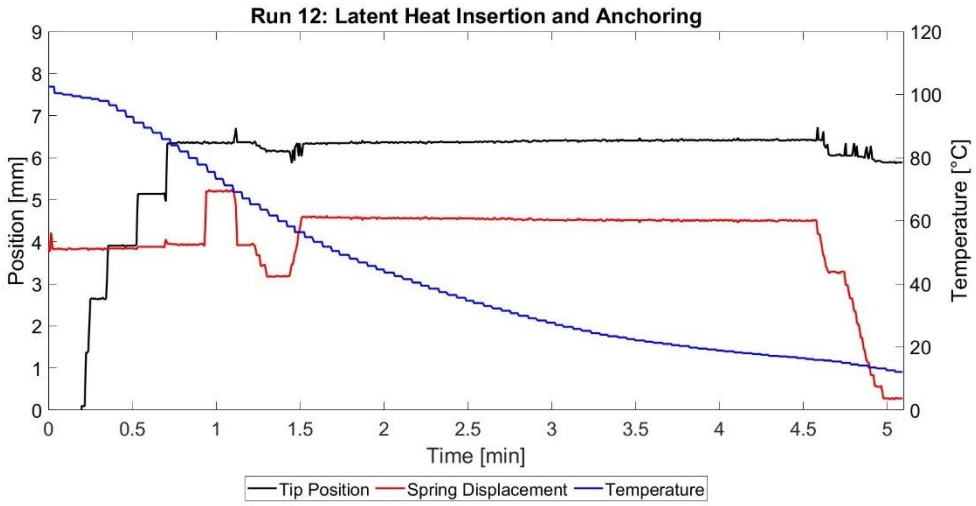

Figure 45: Test run 12 using thermal pick (A) inserted with the heater off leading to controlled thermal stall and cooling followed by an applied anchoring load of 130 N.

4.5.7 Extraction Step

The extraction phase is similar to the insertion phase although the energy costs are lower due to the relatively smaller volumes of thermally drilled ice. Upon extraction, a tapered thermal pick must thermally drill through ices that have built up behind the taper of the inserted portion of the thermal pick. During extraction, the active thermal drilling surface is its angled edge instead of its tip. Extraction of the thermal pick was performed immediately following the insertion phase and behaved similarly to insertion. The measured extraction efficiencies were between 0.11 and 0.62. The volume of ice and corresponding energy required for extraction were

calculated using the insertion depth (D), the tip radius (r_{tip}), and density of ice (ρ_{ice}) according to Equations (37) and (38), respectively.

$$V_{ext} = \int_0^D \pi({r_{tip}}^2 - r^2)\, dD \tag{37}$$

$$E_{ext} = (h_{fus} + c_p \Delta T_{ice})\rho V_{ext} \tag{38}$$

$$\eta_{ext} = \frac{E_{ext}}{E_o} \tag{39}$$

The ice volume requiring thermal drilling during extraction is necessarily lower than that of the insertion phase. However, the thermal energy storage within the thermal pick remains the same if the operational temperature is unchanged. This characteristic allows the rate of extraction to be higher than the rate of insertion. Average extraction velocities of up to 0.68 mm/s were tested, limited primarily by mechanical ground-out considerations of the test rig, rather than the thermal capacity of the thermal pick. The extraction efficiencies can be seen in Figure 46, which shows that the extraction efficiency may be correlated with the average velocity of extraction.

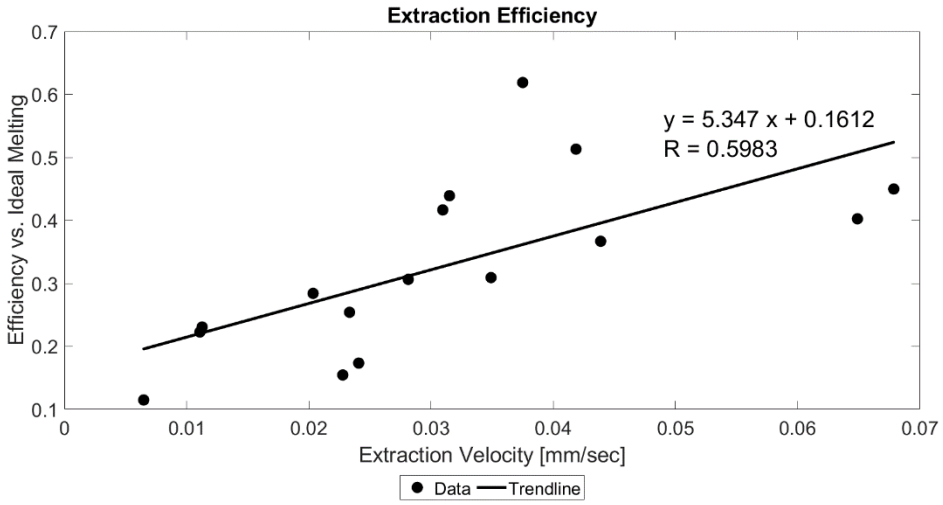

Figure 46: Efficiency relative to ideal melting vs. average extraction velocity for all tests.

4.5.8 Radiative and Internal Conduction Loss

A consequence of heating the thermal pick to its operational temperature is the internal conduction in the test rig. The thermal pick is insulated from the test rig structure through the G-10 insulating tube, although this does not prevent all internal conductive heat transfer. Differential radiative heat loss also occurs due to the temperature of the thermal pick relative to its surroundings, but this heat loss mechanism is assumed to be negligible.

The internal conduction losses were measured under vacuum prior to initiating contact with the ice. This measurement was performed by warming the thermal pick to a target temperature and holding steadily at that temperature using thermostat control. The heater power required to maintain that temperature was recorded as a function of time. The resulting calculated loss of power through internal conduction is shown in Figure 47. This conductive heat loss can represent a significant fraction of the total energy that is expended by the heater, given that the operating temperatures

are frequently greater than 100 °C.

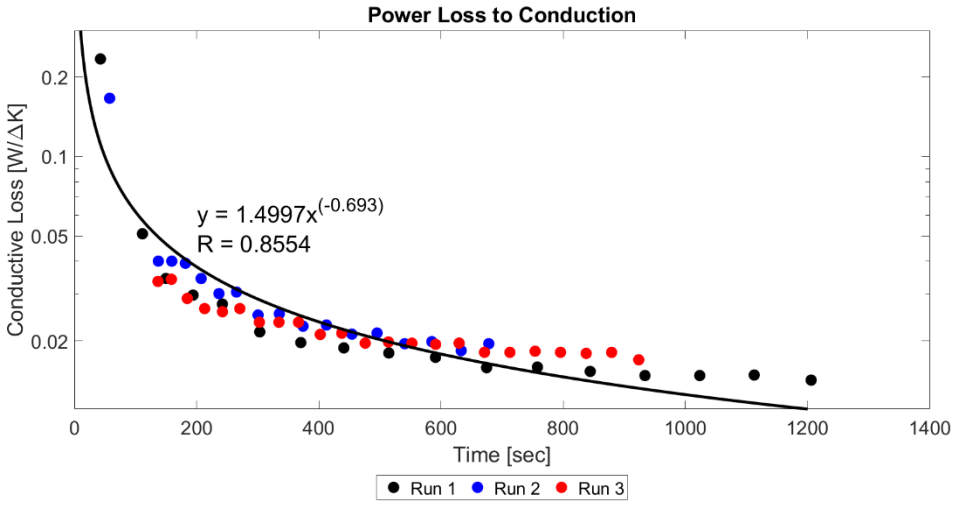

Figure 47: Measured internal conductive losses between the thermal pick and test rig plotted against time.

Figure 48: Conduction-corrected efficiency vs insertion step size of all insertion tests using measured internal conduction rates.

Conduction-corrected data assumes a conservatively estimated constant power loss ($P_{con,int}$) of 12.5 mW/K due to internal conduction and lasting for the entire duration of each test performed. The temperature differential is relative to 20 °C, the

resting temperature of the test rig. Conduction-corrected results allow for a closer examination of the efficiency of the thermal drilling process without the impacts of the characteristics of the thermal insulation approach used. The conduction-corrected efficiency is defined by Equation (40), is shown in Figure 48, and demonstrates an increase in efficiency to between 0.32 and 0.86 for successful tests and between 0.06 and 0.86 for all tests.

$$\eta_{melt,cc} = \frac{(h_{fus} + c_p \Delta T_{ice}) \Delta m_{melt}}{E_o - P_{con,int} t_{total}} \tag{40}$$

4.5.9 Pick Geometry

The three characteristics that define the geometry of the tapered thermal picks used in this study are their length, width, and degree of taper. As shown by terrestrial studies of ice screws, the depth of insertion (d_{total}) and therefore the length of the thermal pick is a determining factor in the strength of an ice anchor [26]. A longer pick may also be capable of penetrating through loose surface ices to stronger ices below. However, a longer pick with a deeper insertion requires more energy due to the increased borehole volume.

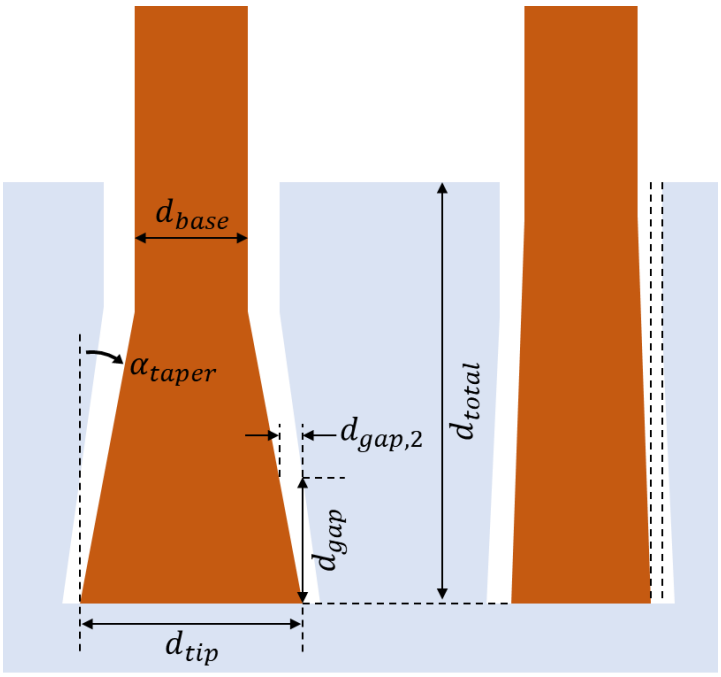

Figure 49: Illustration of the geometry of thermal pick (A) with the measured gap width dimension (d_{gap}) shown.

The width of the base of the thermal pick (d_{base}) determines the bending strength of the thermal pick itself. Bending loads are the expected failure mode for thermal picks and this is explored in Section 5.1. The energy cost associated with increasing the thermal pick tip width (d_{tip}) is approximately proportional to the increase in tip area as shown in Figure 35.

The degree of thermal pick taper (α_{taper}) and consequently the tip-to-base differential is only necessary to ensure that the thermal pick is locked within the ice by re-freezing meltwater. The shallow taper angle of 3.58° on thermal pick (A) locked it under the ice, meaning that only slight tapers are necessary. The gap width is estimated as the measured range of axial motion of a cooled thermal pick within an ice borehole (d_{gap}). This range of motion is observed in Figure 45 (see Appendix A.3) for thermal pick (A) as the difference between the maximum tip position

(thermal pick pushed forward within the borehole as far as possible) and the loaded tip position (thermal pick pulled back within the borehole as far as possible), leading to a conservative gap width estimate of 0.4 mm. Assuming the borehole shape conforms perfectly to the thermal pick and applying the trigonometric correction shown in Equation (41) suggests the true gap width ($d_{gap,2}$) was 0.03 mm, though this was not experimentally confirmed.

$$d_{gap,2} = \tan(\alpha_{taper}) d_{gap} \quad (41)$$

4.5.10 Trapped Air Effects

The porosity of the compressed ice used in the bulk of this testing leaves open the possibility that air bubbles trapped within the ice will impact the test results. If the pressure resulting from the release of this trapped air is comparable to that of the pressure resulting from the vaporization of water ice, then it is considered to be non-negligible. This effect can be estimated by calculating the relative composition of the outgoing gaseous flow. A conservative lower bound of the vaporization of water ice derives from the case where only the ideal volume of meltwater is created at 0 °C, no additional heat is lost to the meltwater, and it expands to vacuum adiabatically. The adiabatic expansion into vacuum results in the production of gas and ice following Equation (16), from which it is determined that 10.6% of the meltwater created will be converted into gas.

The measured density of the compressed ice used is 0.85 g/cm^3, while the density of pure ice is 0.92 g/cm^3, suggesting that air makes up 7.6% of the total test block volume. A cubic centimeter of compressed ice contains 850 mg of water (yielding 90 mg of gaseous water after adiabatic expansion) but only 97 μg of air. The

outgoing flow of gas under this assumption will thus be only 0.0011% air by mass, suggesting that internal air bubbles will have a negligible effect on the local pressure environment resulting from thermal drilling.

4.5.11 Optically Clear Ice

Due to issues with thermal shock prior to testing, test data with optically clear ice are limited. This thermal shock was a consequence of the rapid temperature shifts in test preparation when the initially warm ice was exposed to liquid nitrogen vapor during cooling and when the cryogenic ice was exposed to ambient air prior to the pump-down phase. Any differences between optically clear ice and compressed ice were not able to be definitively established. However, thermally drilling into optically clear ice was able to be achieved without failure, which suggests that both ice types can feasibly be used as an ice anchor.

Figure 50: Borehole in optically clear ice using thermal pick (A). Cracks due to thermal shock of test preparation can be seen.

4.6 Simulated Operations

The practical utilization of a thermal pick is dependent on the total energy cost for anchoring. Due to the lack of active cooling of the ice block and internal

conduction in the test rig, timescales allowing equilibration of a thermal pick to cryogenic temperatures during anchoring was not achievable. However, the energy cost over an entire operational cycle of a thermal pick was simulated using trends established by experimental data.

The simulation of a thermal pick operational cycle requires knowledge of the insertion efficiency, extraction efficiency, conductive loss rate, heater power, and the timeline of operation. The experimental results provide estimates for the efficiencies and conductive loss rates, the heater power is known, and the timeline of operation can be assumed.

The simulation models the stages of warming, extraction, delay, and insertion that make up the hypothetical concept of operations for a thermal pick used by a Europa rover for mobility. The model assumes a -170 °C initial condition for all components, an operational temperature of 160 °C for thermal drilling, a step period of 20 seconds, a step length of 3 mm, a final depth of 3 cm, an insertion/extraction efficiency of 0.3, an average extraction velocity of 0.5 mm/s, a heater power of 30 W, the mass and geometry of thermal pick (A), and a 1 minute delay between the extraction and insertion phases. The delay between insertion and extraction represents the time required to reposition the thermal pick between anchoring positions, during which time internal conductive losses can occur. The rate of internal conduction heat loss is calculated by Equation (42) which is created using the trendline shown in Figure 47.

$$P_{loss} = 1.4997\, t^{-0.693} \Delta T \tag{42}$$

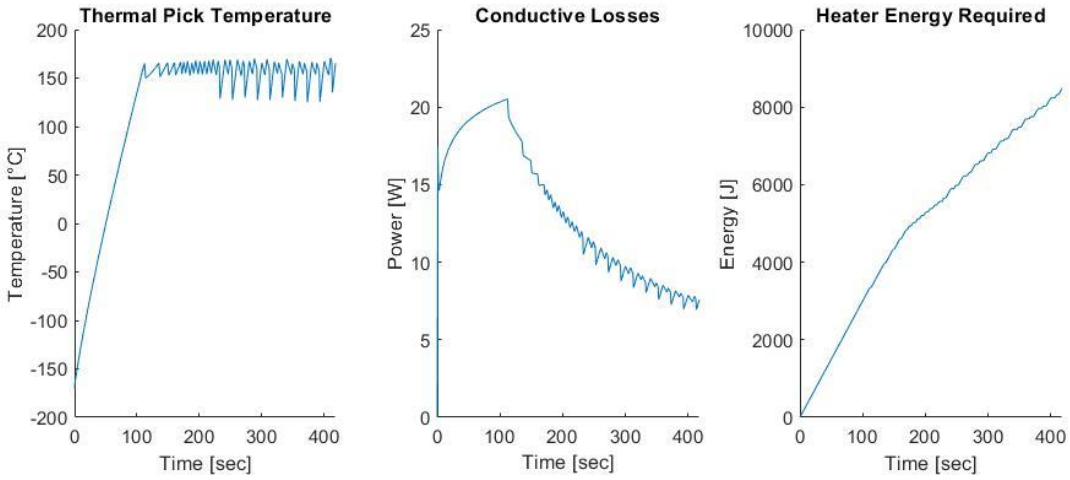

Figure 51: Simulated thermal behavior of thermal pick (A) under Europa conditions using extrapolation of experimentally measured thermal characteristics.

The breakdown of the total energy costs illuminate which aspects of the design can yield the greatest reductions in total energy cost. The modeled energy cost breakdown for thermal pick (A) is as follows.

- Thermal pick warming: 1.13 kJ
- Extraction: 0.52 kJ
- Insertion: 1.12 kJ
- Conduction losses: 5.63 kJ
- Total energy: 8.40 kJ

For the thermal pick (A) and the G-10 insulating tube used in the test rig, conductive losses dominate the energy expenditure of the process. Small changes in the insertion/extraction efficiencies will have a relatively limited effect on the energy cost of the process overall. A design that halves the conductive losses will decrease the total energy cost by 30% (to 5.82 kJ), while a design that doubles the thermal pick cross-sectional area will increase the total energy cost by 23% (to 10.35 kJ). This

illustrates the vital impact of mitigating conductive losses for efficient thermal pick operation.

The insertion and extraction steps in this simulated mode of operation account for 1.64 kJ, which is 19.5% of the total energy cost. If operating conditions and design were optimized so that both insertion and extraction were 100% thermally efficient in the melting regime, then the total simulated energy cost of operation would only drop to 7.29 kJ (13.2% improvement).

4.7 Conclusions

The three requirements for the use of a thermal pick are reasonable energy cost, anchoring strength sufficient to support a rover, and the ability to avoid damaging the ice structure. These three characteristics have been shown and demonstrate the feasibility of using a thermal pick as an ice anchor.

Operation of the thermal pick in each individual phase has been demonstrated and insertion/extraction efficiencies on the order of over >30% have been shown. The efficiencies shown are reliant on active thermal pick control, which is not a capability possessed by steady-state gravity-driven subsurface thermal probes. Moreover, this efficiency range shows that an intermittent insertion approach can significantly reduce the instantaneous and total power costs for a thermal drill relative to the steady-state operational efficiencies of 5% in the cryogenic regime presented in other works.

It has also been shown that when operating in an intermittent melting regime with efficiencies on the order of those demonstrated, that the efficiency of the thermal drilling process ceases to be the dominant driver for the energy cost of operation. The

difference between the ideal and actual energy costs represent a 13.2% shift in the total energy expenditure of operation, suggesting that once the intermittent melting mode of operation is achieved, the energy costs are driven primarily by warming of the thermal pick body and internal conductive losses.

The anchoring loads demonstrated show that ice can be used as an anchor against which the weight of a rover may be supported. While the test apparatus used is limited to a maximum of 130 N anchoring load, this represents the weight of a relatively large rover (100 kg) in the context of Europa exploration. Given that depth is believed to correlate with anchoring strength, anchor depths of 6.5 mm holding 130 N suggest that the >30 mm anchor depths achieved may be capable of holding significantly higher loads.

While the failure mechanisms of the ice are complex, a correlation was demonstrated between ice failure and the β function. These results suggest that a high temperature thermal pick (160 °C) in conjunction with small insertion steps (3 mm) will yield a high β value (30 K/mm) that has a reasonable likelihood of avoiding thermal stall related failure. Maintaining an inter-step delay greater than 20 seconds was also determined to be essential to mitigating ice failure by thermal shock.

Qualitative conclusions on the physical characteristics of the device have also been determined. A shallow taper limits the energy costs of extraction and was not shown to have detrimental effects on anchoring ability. The length and width are limited to what is required to prevent the ice tensile and thermal pick bending failure mechanisms, respectively.

Improving upon the energy cost, reliability, and anchoring strength of a thermal pick requires advances to the test rig and thermal pick adhesive. While incremental improvements on the operational energy cost of a thermal pick can be made through improving the efficiency of the insertion and extraction phases, the primary means by which to reduce the energy cost of a thermal pick is through improving the thermal insulation holding the thermal pick. Improving upon the reliability of a thermal pick requires increasing the operating temperature, which was limited in this study by the thermally conductive epoxy used between the heater and thermal pick body. Confirmation of the potential for higher anchoring strengths requires improvements on the test rig to increase the maximum load that can be applied.

Chapter 5: End Effectors

5.1 Ice Anchor Theory

Designing a thermal pick ice anchor demands the balancing of the energy required for insertion against the anchoring strength that is afforded. Depth is positively correlated with terrestrial ice strength [26], but is also proportional to the energy required for thermal drilling and bending stresses within the thermal pick.

When anchoring to provide stability or mobility for a rover on an icy moon, the direction of the load applied is variable. Off-axial loading causes bending stress to develop within a thermal pick that is proportional to the applied load and the orthogonal distance to the applied load. For this reason, the directionality of the load relative to the thermal pick orientation is always conservatively assumed to be perpendicular. Bending loads must be supported either by ensuring the thermal pick can support the bending stresses or through use of a secondary mechanism.

The ability of a thermal pick to support bending stress is proportional to its second moment of area (I). A tube-shaped thermal pick provides a high bending strength capability by virtue of its material extending out from its axial center, which increases the second moment of area relative to the cross-sectional area as seen in Equation (45). The moment applied by the anchoring load is (M), the design stress is (σ), the radius is (r), and the thermal pick area is (A).

$$\sigma = \frac{Mr}{I} \tag{43}$$

$$I_x = I_y = \frac{\pi}{4}({r_{outer}}^4 - {r_{inner}}^4) \tag{44}$$

$$A = \pi({r_{outer}}^2 - {r_{inner}}^2) \tag{45}$$

$$\frac{I_x}{A} = \frac{({r_{outer}}^2 + {r_{inner}}^2)}{4} \tag{46}$$

This thermal pick geometry works well for terrestrial ice anchors where contact between the side of the thermal pick and borehole is well distributed as a consequence of mechanical insertion, which physically forces ice out of the way as the anchor is inserted. However, thermal drilling systems develop a gap between the side of the thermal pick and the borehole. This gap permits point loading as seen in Figure 52. Additionally, moving to a tubular profile increases the surface area to volume ratio, which can potentially have negative impacts on thermal drilling. All designs in this work assume a solid core with a circular cross-section except where otherwise stated.

5.1.1 Types of Thermal Picks

The optimality of a thermal pick design is defined by a combination of its tensile and bending strengths, energy cost for insertion to a set depth, and complexity. All analysis in comparing designs is normalized by insertion depth. The complexity of a design is a subjective assessment of the number, intricacy, mass, and volume of the components required for operation. The top four thermal pick designs are described in Sections 5.2, 5.3, 5.4, and 5.5, although only the tapered design was adopted for water ice testing and implemented into the end effector designs.

The gap between a thermal pick and the ice borehole that results from thermal drilling causes point loads rather than distributed loading. Two-point loading will cause bending stresses to develop in the thermal pick but can be avoided with a lateral

support mechanism as seen in Figure 52. A laterally supported system induces only tensile loads in the thermal pick but requires the use of an external mechanism.

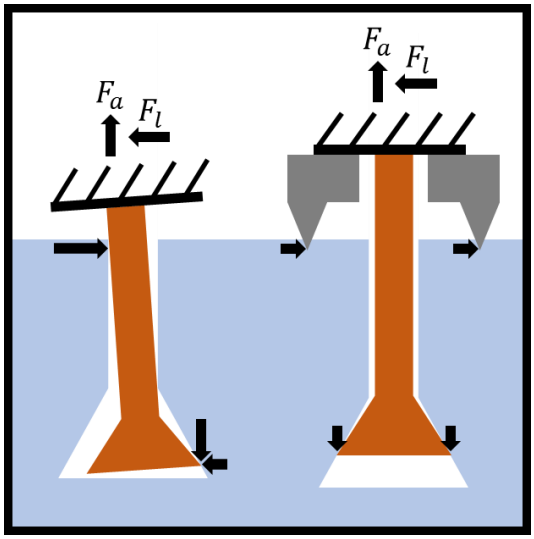

Figure 52: Contact points of an anchored thermal pick due to an applied load without lateral support shown left and with lateral support using an ice gripping mechanism shown right.

5.1.2 Bending Thermal Pick Failure

The four designs considered are shown in Figure 53, Figure 54, Figure 55, and Figure 56 and have a maximum moment arm equal to the depth of insertion (D). Each design is assumed to have the same laterally applied load (F_l), material yield stress (σ_{yield}) and safety factor (SF). This leads to a direct correlation between a thermal pick's ability to support a bending load and its radius (r), cross-sectional area (A), and volume (V) by Equations (50), (51), and (52).

$$M = F_l D \tag{47}$$

$$I = \frac{\pi}{4} r^4 \tag{48}$$

$$\sigma_{yield} = SF \frac{Mr}{I} \tag{49}$$

$$r = \left(\frac{4\ SF\ F_l D}{\pi \sigma_{yield}}\right)^{\frac{1}{3}} \tag{50}$$

$$A = \pi \left(\frac{4\ SF\ F_l D}{\pi \sigma_{yield}}\right)^{\frac{2}{3}} \tag{51}$$

$$V = \pi \left(\frac{4\ SF\ F_l}{\pi \sigma_{yield}}\right)^{\frac{2}{3}} D^{\frac{5}{3}} \tag{52}$$

5.1.3 Tensile Thermal Pick Failure

As is the case with bending thermal pick failure, the thermal picks are all assumed to have a circular cross-section and equivalent axial applied load (F_a), material yield stress (σ_{yield}), and safety factor (SF).

$$\sigma_{yield} = SF \frac{F}{\pi r^2} \tag{53}$$

$$A = \pi r^2 = \frac{SF\ F}{\sigma_{yield}} \tag{54}$$

$$V = \left(\frac{SF\ F}{\sigma_{yield}}\right) D \tag{55}$$

The bending loads will be the primary driver of the required area, leading to power law scaling of thermal pick volume relative to depth. The energy cost of insertion incentivizes the use of lateral supports for deep insertions because the thermal pick volume required to support tensile loads scales linearly with depth.

5.1.4 Ice Failure

While the temperature, pressure, and kilometer-scale geography of Europa have been observed, other surface characteristics relevant to anchoring are unknown.

As such, terrestrial ice anchor testing data is used as a model for what may be expected for thermal pick use on Europa. Terrestrial ice anchor failures have shown that the ice failure mode is that of a tensile bowl and that the ice strength depends on the depth achieved by the thermal pick [26]. For this reason, the depth of the thermal pick insertion (D) is a monotonic predictor for the ice strength in support of an anchoring load, although the exact nature of this relationship is not presumed to be known. Given the desire to create a reliable anchoring hold despite the unpredictability of brittle ice failure mechanisms, increasing the depth of insertion is of the utmost importance.

5.2 Hooked Thermal Pick

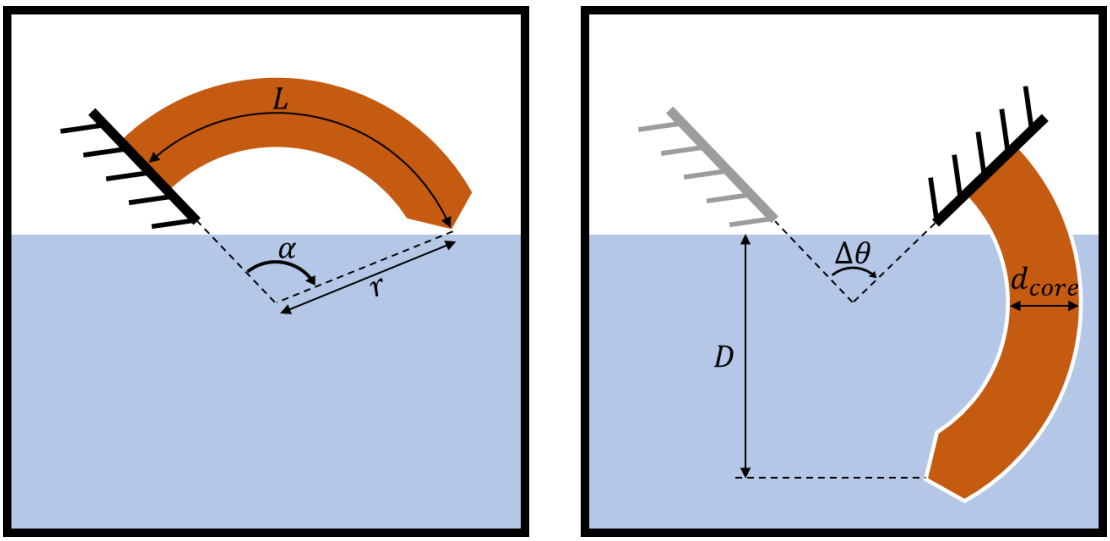

Figure 53: Hooked thermal pick prior to insertion (shown left) and after insertion (shown right).

5.2.1 Description

A hooked thermal pick requires a rotary insertion about the center of curvature to insert beneath the ice, after which only a reverse motion can remove it from the ice. The cross-sectional core of the thermal pick is circular with a diameter of (d_{core}).

5.2.2 Strength

The hooked thermal pick cannot be loaded purely in tension. Tip loading will always result in internal moments regardless of the direction in which it is applied, which makes a hooked design applicable only in cases where bending loads are acceptable.

5.2.3 Volume

Using the assumption of a thermal pick that is thin relative to its length, the borehole volume is proportional to the cross-sectional area and the thermal pick's arc length.

$$D = 2r \sin\left(\frac{\alpha}{2}\right) \tag{56}$$

$$L = r\,\alpha \tag{57}$$

$$V = A\,L = A\,r\,\alpha = \frac{AD\alpha}{2\sin\left(\frac{\alpha}{2}\right)} \tag{58}$$

The energy required for thermal drilling based insertion (E) of the hooked thermal pick can be derived as a function of its insertion depth as seen in Equation (59). Equations (26) and (28) are used to develop the term (E_v), which is the specific energy per unit volume of the thermal drilling process and is assumed to be constant between each thermal pick design.

$$E_v = \frac{E_{i,melt}}{\eta_{melt} V} = \frac{\left(h_{fus} + c_p \Delta T_{ice}\right)\rho}{\eta_{melt}} \tag{59}$$

$$E = VE_v = (ADE_v) * \left[\frac{\alpha}{2 \sin\left(\frac{\alpha}{2}\right)}\right] \tag{60}$$

5.2.4 Complexity

A hooked thermal pick requires only a rotary motor for its insertion with an actuation scheme based on the center of curvature of the hook.

5.3 Key Thermal Pick

5.3.1 Description

The key thermal pick was designed for a sublimation-based insertion. The key portion at the leading edge is not cylindrically symmetrical, so when it is turned by 90° at the end of an insertion, it locks the thermal pick within the ice. When laterally supported, this design can bear pure tensile loads.

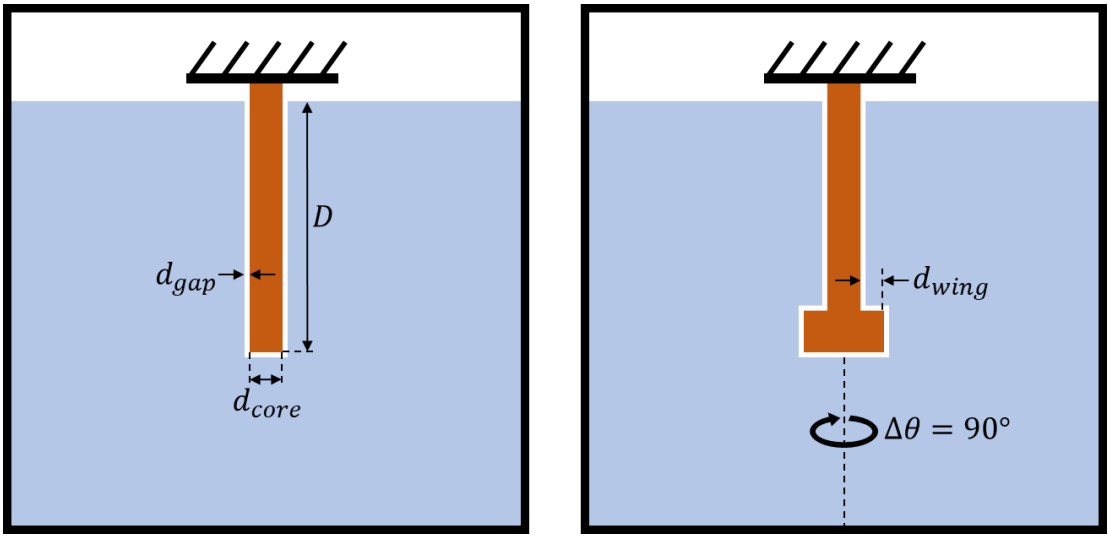

Figure 54: Key thermal pick shown after initial linear insertion (shown left) and after a subsequent 90° rotation (shown right).

5.3.2 Strength

A key thermal pick as shown in Figure 54 is most desirable when loading in tension. This allows for the use of relatively thin thermal picks but requires lateral support as seen in Figure 52. Bending loads require a significant core diameter of the thermal pick relative to its length based on the scaling law in Equation (51).

5.3.3 Volume

The volume bored by a key thermal pick is proportional to its depth and dependent upon the key shape. The term (A) is used to refer to the area of the core of the thermal pick to maintain consistency with the other three designs considered.

$$V = A_{key}L = A_{wing}L + AL \tag{61}$$

$$E = (ADE_v) * \left[1 + \frac{A_{wing}}{A}\right] \tag{62}$$

The depth of the wing of the thermal pick (d_{pick}) is only required to exceed the gap width (d_{gap}) that is created in the thermal drilling process. This permits the thermal pick to become stuck beneath the ice to be used as a tensile thermal pick. The gap width is estimated to be between 0.03 mm and 0.4 mm for water ice (Section 4.5.9) and between 0.45 mm and 0.75 mm for dry ice (Section 3.2.3). This suggests that only a relatively small additional area is required for the key portion of the thermal pick.

5.3.4 Complexity

The key design is the most complex because it requires two separate types of actuation. The first actuation is a linear insertion into the ice, followed by a rotary actuation that locks the key beneath the ice.

5.4 Screw Thermal Pick

5.4.1 Description

A screw design must be fed into the ice using coupled linear and rotational motion matching the pitch of the screw. This creates a threaded ice borehole that holds the screw thermal pick beneath the ice after insertion.

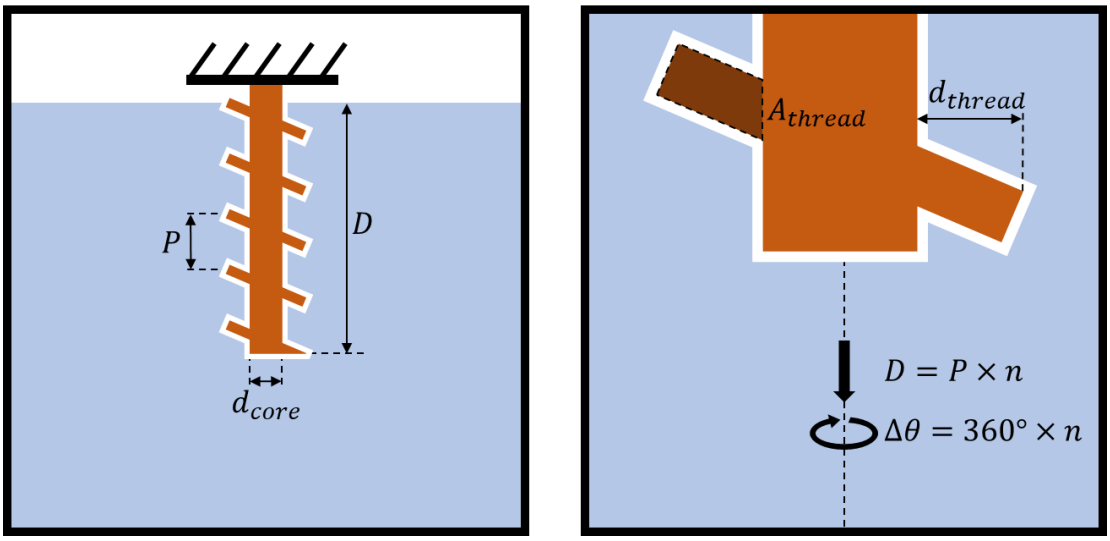

Figure 55: Screw thermal pick after corkscrew insertion into the ice (shown left) and with the thread area and motion coupling (shown right).

5.4.2 Strength

As with a key design, the screw can be loaded at the tip purely in tension without developing significant internal moments. It can be used as either an

unsupported thermal pick that withstands bending loads or one that incurs only tensile loads using a lateral support mechanism.

5.4.3 Volume

The borehole volume of an inserted screw is a combination of the thermal pick core and the additional volume added by the threading. Terrestrial ice screws traditionally have a small thread area (A_{thread}) and a relatively large pitch (P) with few turns (n) and a large radius (r).

$$V = A_{rod}L + A_{thread}L_{helix} \tag{63}$$

$$L_{helix} = n\sqrt{(2\pi r)^2 + P^2} = L\sqrt{\frac{(2\pi r)^2}{P^2} + 1} \tag{64}$$

$$V = LA\left(1 + \frac{A_{thread}}{A}\sqrt{\frac{(2\pi r)^2}{P^2} + 1}\right) \tag{65}$$

$$E = (ADE_v) * \left[1 + \frac{A_{thread}}{A}\sqrt{\frac{(2\pi r)^2}{P^2} + 1}\right] \tag{66}$$

As with the key design, the thread depth is only required to extend past the width of the gap between the ice and thermal pick, which allows it to be small relative to the body of the thermal pick.

5.4.4 Complexity

The screw insertion mechanism requires a coupled linear and rotational insertion. This coupled motion is provided by rotary actuation, a nut, and a screw. The screw used to mate with the nut can be the thermal pick itself, but this requires that the nut be a thermal insulator to inhibit internal conduction during thermal

drilling. A secondary screw can also be used for actuation and its pitch must match that of the thermal pick.

The pitch of the thermal pick should be relatively low to ensure that the actuator is not backdrivable. Linear forces can drive screw actuators of high pitch, which is a property known as backdrivability. In the context of anchoring, backdrivability would allow axial anchoring forces to pull the screw out of the ice.

5.5 Tapered Thermal Pick

5.5.1 Description

The tapered thermal pick is recommended for use where water ice is present. The low pressure of water's triple point allows for the melting and freezing of ice during the thermal drilling process. Meltwater that freezes behind the taper of the tapered thermal pick causes it to be trapped within the ice and enables its use as an anchor. However, this meltwater must be thermally drilled if the thermal pick is to be extracted from the ice, leading to a secondary energy expenditure.

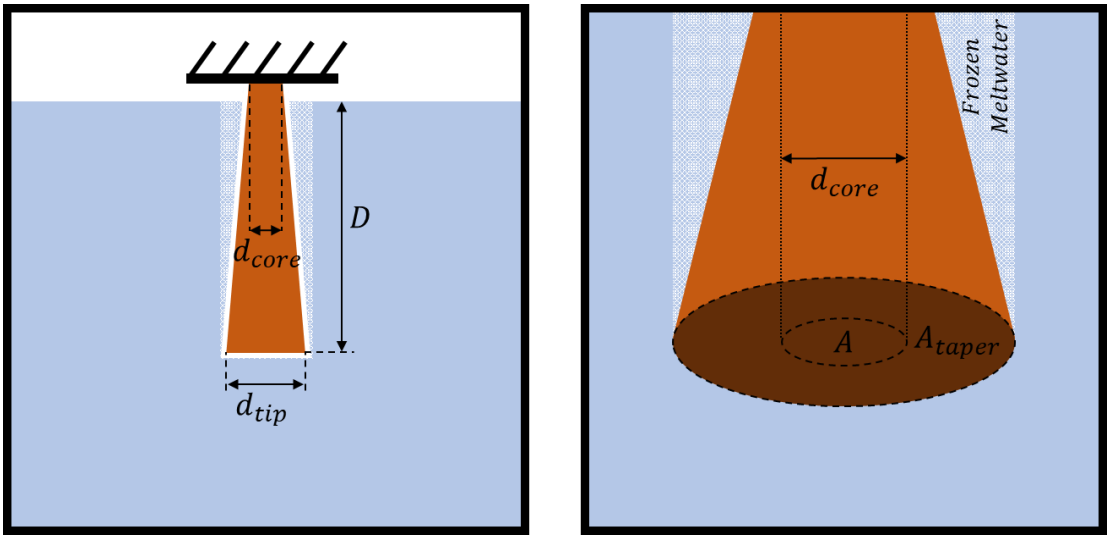

Figure 56: Tapered thermal pick after linear insertion with re-frozen water (shown left) and the areal breakdown of the leading edge (shown right).

5.5.2 Strength

As with the key and screw designs, the tapered thermal pick can be loaded purely in tension using an external lateral stabilization mechanism or bending loads can be permitted with a high width design.

5.5.3 Volume

The borehole volume of a tapered thermal pick is determined by the tip area A_{tip}. As with the key and screw designs, the taper width is only required to extend past the width of the gap between the ice and thermal pick, which allows it to be small relative to the body of the thermal pick.

$$V = A_{tip} = AL + A_{taper}L \tag{67}$$

$$E = (ADE_v) * \left[1 + \frac{A_{taper}}{A}\right] \tag{68}$$

The additional energy cost of extraction is proportional to the cavity volume (V_{cavity}). However, given that the taper area needs not be large relative to the core as discussed in Section 4.5.9, this energy is small.

$$V_{cavity} = \frac{A_{taper} L}{2} \tag{69}$$

$$E_{ext} = (ADE_v) * \left[\frac{A_{taper}}{2A}\right] \tag{70}$$

$$E_{total} = (ADE_v) * \left[1 + \frac{3A_{taper}}{2A}\right] \tag{71}$$

5.5.4 Complexity

The tapered design the least complex because it requires only linear actuation for insertion and extraction.

5.6 Design Selection

All four thermal pick designs have a similar energy costs when controlling for insertion depth as can be seen by comparing Equations (60), (62), (66), and (68). For this reason, the complexity of the mechanism is used as the driving factor in the selection of a design. This makes the tapered thermal pick the optimal choice when water ice melting permits its use. If the target ices are carbon dioxide based, then a screw thermal pick is preferable.

5.7 External Bracing Mechanism

The energy cost of thermal drilling is proportional to the thermal pick volume while the ice strength is proportional to the anchor depth. This allows the scaling laws

determined by using Equations (52) and (55) to define the scaling of the energy cost relative to the anchoring force (F_{anchor}) for both the bending and tensile-only cases.

$$V_{bending} \propto D^{\frac{5}{3}} \tag{72}$$

$$V_{tensile} \propto D \tag{73}$$

$$E_{bending} \propto F_{anchor}{}^{\frac{5}{3}} \tag{74}$$

$$E_{tensile} \propto F_{anchor} \tag{75}$$

This relationship suggests that as the required anchoring depth increases, a thermal pick loaded in tension becomes increasingly desirable.

For an external mechanism such as the one seen in Figure 52 to provide lateral support, it must be through forcible contact with the surface ice. This contact needs to prevent lateral forces from passing to the thermal pick. An external mechanism is unable to provide the downwards force necessary to create the lateral support, but an inserted thermal pick anchor can be leveraged to provide that force. The end effector described in Section 5.10 uses springs to passively provide the force pressing its external bracing mechanism into the ice and the reciprocal force is sustained pick-to-ice anchoring under the ice.

Using an external bracing mechanism that prevents bending loads allows the thermal pick to be made significantly smaller than would otherwise be possible. When operating under tensile loads, even tellurium copper (the material used in this study) with a modest yield stress of 205 MPa, a safety factor of 2, and an anchoring load of 1.3 kN (the weight of one metric ton on Europa), the required core area is 12.7 mm^2 according to Equation (54), which is smaller than even thermal pick (A) that was described in Section 4.1.1.2.

5.8 End Effector Designs

Anchoring will not be feasible if it is discovered that Europan ices are incapable of bearing loads. However, if strong ices are found at or near the surface, then anchoring will be possible. For this reason, two end effectors were designed and prototyped. The first end effector is optimized for strong ices at the surface while the second end effector is optimized for creating deep anchors at minimal energy cost.

The short thermal pick end effector is designed for simplicity and is proposed for applications in which the required anchoring depth is shallow. If strong surface ices are found on Europa or other icy moons, then shallow anchors may be capable of supporting the necessary anchoring loads. This design does not have lateral stabilization since the short thermal picks do not incur large bending loads. This design does not require lateral stabilization because the short thermal picks are not susceptible to bending failure.

The long thermal pick end effector is designed for applications in which the required anchoring depth required is deep. Current estimates of the porosity of Europa's surface suggest that at least the uppermost optical layer is highly porous (95%) [16], the meter-scale ice is slightly less porous (50-75%) [17], and the deeper ices have lower porosities (10%) [18]. It is also possible that a surface crust has formed, which increases the strength of porous surface ices [19]. Since ice strength is shown to depend on porosity [13], confirming this porosity range is necessary.

The design of both end effectors assumes their use on a rover that has limbs that are capable of motion (external actuators). This allows both end effectors to be

passive, only requiring electronics to support the thermal pick heater and thermocouple.

5.9 Short Thermal Pick End Effector Design

The short thermal pick end effector can be seen in Figure 57. It is made of two short thermal picks, an aluminum base, and thermal insulation. Its thermal picks are wide enough to support any bending loads that may develop during anchoring. The thermal picks used for this prototype have a 12.7 mm diameter tip and slight taper and have a maximum insertion depth of 6 mm. This leads to a borehole volume of 0.76 cm^3, which at an efficiency of 0.3 translates to a total insertion energy cost of approximately 2.72 kJ (not including warming, conduction, or extraction). The simplicity of this system will allow it to be modified to suit the needs of a range of rover styles but requires that strong surface ices be present.

5.9.1 Experimental Testing

A block of compressed ice was cooled to cryogenic temperatures using dry ice and then mounted in a raised position to demonstrate wall-climbing capability. The thermal picks were warmed to their operational temperatures using their embedded cartridge heaters and then inserted into the ice in a single motion until they thermally stalled. Since this testing was performed at atmospheric pressures, the thermodynamic behaviors of a thermal pick insertion under vacuum were not observed, although the structural characteristics of the ice during anchoring were assumed to be roughly similar. The thermal picks were allowed to conductively cool for several minutes after being inserted and before anchoring loads were applied.

The end effector was loaded with approximately 20 Nm of torque. The anchoring load applied caused failure of the ice block at its mounting clamps due to their compressive point loads but manually lifting the ice block confirmed that the full torque load could be supported without further failure.

While the cryogenic ice block that was tested was demonstrated to be capable of supporting this torque, it is unknown whether this is indicative of the loads that may be supported by the surface ices of Europa or the other icy moons.

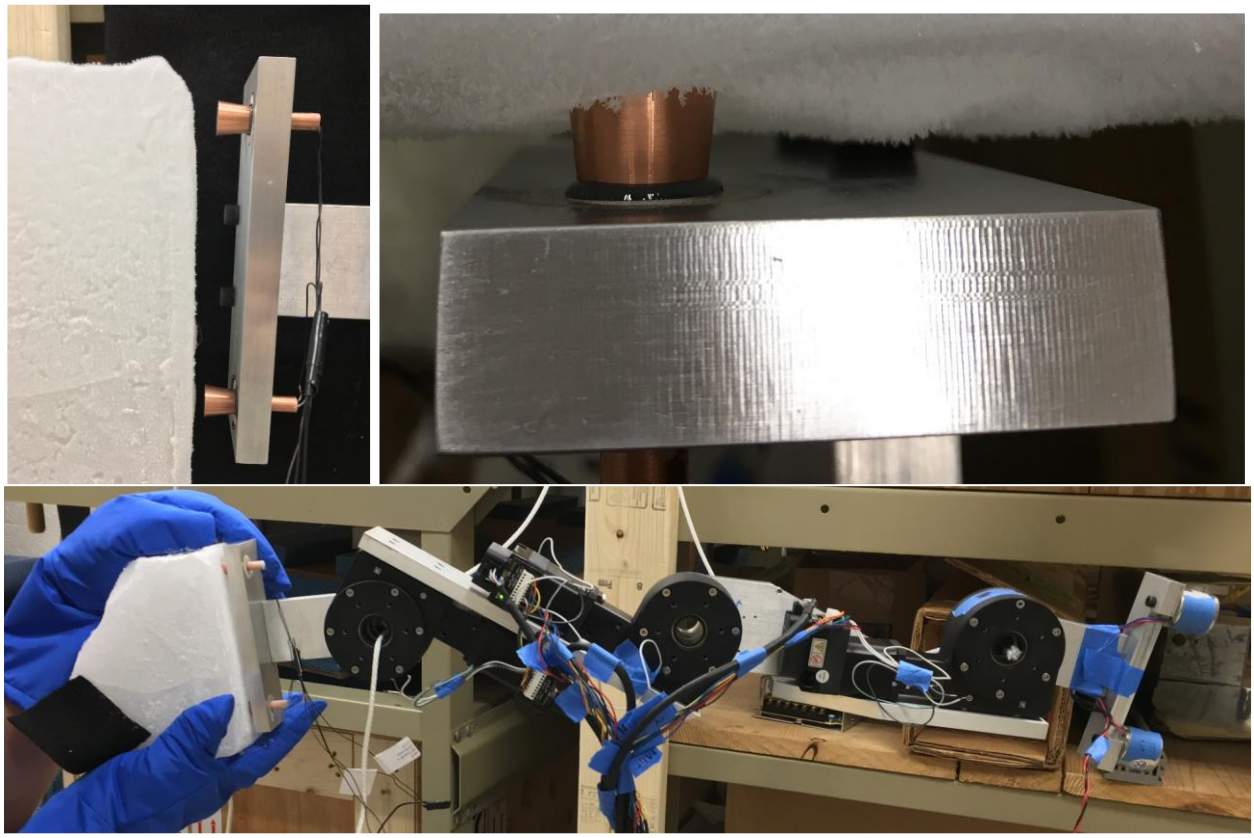

Figure 57: Experimental testing of the small thermal pick end effector bored into cryogenic water ice at atmospheric pressure. Water ice failure due to clamping mechanism (unrelated to the testing) but the end effector still held approximately 20Nm of torque without failure in the cantilevered position.

5.10 Long Thermal Pick End Effector

The long thermal pick end effector is a passive spring-based “heat and press to engage/release” concept proposed for use on a rover that already has actuated limbs. The end effector is made of a leg, external bracing mechanism, thermal pick, and associated components. The end effector requires the application of an external force directed towards the surface of the ice to compress its spring. This force is provided either by rover weight or a previously inserted thermal pick anchor.

The end effector is split into the “upper leg” and “lower leg” which translate relative to one another using sleeve bushings. The external bracing mechanism is attached to the lower and the thermal pick is attached to the upper leg. The spring is connected to both the upper and lower leg, keeping the thermal pick recessed within the lower leg. When the external force is applied, the spring compresses and the thermal pick is exposed. This allows for thermal drilling and eventual anchoring.

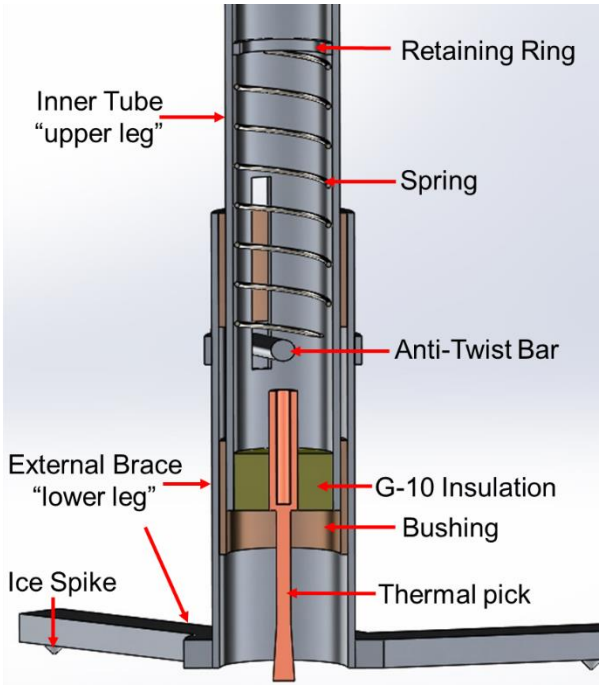

Figure 58: Long thermal pick end effector SolidWorks model. Cross-cut view with internal and external components shown.

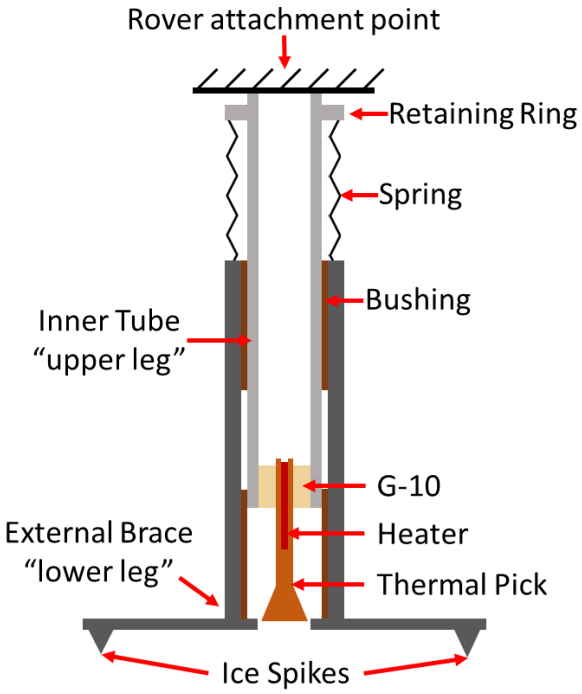

Figure 59: Illustration of the long thermal pick end effector.

5.10.1 Components and Characteristics

The upper and lower leg pieces are made of aluminum 6061 tubing and are separated by frelon-lined bushings, limiting friction during relative axial motion. The anti-twist bar prevents the lower and upper leg pieces from rotating around one another. The G-10 insulation rigidly connects the thermal pick to the upper leg and minimizes internal conduction during thermal drilling.

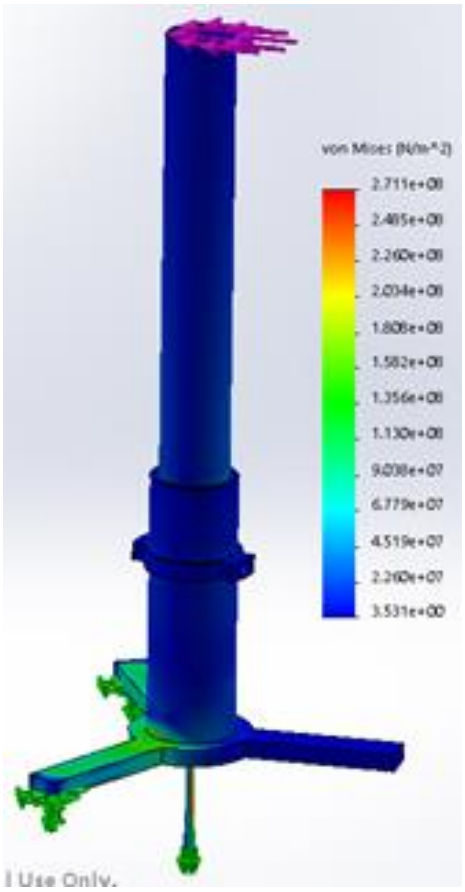

Figure 60: Simulated loading of the long thermal pick end effector. A load of 130N is distributed perpendicular to the top of the end effector.

Thermal pick (A) is used to minimize the energy expenditure given that lateral support enables purely tensile loading of the thermal pick during anchoring. The anchoring load of the end effector supporting the rover is conservatively assumed to

be perpendicular to the axial direction, causing the end effector to be cantilevered about the anchor point. The simulated cantilever strength of this prototype is 130N as seen in Figure 60.

5.10.2 External Bracing Mechanism

The gripping mechanism is used to support lateral forces and moments that arise during the use of the end effector as a thermal pick or during the thermal drilling process. The gripping mechanism can fail either through slipping or tip-over. Slipping is defined as when the lateral force exceeds the friction force between the ice spikes and the ice surface and is dependent upon the friction coefficient (μ_f) and spring force (F_s) according to Equation (76). The friction coefficient is a function of the material properties and contact geometry of the ice spike and the surface ice, which is not studied here. However, cryogenic ices do not have the low surface friction that is typical of terrestrial ices [20].

Tip-over is defined as when the lateral force causes a moment about the anchor point that exceeds the maximum moment supported by the spring force. The moment supported by the spring force is proportional to the moment arm provided by the gripping mechanism (d_{min}) which is a function of the number of spikes (n_{spike}) and their distance from the central axis (d_{spike}) which can be seen in Figure 61. Three spikes that are evenly distributed about the central axis are assumed optimal because this ensures contact for each spike and the greatest minimum moment arm by Equation (77). The moment caused by a lateral force is also proportional to the height of the end effector (L_{EF}).

$$F_{l,slip} = \mu_f F_s \tag{76}$$

$$d_{min} = d_{spike} \cos\left(\frac{\pi}{n_{spike}}\right) \tag{77}$$

$$F_{l,tip} L_{EF} = F_s d_{min} \tag{78}$$

5.10.3 Concept of Operations

The following concept of operations is for rover mobility and is illustrated in Figure 61, Figure 62, and Figure 63. The end effector shown assumes two ice spikes for simplicity of the two-dimensional illustration.

5.10.3.1 State I: Free Motion

State (I) of the end effector is prior to placement at the insertion site. The future insertion site for the end effector is determined in this state and the thermal pick can begin its warming prior to placement if desired. If the thermal pick has recently been extracted from the ice by thermal drilling, then it will be warm and losing heat through internal conduction during State (I). This incentivizes quickly transitioning to placement and insertion.

5.10.3.2 Process I-II: Placement

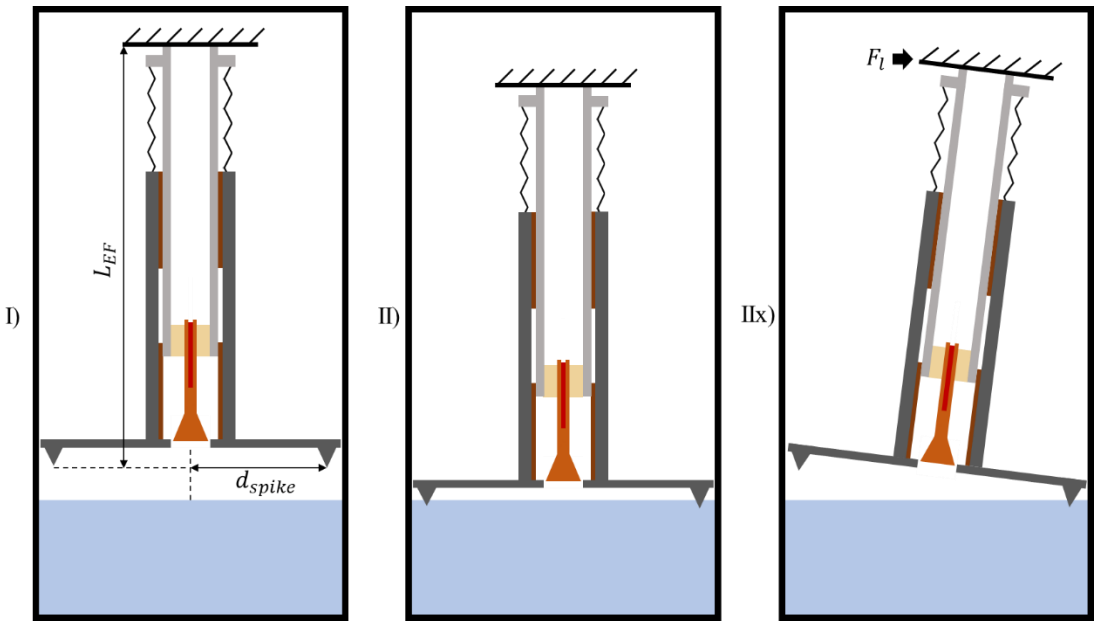

Figure 61: Illustrated concept of operation states I, II, and IIx of the long thermal pick end effector.

This process is the placement of the external bracing mechanism onto the ice surface using the rover's actuators. A stable placement of the external bracing mechanism against the ice is necessary so the thermal pick can be inserted without any lateral motion of the thermal pick. Process (I-II) ends when the external bracing mechanism is securely pressed against the ice and the thermal pick has finished warming to its operational temperature using the embedded heater.

Once in stable contact with the ice, excessive lateral forces (F_l) applied at the rover attachment point will lead to tip-over of the end effector (IIx), preventing the safe insertion of the thermal pick. Since the thermal pick is retracted within the body

of the end effector until the insertion process, this tipping will not result in improper loading of the thermal pick.

5.10.3.3 Process II-IV: Insertion

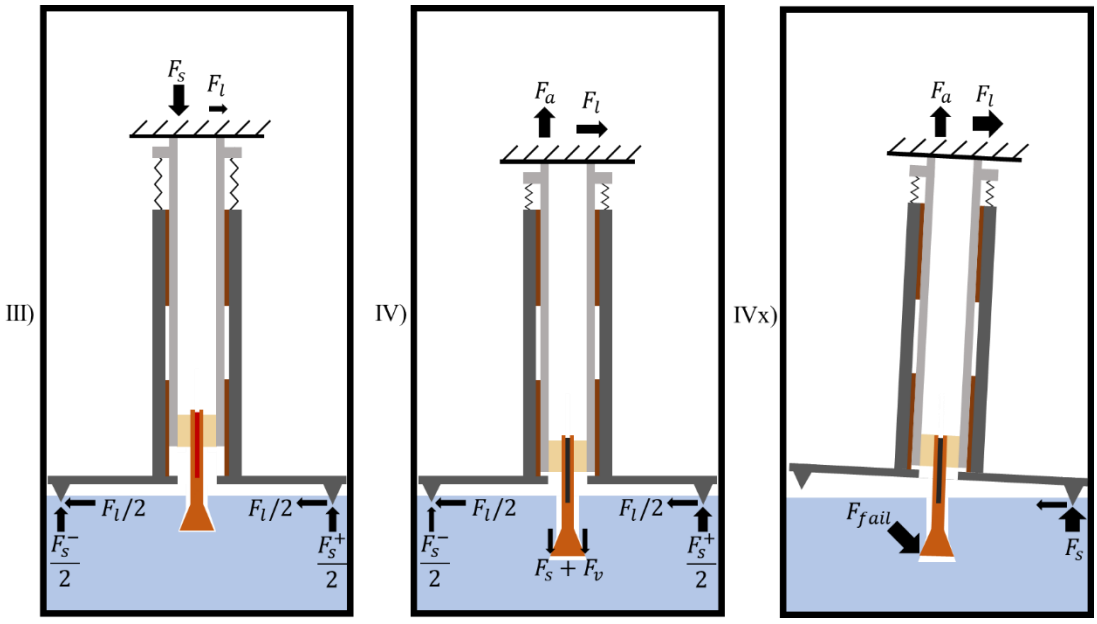

Figure 62: Illustrated concept of operation states III, IV, and IVx of the long thermal pick end effector.

Insertion of the thermal pick uses an applied force that exceeds the spring force (F_s^+). This compresses the spring and drives the thermal pick into the ice, with contact resulting in thermal drilling. During thermal drilling there will be pick-to-ice pressure resisting insertion, requiring an additional application of force. However, experimental testing has shown that this additional force is less than 6.5 N for the thermal picks used. Throughout the entire insertion phase up until anchoring (IV), the spring force is supported by the spikes on the gripping plate, which laterally secures the end effector. Because insertion of the thermal pick is based on intermittent insertion, several intermediate holding phases (III) are required between insertion steps where the applied force is equal to the spring force (F_s).

At any point during insertion of the thermal pick, an applied lateral force (F_l) will result in a differential applied load across the spikes on the gripping plate. If the applied lateral force exceeds the tip-over condition described in Equation (78), then failure of the end effector may occur (IVx).

5.10.3.4 State IV: Anchoring

Once anchored, there is no longer a need to actively control the force applied at the rover attachment point and the end effector can support axial (F_a) and lateral loads (F_l). During anchoring, the contact between the thermal pick and the ice resists the spring force and this continues to drive the ice spikes of the gripping mechanism into the ice surface. When anchored, lateral forces exceeding the tip-over condition by Equations (78) will result in failure. The axial force limit is based on tensile failure of the thermal pick discussed (Section 5.1.3) or the ice (Section 4.5.6).

5.10.3.5 State V: Warming

The warming state is when the thermal pick is heated without physical contact with the ice. An applied force at the rover attachment point that balances the spring force (F_s) will release the contact between the thermal pick and the ice as shown in state (V). This thermally disconnects the thermal pick from the ice, allowing warming without conduction into the ice. Extraction of the thermal pick can begin once the operational temperature is reached.

5.10.3.6 Process V-VI: Extraction

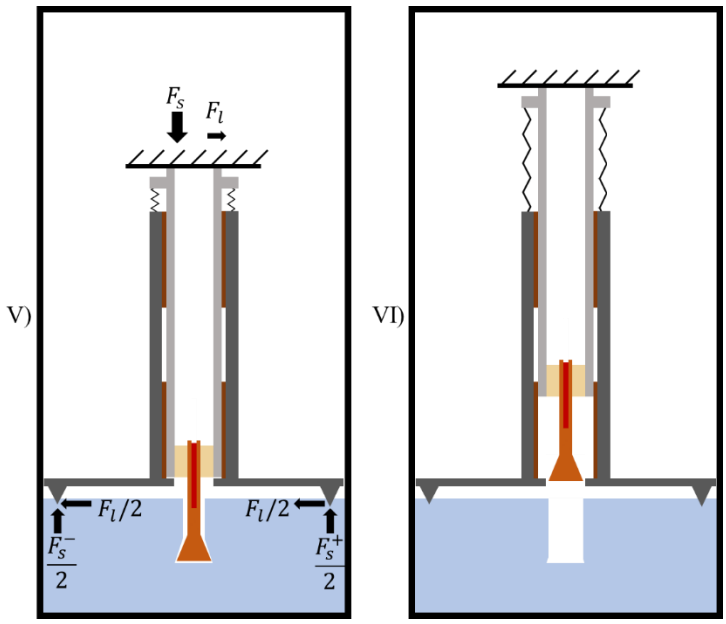

Figure 63: Illustrated concept of operation states V and VI of the long thermal pick end effector.

Extraction of the thermal pick uses intermittent thermal drilling. An applied force slightly less than the spring force (F_s^-) causes the thermal pick to retract back into the end effector. This process is completed when the thermal pick has been fully retracted (VI) and is equivalent to the initial state (I).

5.10.4 Experimental Testing

Due to concerns over violating the tip-over condition, the long thermal pick end effector was manually inserted during experimental testing. Manual insertion of the end effector was performed with a pre-heated thermal pick and cryogenic ice at atmospheric pressure. The ice was cooled using dry ice to a temperature of -60 °C and was secured using the dry ice test rig mount described in Section 4.1.2.11.

Since this experiment was performed at atmospheric pressure, there was no

mechanism to evacuate meltwater from the borehole and so the thermal pick remained exposed to cold liquid and ice. This sustained exposure rapidly cooled the thermal pick and quickly resulted in thermal stall after only a shallow insertion. The heater was then turned off, allowing the thermal pick to equilibrate to the ice temperature. Despite the limited insertion length, a manually applied axial load was unable to cause ice or thermal pick failure.

Lateral cantilever loading was also tested. The end effector successfully held 6.8 Nm but tip-over failure occurred at 13.6 Nm. This failure was a result of the partial force, reducing the spring force and therefore the tip-over moment according to Equation (78). The tip-over failure caused the thermal pick to bend, preventing further testing.

Figure 64: Experimental testing of the long thermal pick end effector bored into cryogenic water ice at atmospheric pressure.

Figure 65: Cantilever loading of the long thermal pick end effector.

5.11 Conclusions

A mechanical analysis of the thermal picks was used to determine their optimal design characteristics. Scaling laws for various end effectors have been presented and show the relative energy cost for each design corresponding to their anchoring depth. Long thermal picks can provide deep anchors but are susceptible to bending. The depth required for an anchoring hold is a function of the ice quality. When long thermal picks are necessitated by weak ices, external bracing mechanisms that prevent bending are incentivized.

The optimal thermal pick design depends on whether the ice will sublimate or melt during thermal drilling. For water ice, the tapered thermal pick design is optimal because of its simplicity since it operates using linear insertion and extraction, leveraging re-freezing effects to lock within the ice. For dry ice, the screw thermal pick design is optimal because it requires only one actuation system that provides coupled linear-rotational motion.

The long thermal pick end effector has an external bracing mechanism to permit the use of a thin thermal pick, driving down energy costs. It is a passive system that leverages rover actuation for its use. The short thermal pick end effector is designed for thermal picks that can withstand bending loads. This end effector design is simple and is made only of the thermal pick(s), thermal insulation, and structures required to mount to a rover.

Experimental testing of both end effectors at atmospheric pressure and thermal pick testing under vacuum show the potential for end effector feasibility. The meter-scale surface conditions on Europa are currently unknown but will have important implications for the use of any ice anchoring system. If the ices on Europa are porous and weak, then anchoring systems may not be viable. However, if ices that are strong enough to support anchoring loads are found at or just below the surface, then the thermal pick end effectors could allow for safe mobility through extreme terrains.

Chapter 6: Conclusions and Future Work

The “thermal pick” system was developed to act as a combined thermal drill and ice anchor for rovers traversing the harsh environments found on Europa or other icy planetary bodies. Thermal drilling using a hot thermal pick excavates an ice borehole in which the thermal pick can anchor, enabling a rover to traverse the Europan surface. The feasibility of the thermal pick concept and the associated components was demonstrated using simulated ambient conditions on Europa, creating the foundation for future application-specific optimization of the system.

Complementary experimentation and design were performed through multiple cycles of theoretical analysis, design, prototyping, and experimental testing. This enabled a continuous evolution of thermal pick designs that would accommodate or leverage the phenomena that were observed in prior rounds of testing. The result of this work is a collection of designs adapted for operating in either cryogenic dry ice on Mars using the sublimation regime or in cryogenic water ice on Europa using the melting regime.

6.1 The Thermal Pick

The thermal pick is a novel system made of a conductive metal body and an embedded heater. To serve as a thermal drill, the body of the thermal pick stores the energy provided by the heater and rapidly conducts that heat into the ice when contact is initiated. After thermal drilling has created a borehole, the thermal pick that is inside it can function as an anchor. This requires that the body of the thermal pick be

capable of supporting the weight of a rover in motion. This simple concept provides a low mass, low energy, and high reliability approach to anchoring into surface ices.

A range of thermal pick shapes were analyzed and assessed for their predicted anchoring strength and energy costs. A tapered thermal pick with linear insertion and extraction was determined to be the optimal design for water ice use where re-freezing meltwater can seal the thermal pick within the ice. Screw thermal picks were determined to be optimal for dry ice use.

6.2 The End Effector

An end effector is a complete system that is made of a thermal pick, thermal insulation, and stabilizing mechanisms where necessary. The end effectors designed in this work are for use on a rover and leverage existing actuation. The type of end effector used will depend on the rover's weight and the strength of the ice.

Large rovers and weak ices will necessitate the use of end effectors optimized for deep anchor holds. The long thermal pick end effector is designed for such missions. An external gripping mechanism attached to the bottom of the end effector uses a set of ice spikes to brace against the ice, providing lateral stability that prevents bending of the thermal pick. A constant force between the ice spikes and the ice is passively maintained by a compressed spring. This approach permits the use of long and thin thermal picks, yielding deep anchors for minimal energy cost.

The short thermal pick end effector is designed for missions where strong surface ices are expected. It uses short and strong thermal picks that hold the full weight of the rover. This end effector requires no stabilizing mechanisms, giving it a small profile that is adaptable to various rover designs.

The end effector designs are passive and have few moving parts, which is advantageous for autonomous robotics where reliability is of paramount importance. Thermal gradients created during the thermal drilling process can damage the ice and so operational conditions that mitigate this failure type were developed.

Using a thermal drill generally requires substantial energy and could be burdensome for autonomous planetary robotics. An intermittent thermal drilling approach was developed that simultaneously minimizes the total energy cost and the peak heater power required. This is achieved because intermittent drilling limits conduction into the ice, which is the primary mechanism for heat loss.

6.3 Anchoring into Carbon Dioxide Ices

Thermal drilling experimentation using dry ice led to an understanding of the sublimation process and its implications for thermal pick insertion and anchoring. The phenomena observed in the sublimation regime all stem from the rapid production of gas. These are the pushback force, reduced friction, and heat loss into the escaping gas flow.

The pushback force is the result of gas pressure building up across the leading edge of a thermal pick. It can separate the thermal pick from the ice, reducing heat transfer rates and slowing the thermal drilling process. Countering the pushback force was achieved by controlling the tip shape and applying external forces.

The reduced friction caused thermal picks to slip laterally on slanted ice surfaces during initial insertion into the ice. This resulted in oblong boreholes that are energetically inefficient. Reduced friction was countered with high stiffness components and the addition of stabilizing mechanisms.

The heat lost into the escaping gas flow increases the energy cost of thermal drilling. Thermally insulated walls did not provide significant benefit. However, smooth wall geometry and lower operating temperatures both increase thermal efficiency.

Sublimation is the dominant mode of thermal drilling for dry ice due to the high triple point pressure of carbon dioxide. The screw thermal picks that are recommended for dry ice were shown to have efficiencies of over 75%. Future work will be required to determine the anchoring strength of dry ice anchors in simulated planetary conditions and for the development of an end effector design that accommodates coupled linear and rotational motion.

6.4 Anchoring into Cryogenic Vacuum Water Ices

Steady-state thermal drilling in cryogenic water ice at vacuum pressure has already been demonstrated by prior research to result in sublimation of the surface ice with brief periods of melting. These studies have shown that thermal drilling water ice requires a large energy expenditure that is driven by conductive heat loss. To mitigate these conductive losses, an intermittent thermal drilling approach was developed.

Intermittent thermal drilling leverages the thermal storage capacity of a hot thermal pick to create short periods of rapid thermal drilling activity separated by delay periods. When a hot thermal pick is pressed against water ice, the ice melts and the thermal pick begins to cool. During delay periods when the thermal pick stops moving, conductive losses are halted by thermally severing conduction paths between the thermal pick and the ice. Each press-halt cycle drills the borehole deeper, at

efficiencies between 20% and 50% relative to an ideal melting process. This intermittent approach also decouples thermal drilling efficiency from heater power, easing the burden on a rover's power system.

The large range in measured efficiencies and the lack of specific trends in test conditions is indicative of the natural variability and impact of internal conductive losses. However, even a 20% efficiency relative to an ideal melting process represents a dramatic reduction in energy cost relative to the sublimation and melting systems of prior works.

The melting that occurs during intermittent thermal drilling permits re-freeze anchors to be used. Tapered anchors were designed that leverage the conformal re-freezing of meltwater to lock the anchor into the ice.

A consequence of intermittent thermal drilling is the susceptibility of the ice borehole to thermal shock and to re-freeze expansion cracking. Melting under cryogenic ambient conditions may create large thermal gradients and differential expansion/contraction that cause ice to crack in a process called thermal shock. This failure was mitigated by delay periods of greater than 20 seconds. Cracking of the ice is also possible when meltwater re-freezes in a closed volume if the thermal pick cools excessively. A β-function was developed that describes the relationship between the usable thermal reserves and the energy necessary for a thermal drilling step. The β-function was demonstrated to correlate with re-freeze expansion cracking, with high β values indicating resilience to this failure mode. A high β value is achieved through high operating temperatures and small step sizes.

Anchoring tests were performed using cryogenic blocks of water ice and the maximum anchoring load of 130 N was applied at each anchoring test without a single observed failure. In an effort to observe anchoring failure, the minimum feasible anchor depth and width was used but still successfully held the full anchoring load. This suggests that high anchoring forces can be supported if Europa's surface is of similar structure to the test ices used.

The total operational energy cost of a thermal pick undergoing its full usage cycle was simulated. Surprisingly, these simulations showed that internal conductive losses dominated the energy expenditure for the operation of a thermal pick. Internal conductive losses occur via the thermal insulation holding the thermal pick and may be reduced by further design optimization. A simulated total energy cost of 8.40 kJ for a 3 cm insertion of thermal pick (A) means that even a small planetary rover with limited power generation could use a thermal pick for anchoring.

6.5 Path Forward

Advancing the thermal pick and end effector concepts will require continued design iteration, modifications to the test rig, and ice simulants based on observations of the surface of Europa or other planetary bodies.

The thermal pick end effector systems described in this work are prototypes made with off-the-shelf components and limited custom machining. With continued design iteration, they could see improvements to their mass, volume, and strength. While the complete end effector systems have been tested in cryogenic water ice at atmospheric pressure, testing of the complete end effector in cryogenic water ice under vacuum would further demonstrate the feasibility of the system. Development

of a screw-type end effector for sublimation of dry ice would demonstrate the applicability of this concept for Mars or other planetary bodies with carbon dioxide ices.

Future testing with an improved test rig could provide improved thermal drilling and anchoring data. Internal conduction between the thermal pick and the G-10 insulating tube accounted for the majority of the energy expended during the thermal drilling process. Improving the thermal insulation quality would reduce the energy required for thermal drilling and improve the accuracy of thermal drilling data that corrects for this heat loss mode. A test rig designed to withstand higher anchoring loads could be used to demonstrate the applicability of this concept to rovers larger than 100kg. Active liquid nitrogen cooling of the ice would allow for longer tests durations, permitting longer duration operations to be tested while maintaining Europa-realistic ice temperatures. Finally, a test rig designed for vertical insertion would allow the testing of weak and/or porous ices that may better represent the surface of Europa.

Intermittent thermal drilling was designed for rovers exploring Europa's icy surface, but the approach could potentially be adapted to subsurface thermal drilling. Subsurface drilling to access a liquid ocean has great scientific appeal and is an active area of research. Since subsurface thermal drills are not exposed to vacuum after an initial insertion phase, direct use of this thermal pick solution is not possible. However, the main problems facing subsurface thermal drilling are conductive heat loss and the need for high power heaters, which are solved by intermittent thermal drilling.

Appendices

A.1 Cryogenic Water Ice Test Runs

The plots in this appendix show all the temperature, spring displacement, and thermal pick tip position measurements for each cryogenic water ice test. The calculated values associated with these test runs is shown in Table 3.

The thermal pick temperature as measured by the thermocouple is plotted against the right axis scale. The position of the tip of the thermal pick and the spring displacement are plotted against the left axis scale. Brief dips in the measured tip position prior to insertion steps and similar peaks prior to extraction steps are erroneous and caused by spring displacement readings taken prior to updating the slide position. The slide position updates after a step is completed, after which the tip position is correctly measured.

Non-zero baseline spring displacements represent the use of both the constant force springs and extension spring described in Sections 4.1.2.8 and 4.1.2.9, respectively. Spring displacements with a zero baseline represent the use of only constant force springs.

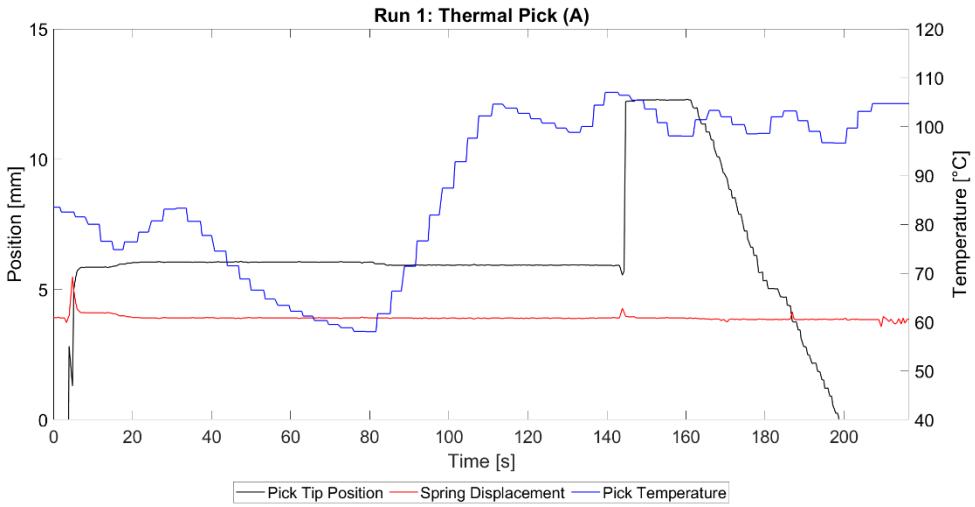

Figure 66: Test run 1 on cryogenic water ice under vacuum.

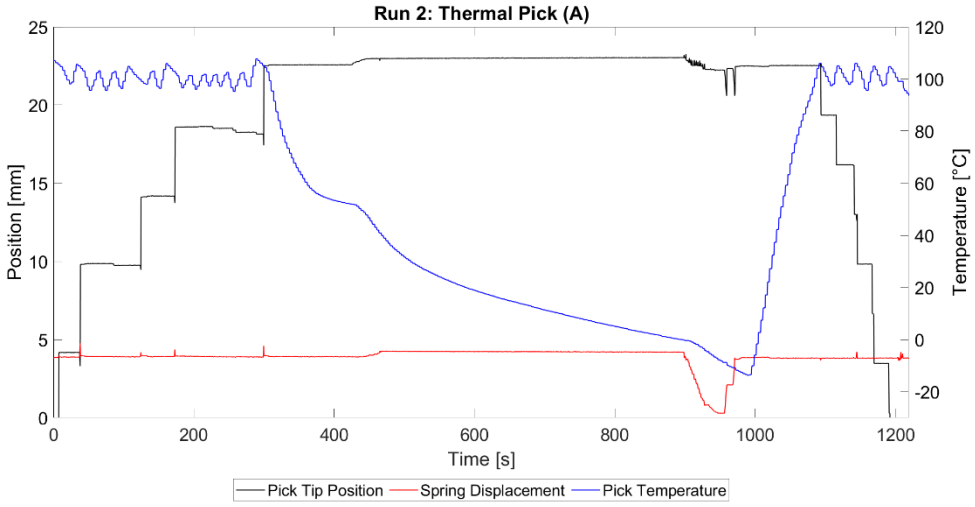

Figure 67: Test run 2 on cryogenic water ice under vacuum.

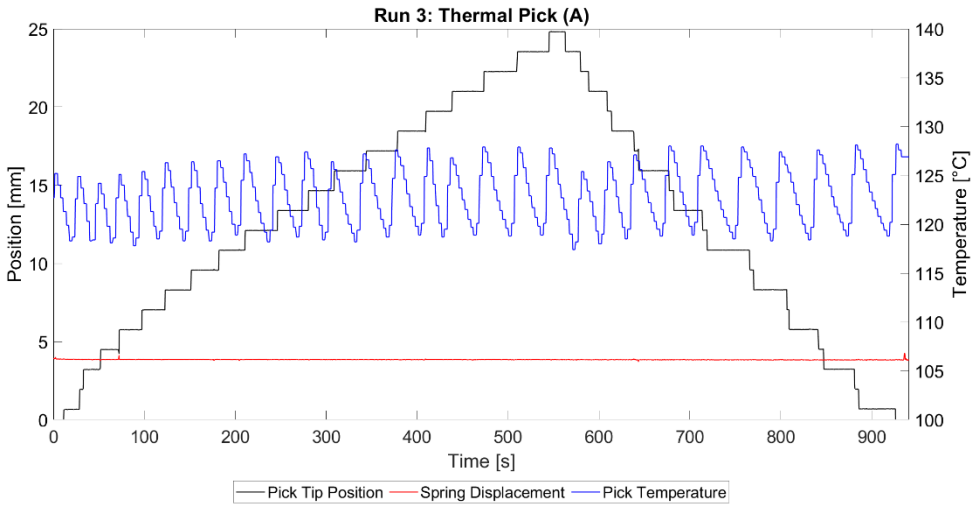

Figure 68: Test run 3 on cryogenic water ice under vacuum.

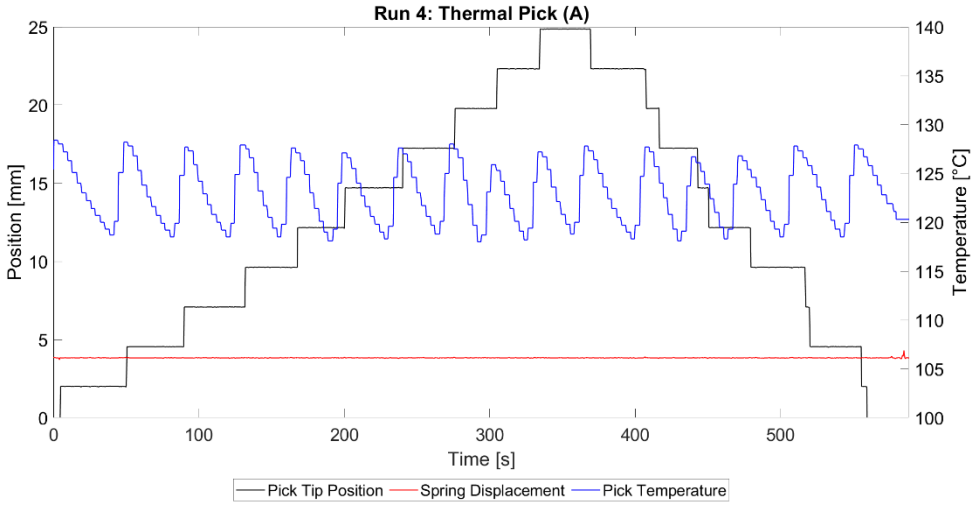

Figure 69: Test run 4 on cryogenic water ice under vacuum.

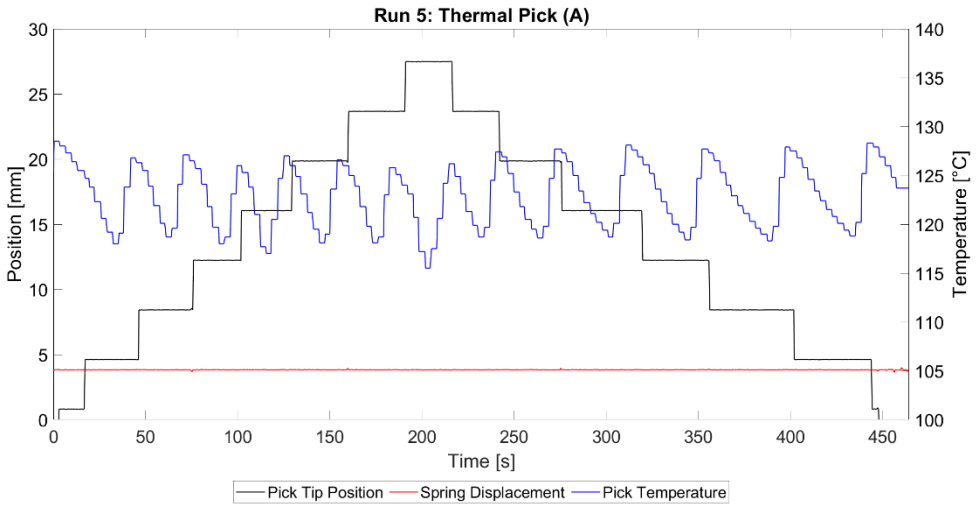

Figure 70: Test run 5 on cryogenic water ice under vacuum.

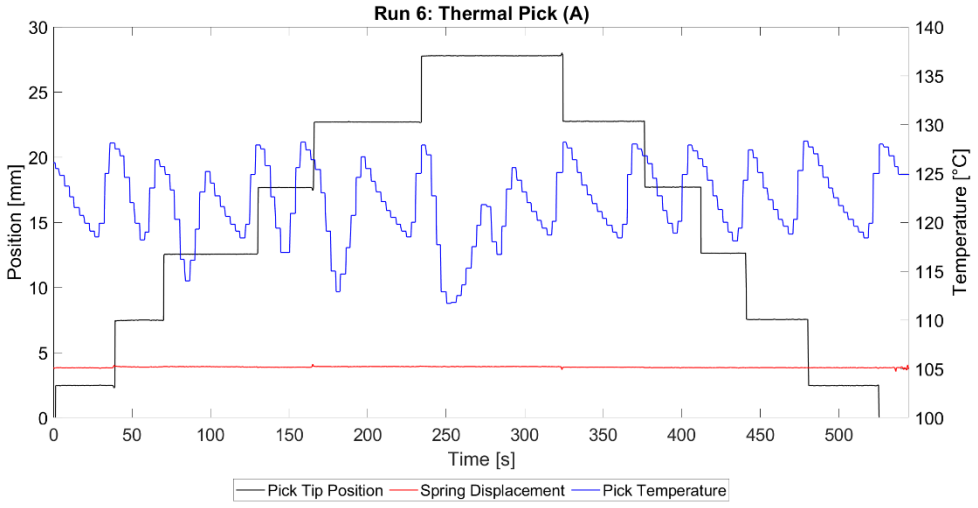

Figure 71: Test run 6 on cryogenic water ice under vacuum.

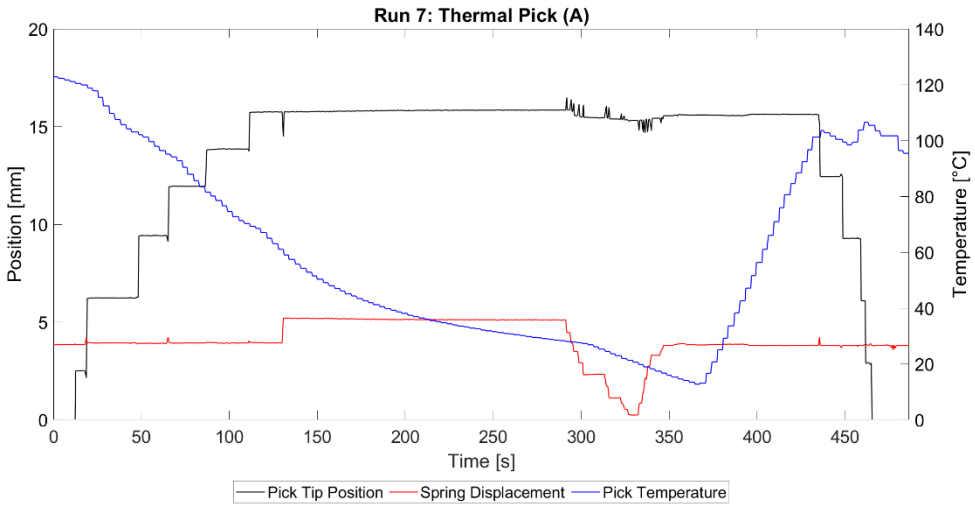

Figure 72: Test run 7 on cryogenic water ice under vacuum.

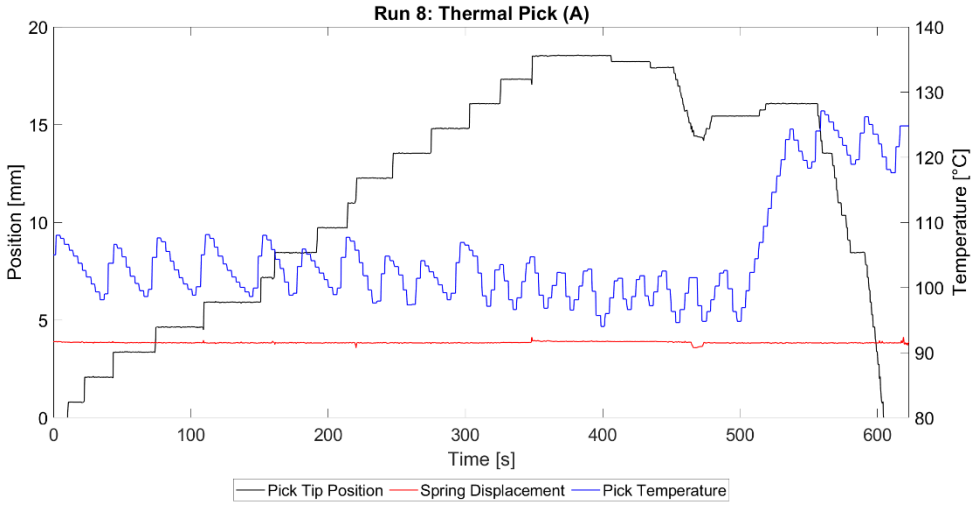

Figure 73: Test run 8 on cryogenic water ice under vacuum.

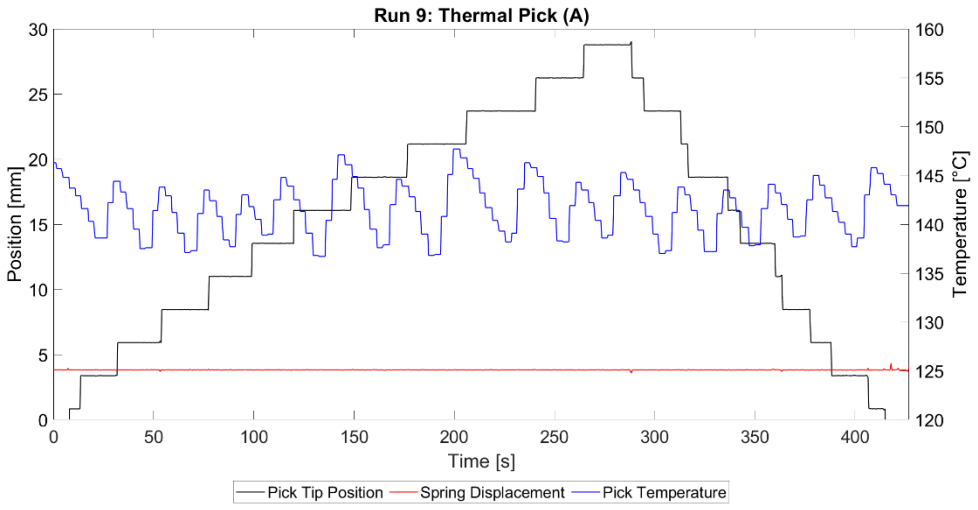

Figure 74: Test run 9 on cryogenic water ice under vacuum.

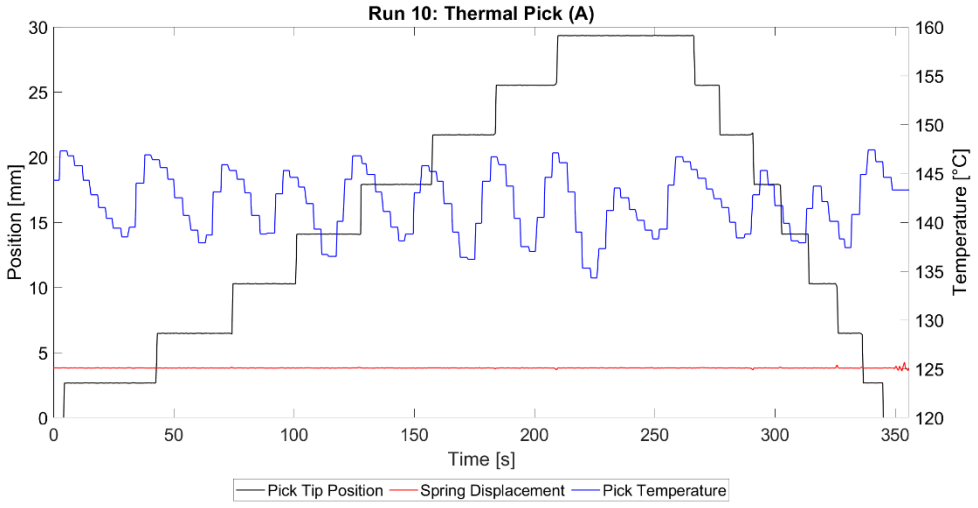

Figure 75: Test run 10 on cryogenic water ice under vacuum.

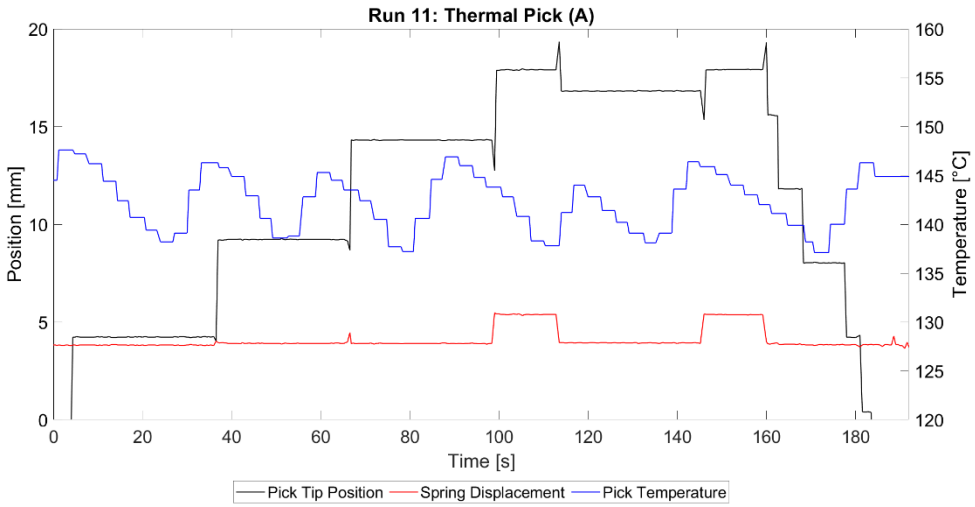

Figure 76: Test run 11 on cryogenic water ice under vacuum.

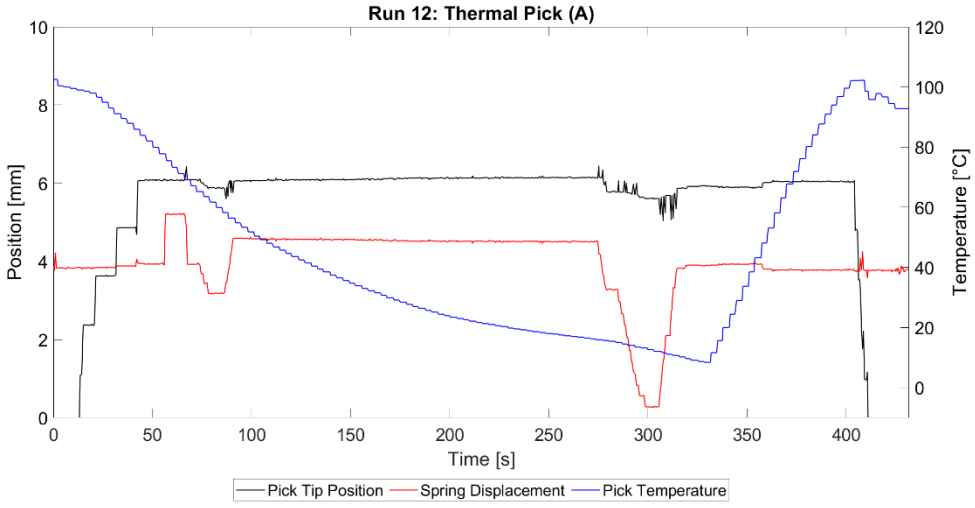

Figure 77: Test run 12 on cryogenic water ice under vacuum.

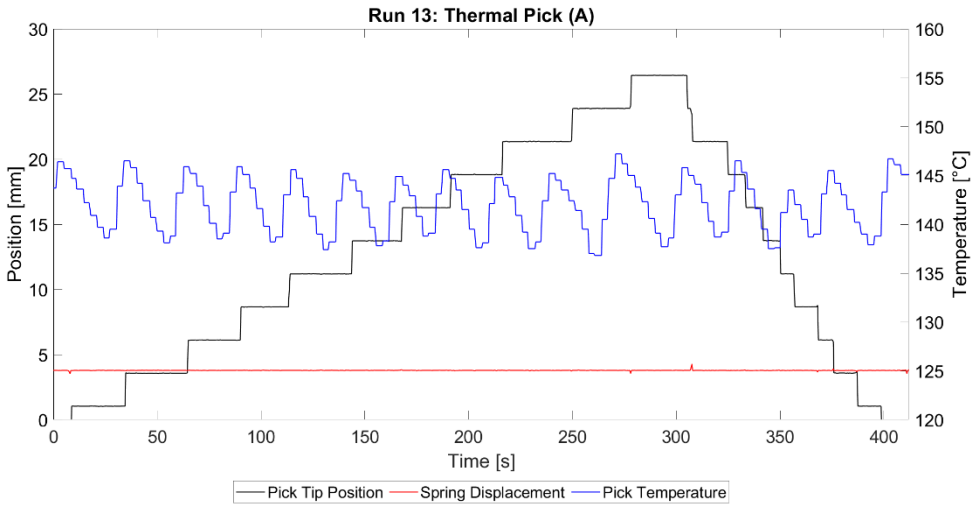

Figure 78: Test run 13 on cryogenic water ice under vacuum.

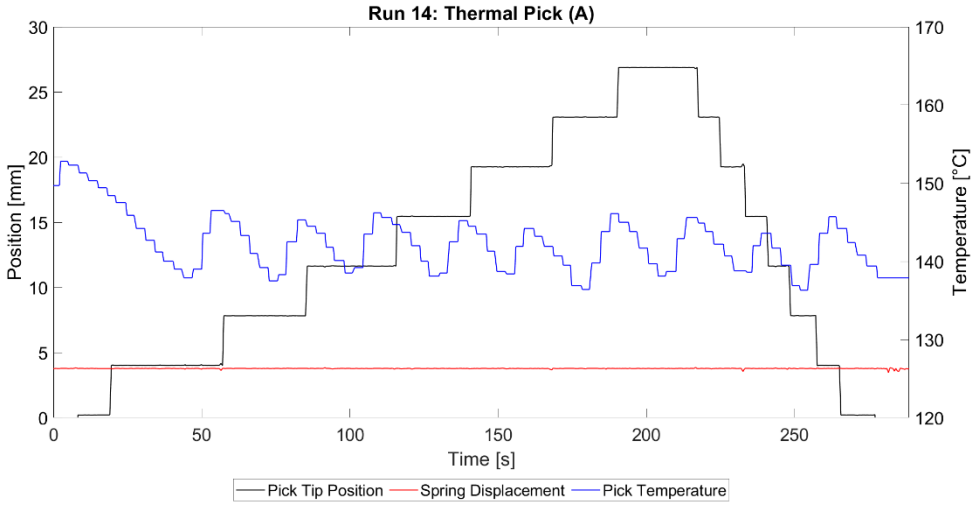

Figure 79: Test run 14 on cryogenic water ice under vacuum.

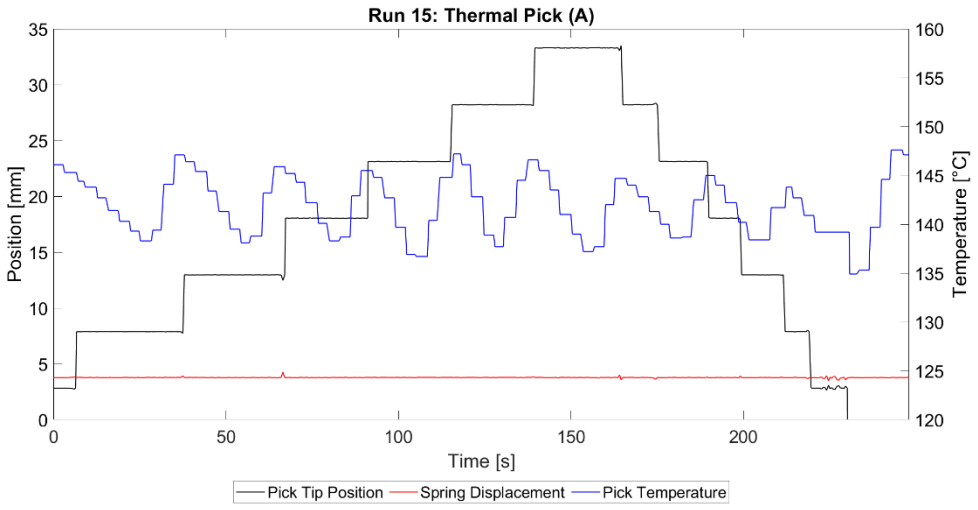

Figure 80: Test run 15 on cryogenic water ice under vacuum.

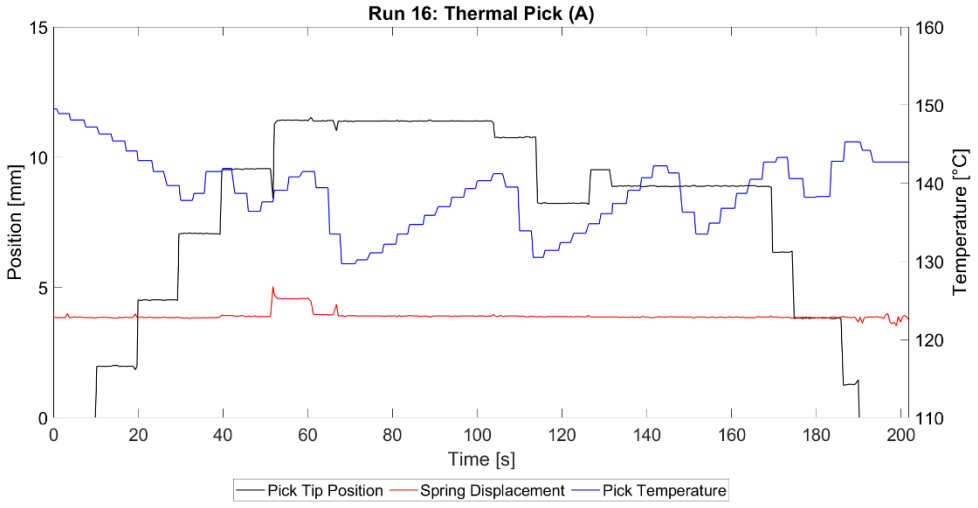

Figure 81: Test run 16 on cryogenic water ice under vacuum.

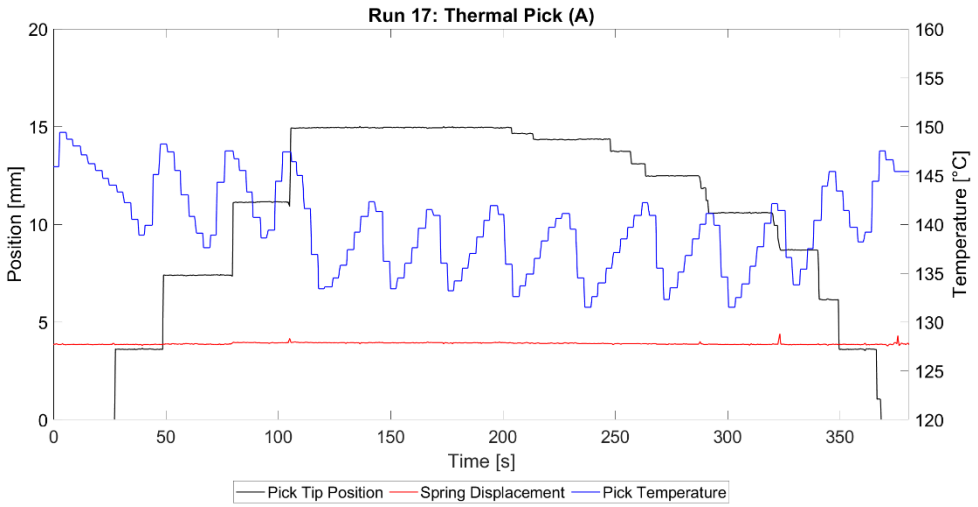

Figure 82: Test run 17 on cryogenic water ice under vacuum.

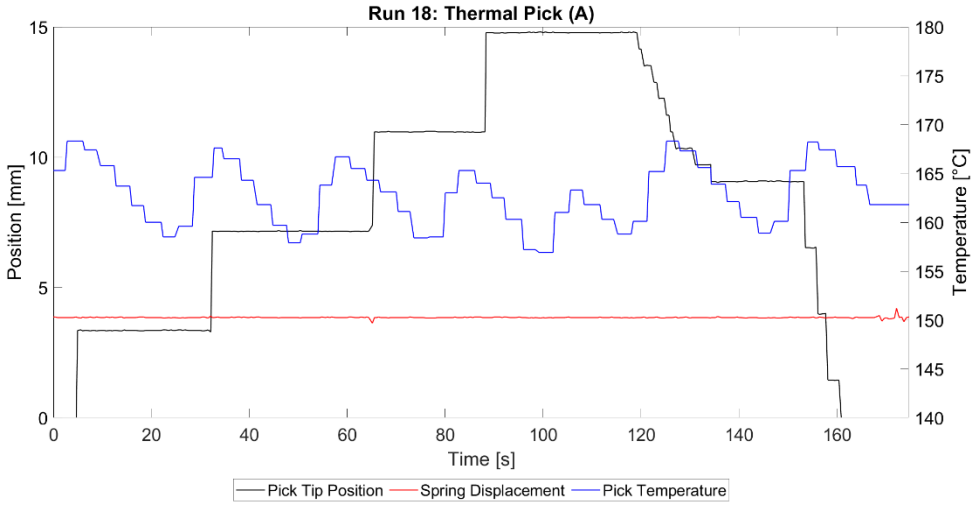

Figure 83: Test run 18 on cryogenic water ice under vacuum.

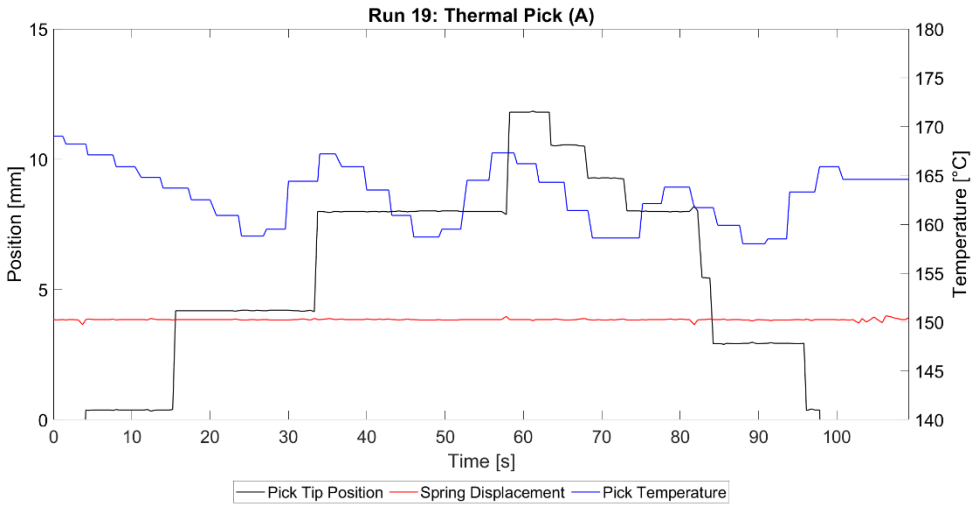

Figure 84: Test run 19 on cryogenic water ice under vacuum.

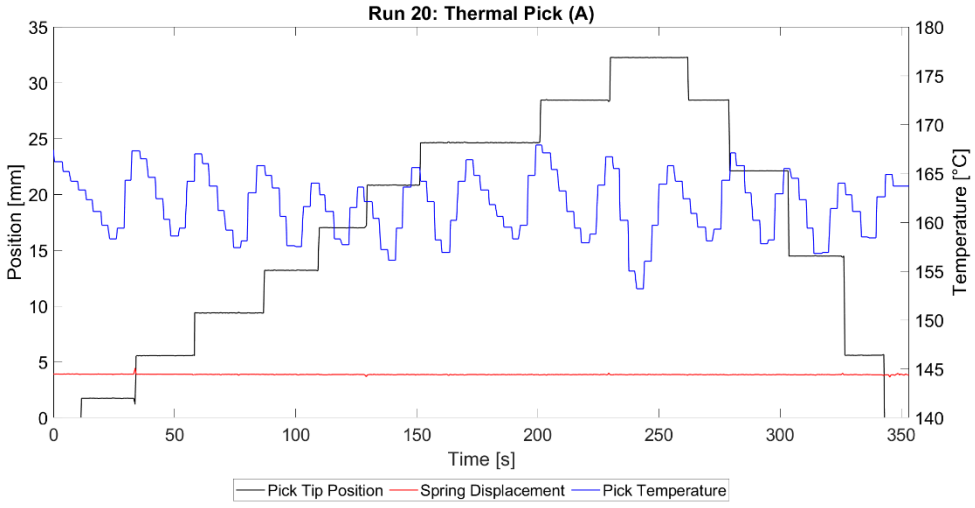

Figure 85: Test run 20 on cryogenic water ice under vacuum.

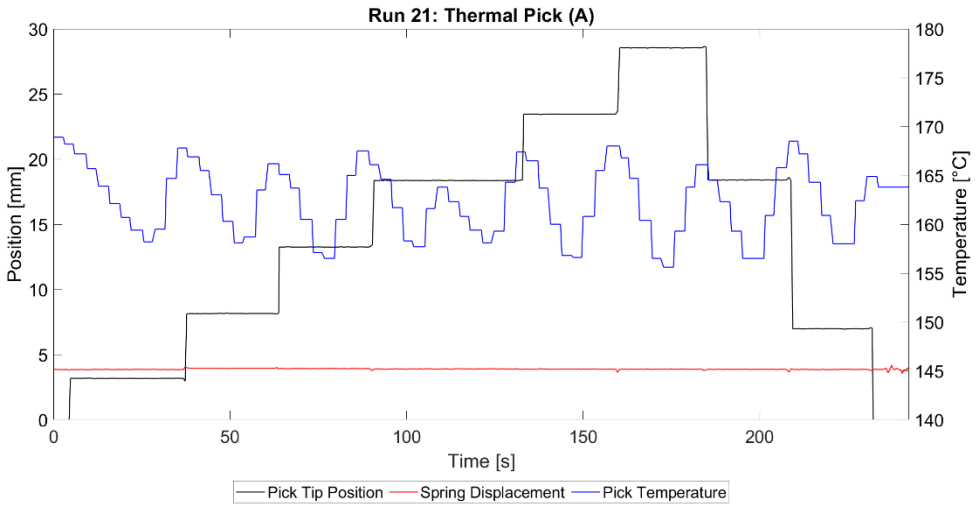

Figure 86: Test run 21 on cryogenic water ice under vacuum.

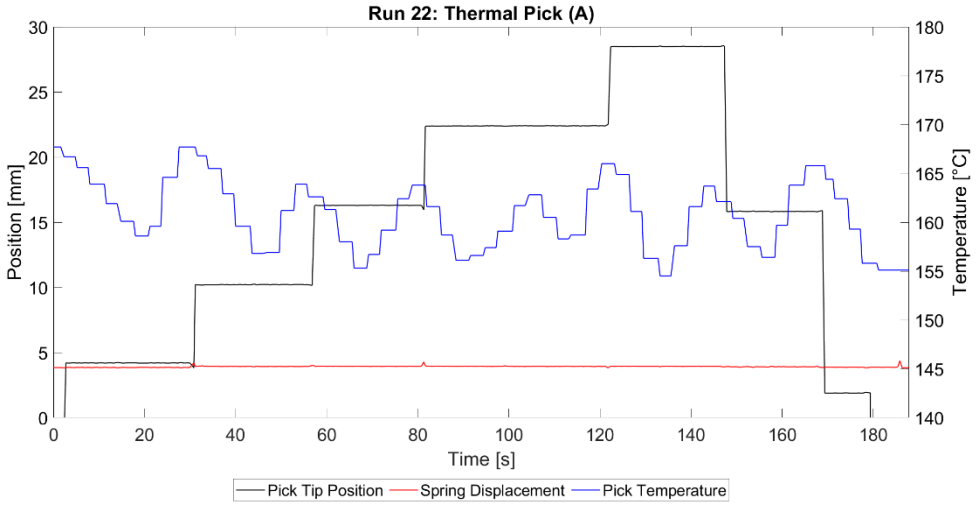

Figure 87: Test run 22 on cryogenic water ice under vacuum.

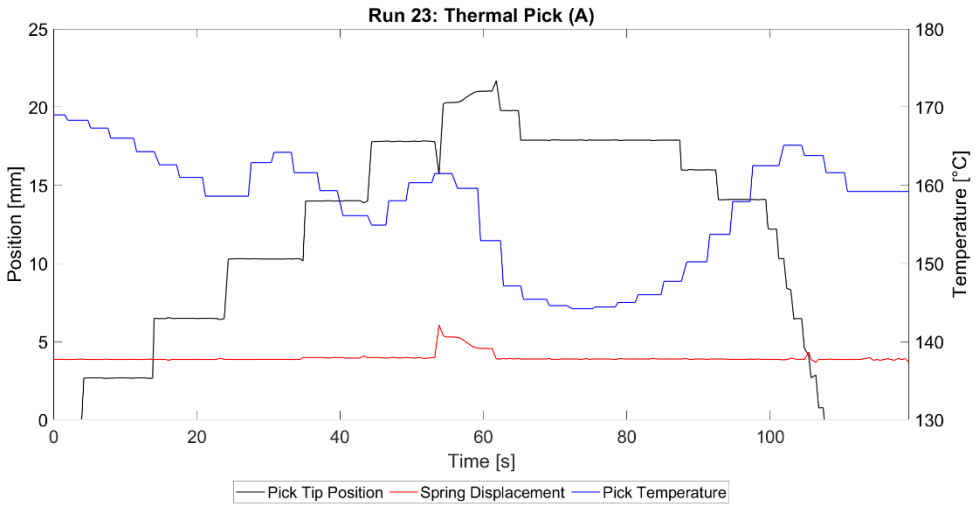

Figure 88: Test run 23 on cryogenic water ice under vacuum.

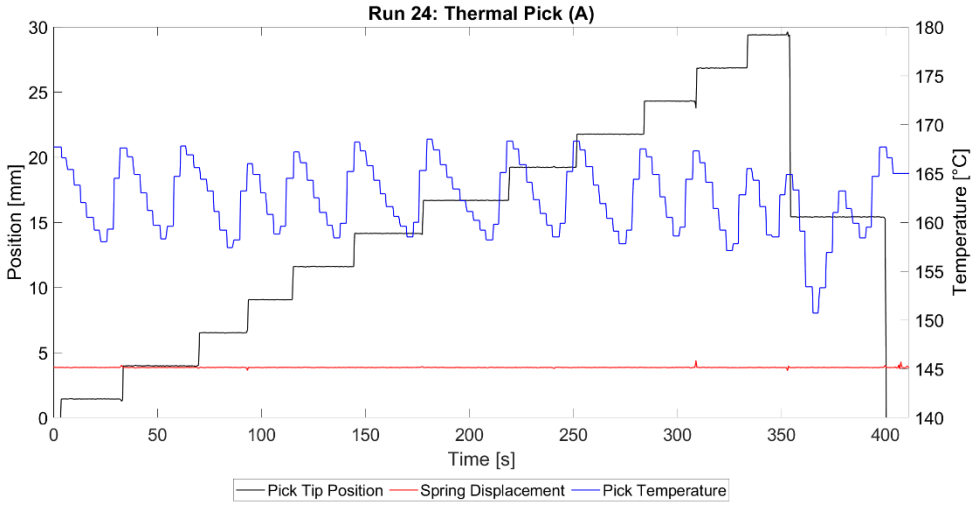

Figure 89: Test run 24 on cryogenic water ice under vacuum.

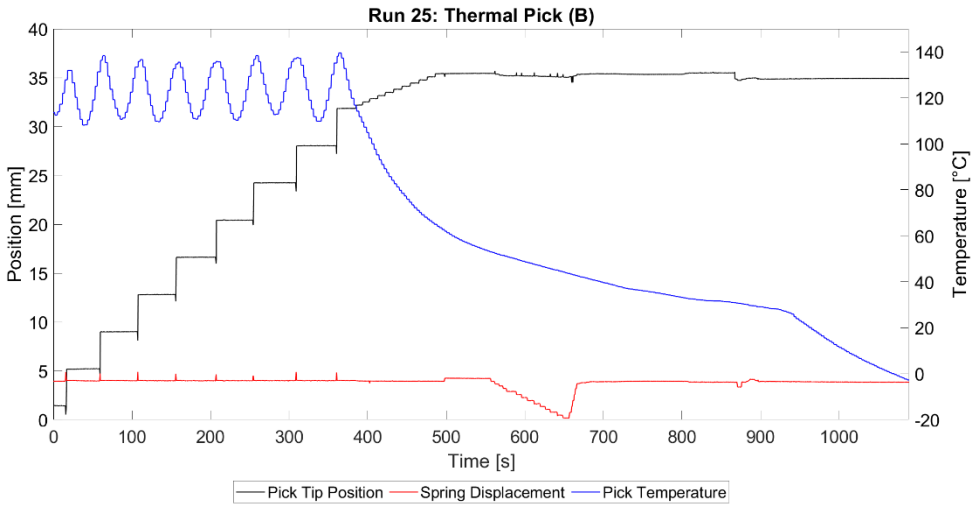

Figure 90: Test run 25 on cryogenic water ice under vacuum.

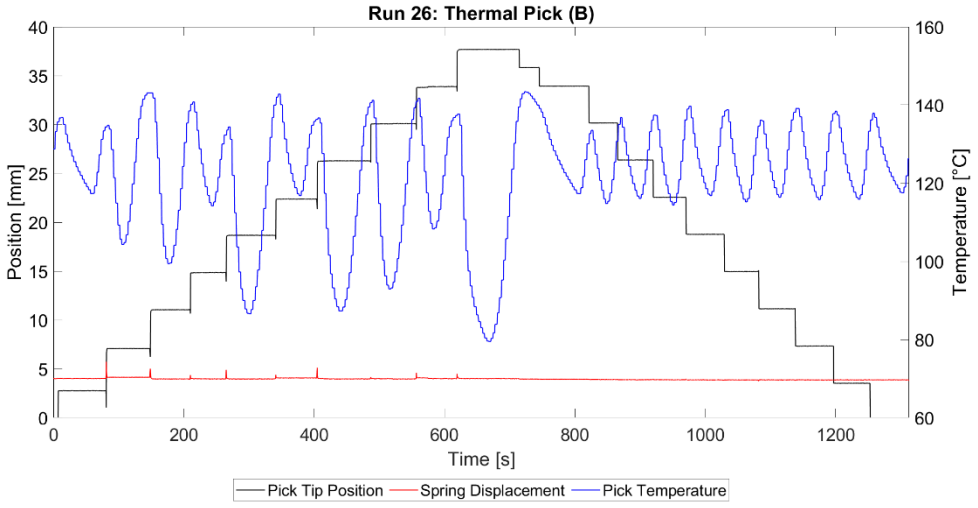

Figure 91: Test run 26 on cryogenic water ice under vacuum.

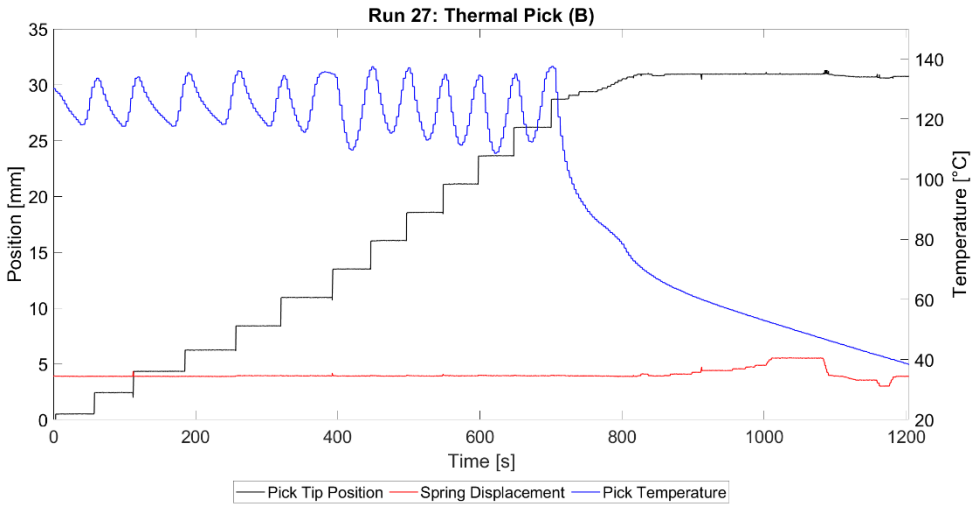

Figure 92: Test run 27 on cryogenic water ice under vacuum.

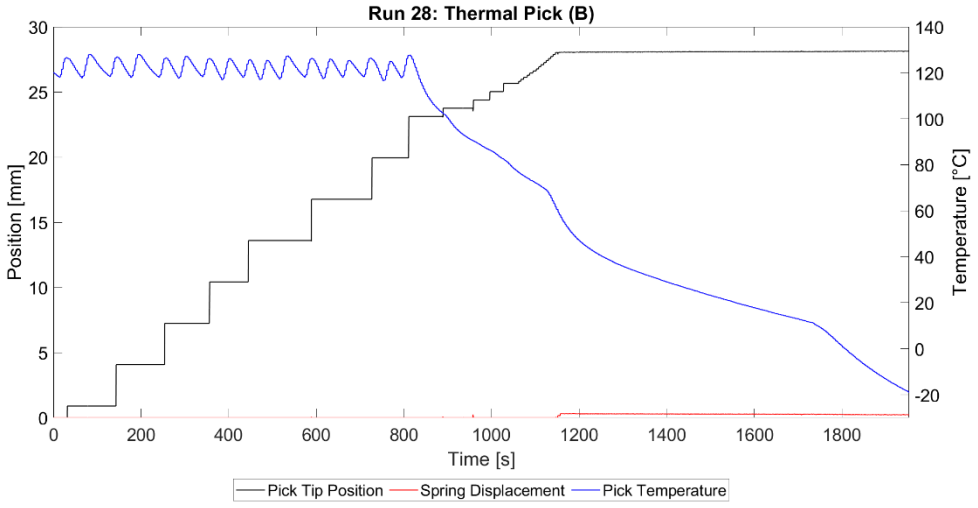

Figure 93: Test run 28 on cryogenic water ice under vacuum.

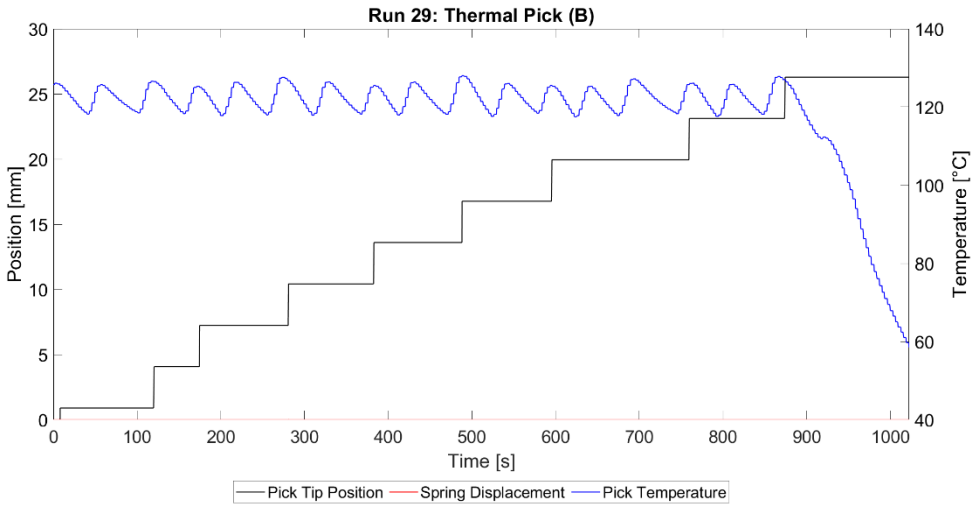

Figure 94: Test run 29 on cryogenic water ice under vacuum.

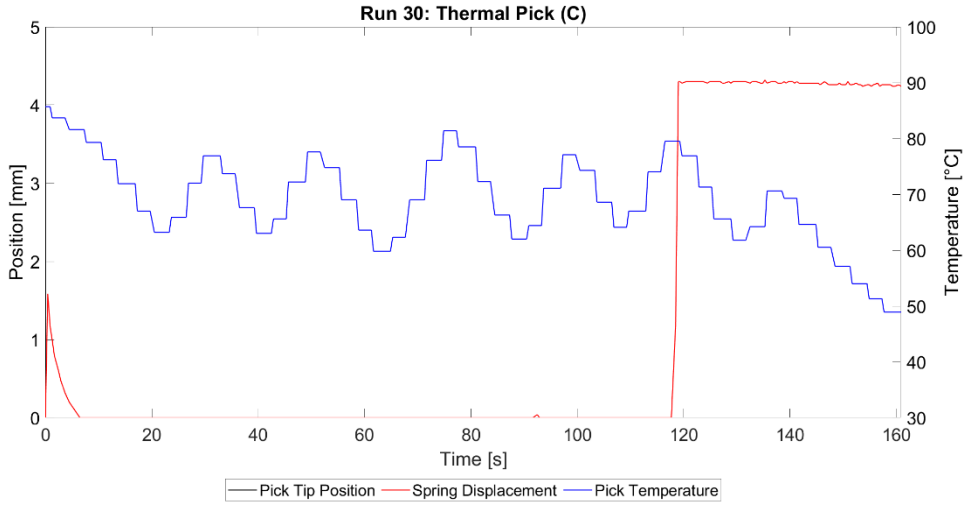

Figure 95: Test run 30 on cryogenic water ice under vacuum.

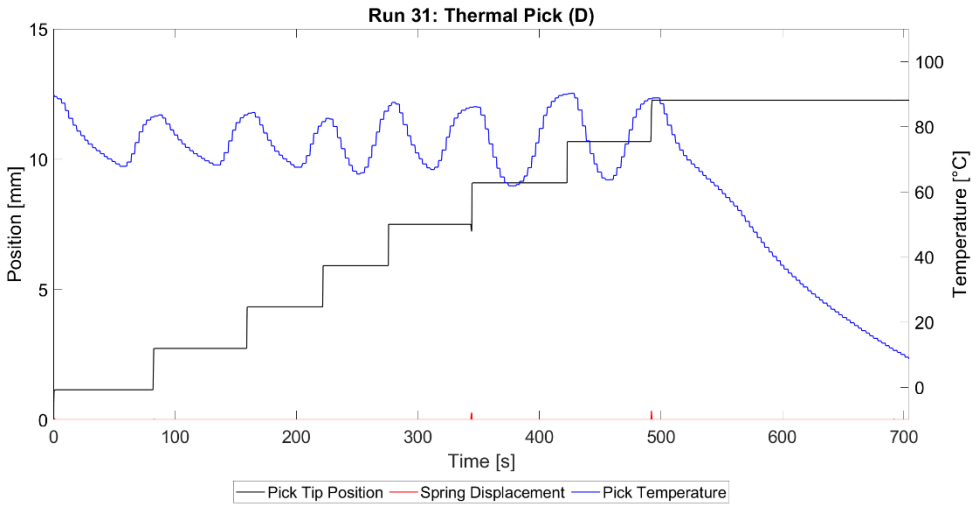

Figure 96: Test run 31 on cryogenic water ice under vacuum.

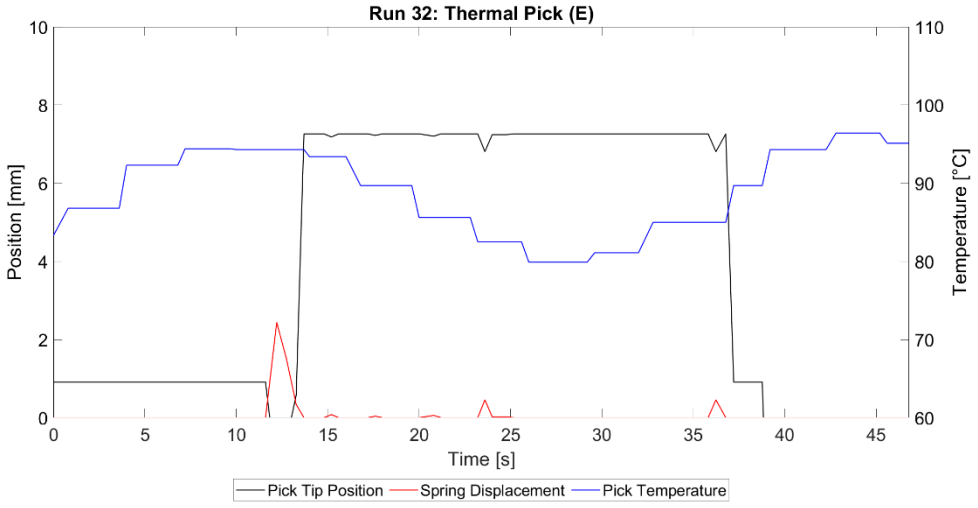

Figure 97: Test run 32 on cryogenic water ice under vacuum.

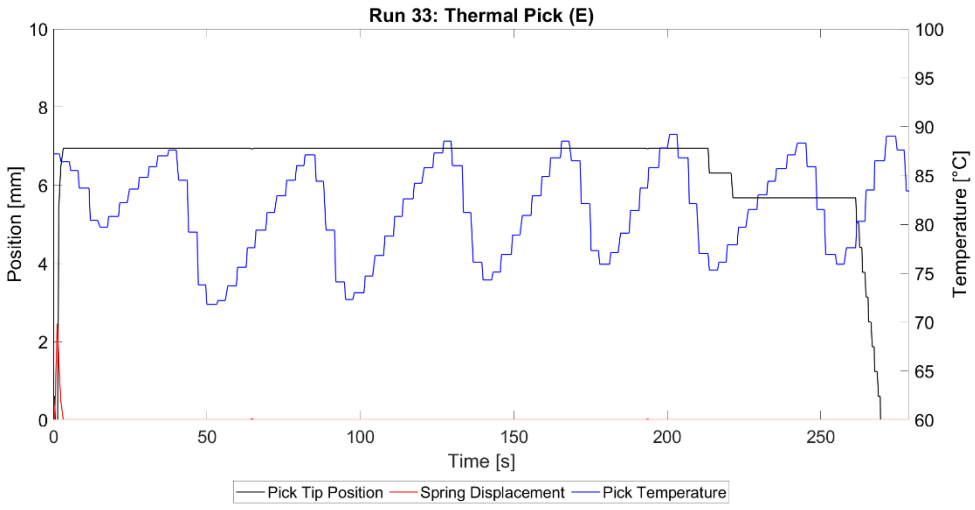

Figure 98: Test run 33 on cryogenic water ice under vacuum.

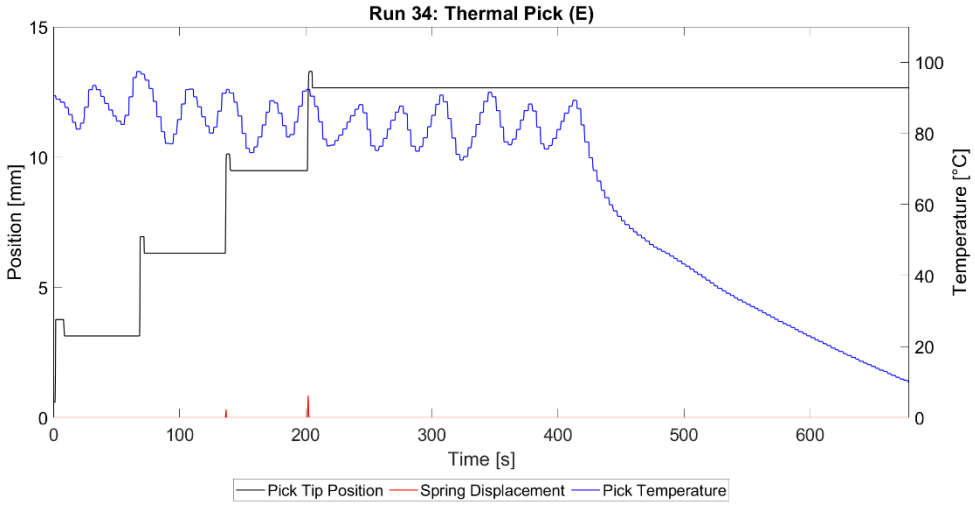

Figure 99: Test run 34 on cryogenic water ice under vacuum.

A.2 Notes from Table 3

Low β: The low temperature relative to the step size is the suspected cause of failure by thermal stall. In these cases, the thermal pick could not sustain the melting regime for long enough to complete the desired step.

Low Temp vs. Depth: The low temperature relative to the total depth reached is the suspected cause of failure. The heat loss through the walls of a thermal pick are a function of total depth, making low temperature problematic for deep insertions.

First step failure: This indicates that the ice fractured and formed a conduction path on the first attempted step, meaning that the energy and efficiency could not be determined.

Low Period: The short inter-step delay period us the suspected cause of failure. Thermal shock occurs when thermal gradients build and thermal drilling with minimal delay will expose the cryogenic ice borehole walls to relatively high temperatures.

Latent Heat Insertion: This indicates that the heater was left off for the duration of the test. Only the latent heat resulting from an initially raised temperature was used for thermal drilling into the ice.

Clear Ice: This indicates that optically clear ice was used for testing rather than a compressed ice block.

A.3 Interpretation of a Test Data Stream

The following is a detailed review of the events occurring in test run 12 as shown in Figure 45. The numbered states marked on the plot indicate their timing and they are positioned adjacent to the relevant plotted values.

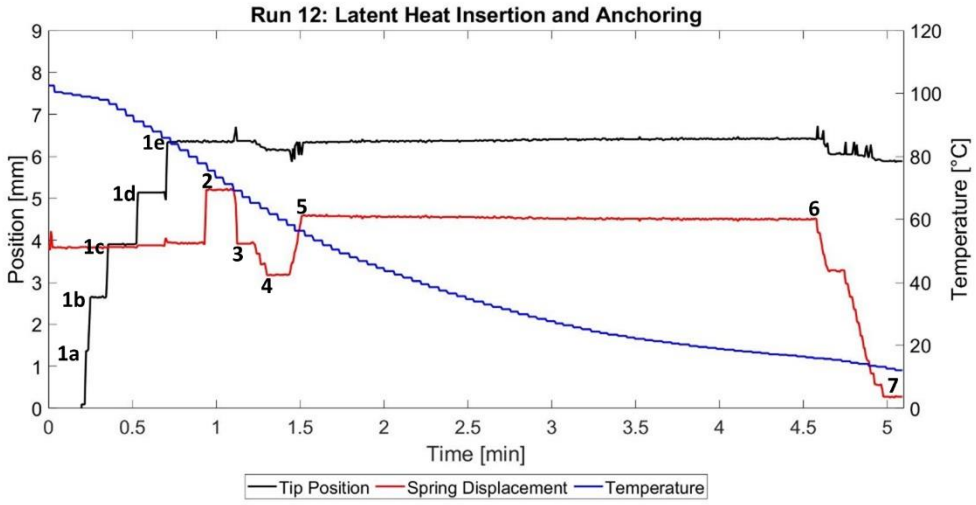

Figure 100: Annotated test run 12.

States 1a-1e: Five insertion steps into the ice were taken without any observed resistance. The tip of the thermal pick underwent 5 distinct steps into the ice of 1.27 mm each. The spring displacement was constant despite taking these insertion steps, which means that any resistance from the ice against the pick's insertion occurred at a tip pressure less than 1499 kPa (26.68 N) and therefore did not compress the constant force springs.

State 2: A positive spring displacement equivalent to the step size of 1.27 mm was observed without the tip position changing. This means that a sixth insertion step was attempted but the thermal pick was unable to advance because of the decreasing tip temperature. The measured temperature at the thermocouple is approximately

75 °C but the tip temperature was lower due to thermal inertia. For this reason, it is believed that thermal drilling cannot occur below approximately 70 °C.

State 3: The spring displacement returned to its initial value, indicating a return to the neutral spring position.

State 4: A negative spring displacement was observed alongside a slight dip in tip position. This indicates that the thermal pick was pulled back against the ice in an anchored position. The negative spring displacement means the ice is supporting the pick against an anchoring load. The slight dip in tip position shows that the thermal pick has some limited space within which it can move freely within the ice borehole.

State 5: A positive spring displacement was observed alongside a slight bump in tip position. The thermal pick was pressed on its tip surface against the ice at the bottom of the borehole to undergo active cooling.

State 6: The temperature of the thermal pick was deemed to be low enough that the anchoring phase could begin.

State 7: A large negative spring displacement was observed resulting from many small attempted extraction steps. The extension spring applied an anchoring load (130 N) that was supported by the ice. The tip position measured in this state (anchored against the top of the borehole) relative to the tip position measured in state 6 (pressed against the bottom of the borehole) was used to determine the borehole gap width.

Bibliography

[1] B. E. Schmidt, D. D. Blankenship, G. W. Patterson and P. M. Schenk, "Active formation of 'chaos terrain' over shallow subsurface water on Europa," *Nature,* vol. 479, pp. 502-505, 2011.

[2] J. L. Noviello, Z. A. Torrano, A. R. Rhoden and K. N. Singer, "Mapping Europa's microfeatures in regional mosaics: New constraints on formation models," *Icarus,* vol. 329, pp. 101-123, 2019.

[3] M. W. Klaser, J. Gross, S. Tindall, R. W. Schlische and C. J. Potter, "Europa's ice tectonics: New insights from physical wax experiments with implications for subduction initiation and global resurfacing processes," *Icarus,* vol. 321, pp. 593-607, 2019.

[4] E. J. Leonard, R. T. Pappalardo and A. Yin, "Analysis of very-high-resolution Galileo images and implications for resurfacing mechanisms on Europa," *Icarus,* vol. 312, pp. 100-120, 2018.

[5] D. E. J. Hobley, J. M. Moore, A. D. Howard and O. M. Umurhan, "Formation of metre-scale bladed roughness on Europa's surface by ablation of ice," *Nature Geoscience,* vol. 11, pp. 901-904, 2018.

[6] K. P. Hand, D. Berisford, T. Daimaru, J. Foster, A. E. Hofmann and B. Furst, "Penitente formation is unlikely on Europa," *Nature Geoscience,* vol. 13, pp. 17-19, 2020.

[7] M. Poinelli, E. Larour, J. Castillo-Rogez and B. Vermeersen, "Crevasse Propagation on Brittle Ice: Application to Cycloids on Europa," *Geophysical Research Letters,* vol. 46, no. 21, pp. 11,756-11,763, 2019.

[8] R. Greenberg and P. B. Sak, "The ridges of Europa: Extensions of adjacent topography onto their flanks," *Earth and Planetary Science Letters,* vol. 389, pp. 43-51, 2014.

[9] E. Lesage, H. Massol and F. Schmidt, "Cryomagma ascent on Europa," *Icarus,* vol. 335, 2020.

[10] Y. Ashkenazy, "The surface temperature of Europa," *Heliyon,* vol. 5, no. 6, 2019.

[11] Christina Plainaki, Tim A. Cassidy, Valery I. Shematovich, et al., "Towards a Global Unified Model of Europa's Tenuous Atmosphere," *Space Sci Rev,* vol. 214, no. 40, 2017.

[12] E. M. Schulson, "Brittle failure of ice," *Engineering Fracture Mechanics,* vol. 68, pp. 1839-1887, 2001.

[13] K. L. Litwin, B. R. Zygielbaum, P. J. Polito and L. S. Sklar, "Influence of temperature, composition, and grain size on the tensile failure of water ice; Implications for erosion on Titan," *Journal of Geophysical Research,* vol. 117, no. E8, 2012.

[14] M. Arakawa and N. Maeno, "Mechanical strength of polycrystalline ice under uniaxial compression," *Cold Regions Science and Technology,* vol. 26, no. 3, pp. 215-229, 1997.

[15] C. A. Hibbitts, K. Stockstill-Cahill, B. Wing and C. Paranicas, "Color centers in salts - Evidence for the presence of sulfates on Europa," *Icarus,* vol. 326, pp. 37-47, 2019.

[16] A. R. Hendrix, D. L. Domingue and K. King, "The icy Galilean satellites: ultraviolet phase curve analysis," *Icarus,* vol. 173, no. 1, pp. 29-49, 2005.

[17] G. J. Black, D. B. Campbell and P. D. Nicholson, "Icy Galilean Satellites: Modeling Radar Reflectivities," *Icarus,* vol. 151, no. 2, pp. 167-180, 2001.

[18] Brandon C. Johnson, Rachel Y. Sheppard, Alyssa C. Pascuzzo, et al., "Porosity and Salt Content Determine if Subducation Can Occur in Europa's Ice Shell," *Journal of Geophysical Research: Planets,* vol. 122, no. 12, pp. 2765-2778, 2017.

[19] B. Gundlach, J. Ratte, J. Blum, J. Oesert and S. N. Gorb, "Sintering and sublimation of micrometre-sized water-ice particles: the formation of surface crusts on icy Solar System bodies," *Monthly Notices of the Royal Astronomical Society,* vol. 479, pp. 5272-5287, 2018.

[20] B. A. Marmo, J. R. Blackford and C. E. Jeffree, "Ice friction, wear features and their dependence on sliding velocity and temperature," *Journal of Glaciology,* vol. 51, no. 174, pp. 391-398, 2005.

[21] Y.-C. Yen, "Review of thermal properties of snow, ice and sea ice," United States Army Corps of Engineers, Cold Regions Research and Engineering Laboratory, Hanover, 1981.

[22] J. Garry and I. Wright, "Coring experiments with cryogenic water and carbon dioxide ices-toward planetary surface operations," *Planetary and Space Science,* vol. 52, pp. 823-831, 2004.

[23] A. Curtis, M. Martone and A. Parness, "Roving on Ice: Field Testing an Ice Screw End Effector and Sample Collection Tool," in *IEEE Aerospace Conference*, Big Sky, MT, 2018.

[24] J. Duncombe, "Meet IceWorm: NASA’s New Ice-Climbing Robot," Eos, 27 February 2020. [Online]. Available: https://eos.org/articles/meet-iceworm-nasas-new-ice-climbing-robot.

[25] B. H. Wilcox, "A Deep Subsurface Ice Probe for Europa," 10 10 2017. [Online]. Available: https://www.kiss.caltech.edu/workshops/oceanworlds/presentations/Wilcox.pdf. [Accessed 25 3 2020].

[26] J. M. Beverly and W. S. Attaway, "Ice Climbing Anchor Strength: An In-Depth Analysis," [Online]. Available: http://hmga.gr/storehouse/word-acrobat/Ice%20Climbing%20Anchor%20Strength%20-%20MRA%202009%20-%20Marc%20Beverly.pdf.

[27] K. Schüller and J. Kowalski, "Melting probe technology for subsurface exploration of extraterrestrial ice - Critical refreezing length and the role of gravity," *Icarus,* vol. 317, pp. 1-9, 2019.

[28] H. Aamot, Heat transfer and performance of a thermal probe for glaciers. CRREL Special Report 194, Hanover, New Hampshire: Cold Regions Research and Engineering Laboratory, 1967.

[29] K. Schüller, J. Kowalski and P. Raback, "Curvilinear melting - A preliminary experimental and numerical study," *International Journal of Heat and Mass Transfer,* vol. 92, pp. 884-892, 2016.

[30] R. D. Lorenz, "Thermal Drilling in Planetary Ices: An Analytic Solution with Application to Planetary Protection Problems of Radioisotope Power Sources," *Astrobiology,* vol. 12, no. 8, pp. 799-802, 2012.

[31] J. Biele, S. Ulamec, M. Hilchenbach and N. I. Kömle, "In situ analysis of Europa ices by short-range melting probes," *Advances in Space Research,* vol. 48, pp. 755-763, 2011.

[32] N. I. Kömle, P. Tiefenbacher and A. Kahr, "Melting probe experiments under Mars surface conditions - the influence of dust layers, CO2-ice and porosity," *Icarus,* vol. 315, pp. 7-19, 2018.

[33] P. Weiss, K. L. Yung, T. C. Ng, N. Kömle, G. Kargl and E. Kaufmann, "Study of a thermal drill head for the exploration of subsurface planetary ice layers," *Planetary and Space Science,* vol. 56, pp. 1280-1292, 2008.

[34] E. Kaufmann, G. Kargl, N. I. Kömle, M. Steller, J. Hasiba, F. Tatschl, S. Ulamec, J. Biele, M. Engelhardt and J. Romstedt, "Melting and Sublimation of Planetary Ices Under Low Pressure Conditions: Laboratory Experiments with a Melting Probe Prototype," *Earth Moon Planet,* vol. 105, pp. 11-29, 2009.

[35] P. G. Talalay, Y. Li, M. A. Sysoev, J. Hong, X. Li and X. Fan, "Thermal tips for ice hot-point drilling: Experiments and preliminary thermal modeling," *Cold Regions Science and Tehcnology,* vol. 160, pp. 97-109, 2019.

[36] B. Dachwald, J. Mikucki, S. Tulaczyk, I. Digel, C. Espe, M. Feldmann, G. Francke, J. Kowalski and C. Xu, "IceMole: a maneuverable probe for clean in situ analysis and sampling of subsurface ice and subglacial aquatic ecosystems," *Annals of Glaciology,* vol. 55, no. 65, pp. 14-22, 2014.

[37] M. F. Horne, "Thermal probe design for Europa sample acquisition," *Acta Astronautica,* vol. 142, pp. 29-36, 2018.

[38] Y. Li, P. G. Talalay, M. A. Sysoev, V. S. Zagorodnov, X. Li and X. Fan, "Thermal Heads for Melt Drilling to Subglacial Lakes: Design and Testing," *Astrobiology,* vol. 20, no. 1, pp. 142-156, 2020.

[39] N. I. Kömle, P. Tiefenbacher, P. Weiss and A. Bendiukova, "Melting probes revisited - Ice penetration experiments under Mars surface pressure conditions," *Icarus,* vol. 308, pp. 117-127, 2018.

[40] M. Treffer, N. I. Kömle, G. Kargl, E. Kaufmann, S. Ulamec, J. Biele, A. Ivanov and O. Funke, "Preliminary studies concerning subsurface probes for the

exploration of icy planetary bodies," *Plametary and Space Science,* vol. 54, no. 6, pp. 621-634, 2006.

[41] S. Ulamec, J. Biele, O. Funke and M. Engelhardt, "Access to glacial and subglacial environments in the Solar System by melting probe technology," *Reviews in Environmental Science and Bio/Technology,* vol. 6, no. 1-3, pp. 71-94, 2007.

[42] A. Davis, "A Prototype Ice-Melting Probe for Collecting Biological Samples from Cryogenic Ice at Low Pressure," *Astrobiology,* vol. 17, no. 8, pp. 709-720, 2017.

[43] Zacny, Kris; Mueller, Juergen; Costa, Tighe; et al., "SLUSH: Europa Hybrid Deep Drill," in *IEEE Aerospace Conference*, Big Sky, MT, 2018.

[44] J. Leidenfrost, De aquae communis nonnullis qualitatibus tractatus, Ovenius, Duisburg, 1756.

[45] M. Adda-Bedia, S. Kumar, F. Lechenault, S. Moulinet, M. Schillaci and D. Vella, "Inverse Leidenfrost Effect: Levitating Drops on Liquid Nitrogen," *Langmuir,* vol. 32, pp. 4179-4188, 2016.

[46] G. G. Wells, R. Ledesma-Aguilar, G. McHale and K. Sefiane, "A sublimation heat engine," *Nature Communications,* p. 6:6390 doi: 10.1038/ncomms7390, 2015.

[47] S. Martynov, W. Zheng and H. Mahgerefteh, "Numerical study of the effect of heat transfer on solid phase formation during decompression of CO2 in pipelines," *MATEC Web Conf,* vol. 240, 2018.

[48] S. Martynov, W. Zheng, H. Mahgerefteh, S. Brown, J. Hebrard, D. Jamois and C. Proust, "Computational and Experimental Study of Solid-Phase Formation during Decompression of High-Pressure CO2 Pipelines," *Industrial & Engineering Chemistry Research,* vol. 57, no. 20, pp. 7054-7063, 2018.

[49] J. Kowalski, P. Linder, S. Zierke, et al., "Navigation technology for exploration of glacier ice with maneuverable melting probes," *Cold Regions Science and Technology,* vol. 123, pp. 53-70, 2016.